THE UNIVERSITY OF ALBERTA

QUATERNARY PALEOMAGNETIC/GEOMAGNETIC STUDIES IN WESTERN CANADA

by

© CLAYTON JOHN OBERG

A THESIS

SUBMITTED TO THE FACULTY OF GRADUATE STUDIES AND RESEARCH

IN PARTIAL FULFILMENT OF THE REQUIREMENTS FOR THE DEGREE

OF MASTER OF SCIENCE

IN

GEOPHYSICS

DEPARTMENT OF PHYSICS

EDMONTON, ALBERTA

FALL, 1978

ABSTRACT

Paleomagnetic results from 5 stratigraphic sequences are reported. four of these concern the time interval 12,000 to 13,000 years B.P. The motivation behind them was two-fold; first to seek evidence corroborating the existence of as extremely young geomagnetic polarity reversal - the so-called Gothenburg event, and second to explore the feasibility of using paleomagnetic signatures for stratigraphic correlation. No evidence for a geomagnetic reversal was found and evidence is growing that this event, if it existed at all, was more likely a non-dipole excursion of limited regional extent rather than a global polarity reversal. An enhanced clockwise secular variation loop was observed, and it is felt that this is indicative of some unusually intense non-dipole feature drifting westward past the sampling locality. This loop was identified at two localities some 250 km apart and the resulting correlation is of considerable significance geologically in that it establishes a stratigraphic relationship between two important volcanic tephras which had previously been unknown.

The fifth section involves a detailed study of a single 9,000 year paleomagnetic sequence. No geomagnetic excursions are found, and the absence of the Lake Mungo excursion is regarded as evidence supporting the spatially restricted nature of such phenomena.

Spectral analysis (using the MEM technique) reveals the

presence of two types of periodic looping motion in the Riggins Road data. Highly elliptical counterclockwise looping with a period of roughly 5,000 years probably reflects a counterclockwise "wobble" of the dipole axis as suggested by other workers. The circular clockwise looping motion of period 1,900 years indicates the presence of westward drift of the non-dipole field some 30,000 years ago.

The complex MEM technique is investigated by means of synthetic data sets in an effort to assess the validity of results obtained from very noisy records. Some interesting conclusions are obtained, the most important of which is that it enables one to identify both the frequency and sense of looping signals in the presence of noise levels twice that of the signal amplitude which makes it an ideal tool for analysing the type of time sequences encountered in paleomagnetism.

ACKNOWLEDGEMENTS

I would like to thank both my wife Barbara and my parents for their patience and support throughout my years in graduate school as well as Elsie and Harold Moore for generously providing the living accomodation that I so frequently required while completing this thesis. I am grateful to Dr. Gerry Hoye who participated in most of the field work and helped in the preparation of the final manuscript. I am also most grateful to Dr. John Westgate whose assistance in the field and geological guidance was of fundamental importance throughout this study. Finally I would like to thank my supervisor Dr. M. E. Evans without whose abundant support, guidance, and encouragement none of this work would have been possible.

TABLE OF CONTENTS

*****

TABLE OF CONTENTS

LIST OF TABLES

LIST OF FIGURES

LIST OF FIGURES

CHAPTER 1

Introduction

1.1 The Geomagnetic Field

This thesis deals with the presentation, analysis, and possible implications of paleomagnetic data obtained from several young (< 40,000 yrs.) geological sequences. Such being the case, a brief overview of what is currently known (or hypothesized) about the earth's magnetic field and its behavior with time is first presented.

To a very good approximation, the geomagnetic field can be represented by that of a magnetic dipole situated at the earth's center. The dipole axis presently intersects the surface at 78.7° N, 289.5° E, about 11.5° from the rotation axis, and has remained in this position for as long as detailed world wide geomagnetic data have been available (roughly 150 years). Paleomagnetic data however shows that over much longer time periods (thousands to millions of years), the position of the geomagnetic pole has varied considerably. Motions taking place over millions of years or longer are generally called polar wander and play a very important role in global tectonic theory. Their time scale is much longer than the intervals studied in this thesis however.

Changes in dipole orientation with periods of about 10^4 years also take place and these are often graphically referred to as "dipole wobble". There is as yet no widely accepted

theory as to the precise nature and period associated with this motion (Kawai and Hirooka, 1967; McDonald and Gunst,1968), but most authors agree that if averaged over a sufficient length of time the geomagnetic axis coincides closely with the rotation axis. In other words the time averaged geomagnetic field is thought to approximate that of a geocentric axial dipole.

The actual degree to which the earth's field is dipolar is a matter of considerable importance in both paleomagnetism and geomagnetism since it allows one to specify a mathematical relationship between field direction at a given location on the earth's surface and the position of the corresponding geomagnetic pole. This relationship is as follows (Irving, 1964);

$$L' = \arcsin(\sin(L)\cos(P) + \cos(L)\sin(P)\cos(D))$$

$$\phi' = \phi + \arcsin(\sin(P)\sin(D)/\cos(L')) \quad (\text{for } \cos(P) > \sin(L)\sin(L'))$$

$$\phi' = \phi + 180 - \arcsin(\sin(P)\sin(D)/\cos(L')) \quad (\text{for } \cos(P) < \sin(L)\sin(L'))$$

where L' = latitude of pole

ϕ' = longitude of pole

L = latitude of field location

ϕ = longitude of field location

D = magnetic declination

and P = geomagnetic colatitude which is given by;

$$2\cot(P) = \tan(I)$$

where I = magnetic inclination

These formulae enable paleomagnetists to reconstruct the relative positions of the continents, and their associated lithospheric plates over geologic periods of time, and thereby provide much of the basis of the modern theory of plate tectonics. The same formulae are also used extensively by geomagnetists, both to study the motion of the pole itself, and as a means of comparing directional data obtained from widely separated locations. If sufficient time averaging has been achieved one speaks of "paleomagnetic poles", whereas if insufficient averaging has taken place one speaks of "virtual geomagnetic poles" (VGP's) (McElhinny, 1973).

Obviously if the earth's field were always perfectly dipolar VGP's obtained from geomagnetic directional data would vary only as a function of time and not as a function of the location from which the data were obtained. Analysis of world wide directional data obtained from the present field however, indicates that this is far from true. Figure 1-1 shows that VGP's obtained from globally distributed sites typically vary 10° to 20° from the actual geomagnetic pole. The part of the field responsible for this deviation is called the non-dipole field.

The dipole and non-dipole geomagnetic fields can be distinguished by spherical harmonic analysis of the entire field, the dipole field being represented by the lowest order terms in the expansion, and the non-dipole part being

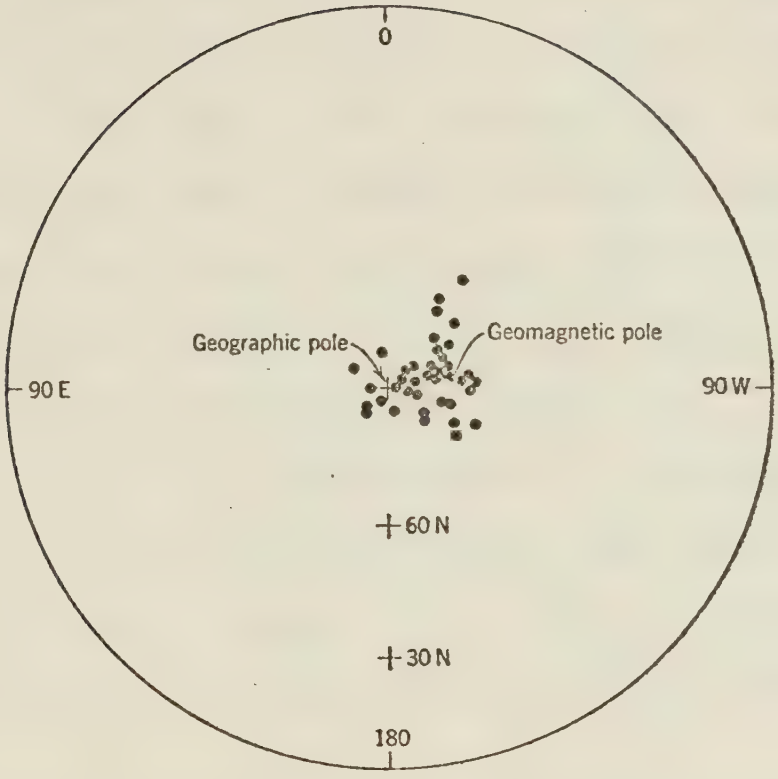

Fig. 1-1: Virtual geomagnetic poles (VGP's) calculated from observatory data for 1945 (after Cox and Doell,1960).

represented by all higher order terms. The justification for regarding the fields separately is that they are thought to arise from two physically distinct processes in the earth's core. The dipole field is believed to be governed by a single self exciting dynamo produced by means of large-scale fluid motion in the outer core (Jacobs, 1975). It is most likely driven by some form of convection and controlled to a large extent by those forces associated with the earth's rotation which would account for its axial nature. The non-dipole field, on the other hand, is thought to arise from small scale eddies or perturbations of the main current system close to the outer core boundary. Such features could be governed to some extent by either thermal or topographical irregularities at the core-mantle interface.

At the earth's surface the non-dipole strength is typically about 1/20 that of the dipole field (Irving, 1964). The non-dipole field however is responsible for essentially all of the shorter period (tens to thousands of years) changes -- the so-called secular variation. Such variations have been observed directly for the last few centuries at various locations throughout the world. The magnitude of these geomagnetic directional fluctuations is typically of the order of 10° to 20°. The best known examples are those recorded at London and Paris (Fig. 1-2) which describe almost complete loops in magnetic direction with an apparent period of about 500 years.

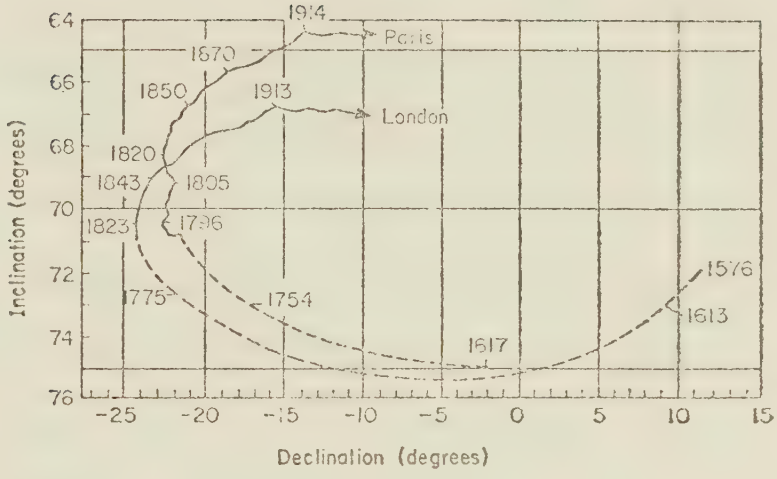

Fig. 1-2: Variation of declination and inclination at London and Paris from observatory data (after Gaiber-Puertas, 1953).

The non-dipole field is generally displayed by means of isomagnetic maps on which one of the field elements (e.g. declination, inclination, intensity) is contoured. The contours on such maps tend to close about regions of continental dimensions forming clearly visible cells several of which are present over the earth's surface (Fig. 1-3). Many of these features appear to grow and decay with lifetimes in the order of hundreds of years, whereas others appear to be stable over much longer periods of time. Perhaps the most interesting feature of the non-dipole field is its tendency to drift westward. Although observation of individual non-dipole features over the past century indicates that these features often follow quite different paths, and move at quite different rates with respect to one another, the overall tendency toward westward drift is unmistakable, the average drift rate being an easily observable 0.18° per year (Bullard et al., 1950).

Although few deny its existence, much concerning the actual nature of the westward drift remains unclear. The actual drift rate, for instance, is difficult to define, as the value obtained, even for a world wide average, depends on the method of analysis used. The value quoted above was obtained from calculations involving the non-dipole field elements directly. Analysis of the time derivatives of these same elements (the secular variation field) through comparison of isoporic charts for different epochs, gives a significantly higher drift rate (0.32° per year, Bullard et

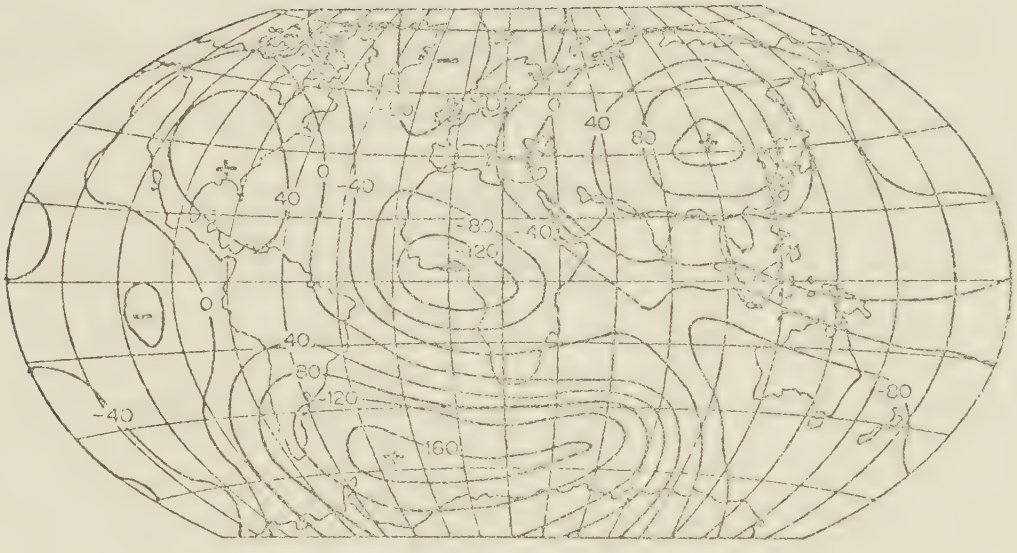

Fig. 1-3: The non-dipole field for 1945. The contours give the vertical component at intervals of 4×10^{-3} mT (after Bullard et al 1950).

al., 1950). Yukutake and Tachinika (1968), attribute this difference to the presence of large stationary anomalies which tend to lower the mean drift rate calculated from the non-dipole field. Provided these anomalies do not fluctuate rapidly in intensity, their presence should not affect the velocity obtained through analysis of the secular variation field. Thus Yukutake and Tachinaka conclude that the higher the two velocities more truly reflects the velocity of the "drifting" portion of the non-dipole field. Simply dividing the non-dipole field into standing and drifting parts does not fully explain the marked regional variation in drift velocity. This is especially true in Canada and Alaska where very small, but definitely measurable, negative (eastward) drift rates have been observed (Cain and Hendricks, 1968; Yukutake, 1962).

In addition to its present, rather complex, nature there is evidence to suggest that westward drift has changed with time as well. For example Harwood and Malin (1976) show that the rate of westward drift decreased by almost 50 percent over the last few decades. Such a remarkably rapid change raises some doubt as to the long term stability of westward drift. Indeed, Hide and Malin (1970) have suggested that the drift may be a transient phenomenon initiated some 500 years ago. In contrast to these observations, archaeomagnetic studies suggest that at least some features of magnetic declination and inclination have probably been drifting westward for roughly 1000 years or more (Yukutake,

1962, 1967; Tarkhov 1965; Burlatskaya et al. 1965, 1968). Futhermore Bucha et al. (1970) have shown that a maximum in geomagnetic intensity may have been drifting westward for as long as 3000 years. Clearly there is considerable uncertainty regarding the long term nature of the secular variation. Runcorn (1959), and Skiles (1970) have pointed out a means by which paleomagnetic data from a single location, can be used to infer the presence and direction of drift. This technique, and its application to a particular set of paleomagnetic data is the subject of Chapter 3.

Another geomagnetic phenomenon of considerable importance is that of polarity reversals. In contrast to the temporal variations discussed above, these are dipole features and are associated with much longer time intervals. The last well established reversal occurred 0.69 X 10^6 years ago at the base of the present Brunhes polarity epoch. Recently, Morner et al. (1971) in Sweden claimed to have established a short reversal dated at approximately 12,000 yrs. B.P. and subsequently named the Gothenburg event. Corroboration of this event in widely separated geographic localities was necessary to establish it as a genuine reversal, and this was the original motivation behind the work described in Chapter 2. If verified, such extremely young and short events would be very important to geomagnetists in terms of the overall polarity spectrum and the mechanism of reversals, and to geologists as high resolution global time markers. Both these topics are discussed in

Chapter 2. It emerges that there probably are real geomagnetic events of this type but they do not represent genuine reversals. Currently they are given the label "geomagnetic excursions", several of which have been reported from around the globe. They are thought to arise from sudden, rapid enhancements of particular non-dipole features in the outermost core and thus affect only limited geographic areas (Harrison and Ramirez, 1975). Verosub and Banerjee (1977) have recently provided a comprehensive review of the appropriate evidence for these features and conclude that the existence of any proposed excursion is not yet "sufficiently well established for its reality to be beyond question" (p. 153).

1.2 Methods and Techniques

The laboratory techniques involved in the measurement of the magnetic remanence vector corresponding to a given paleomagnetic specimen are now routine, and have been well documented (see e.g. McElhinny 1973). Measurements were carried out using two commercial magnetometers, a Schonstedt model SM1 slow spinner, and a Digico Balanced Fluxgate system (Molyneux, 1971). Specimens were partially demagnetized in alternating magnetic fields (A.F. demagnetization), using an apparatus built and described by Murthy (1969), in an attempt to remove unwanted secondary components of magnetization. The actual fields used in demagnetization, are given later in the thesis as each set

of paleomagnetic data is discussed.

Collecting of oriented specimens in the field presented some difficulty, as the material sampled was unconsolidated sediment. Two methods were used. One involved driving a brass channel horizontally into the vertical face of the outcrop; the other utilized small plastic cubes (available commercially) which were pressed into the sediment. Both techniques are described in detail in Appendix 1. A total of 136 stratigraphic horizons from 5 separate localities were collected. The number of independently oriented samples was 173, involving 225 individual specimens and a total of some 1000 measurements of remanence.

Results are analysed using standard Fisher (1953) statistics, which can be regarded as the spherical analogue of Gaussian statistics. S. I. units are used throughout the thesis but since much geophysical literature is still written in cgs units, conversions for the most common parameters are given here:

Magnetic Induction; 10^{-5} Gauss = 1 gamma

= 1 nanotesla

Intensity of Magnetization; 10^{-3} emu cm^{-3} = 1 amp/m

CHAPTER 2

Late Quaternary Paleomagnetic Results from Southeastern Alberta and West Central Montana

2.1 Introduction

This chapter describes a paleomagnetic investigation of sedimentary deposits in the age range 12,000 to 13,000 years, initially undertaken to seek evidence corroborating the existence of the so-called "Gothenburg Event", a supposed geomagnetic reversal recently reported from Sweden (Morner et al., 1971; Morner and Lanser, 1974). Recognition of this extremely young reversal would have been of considerable significance both geophysically and geologically.

A feasibility study was carried out on a section in southeastern Alberta. No reversal was observed, but an apparently reliable geomagnetic record was obtained and it was decided to extend the study to other sections with two objectives in mind. First, to check the reality of certain distinctive features observed and thus improve our knowledge of long-term geomagnetic field behavior, and second to assess the possibility of using magnetic records as a means of regional geological correlation. Samples were therefore collected from three further stratigraphic sections.

The four sections investigated are referred to by local geographical names -- Irvine, Choteau, Manyberries, and Diversion Lake (Fig. 2-1). Of these the first two are about

Fig. 2-1: Location map showing geographic and stratigraphic distribution of samples collected. The dash-dot lines indicate the minimum fall-out area for the appropriate Glacier Peak tephra.

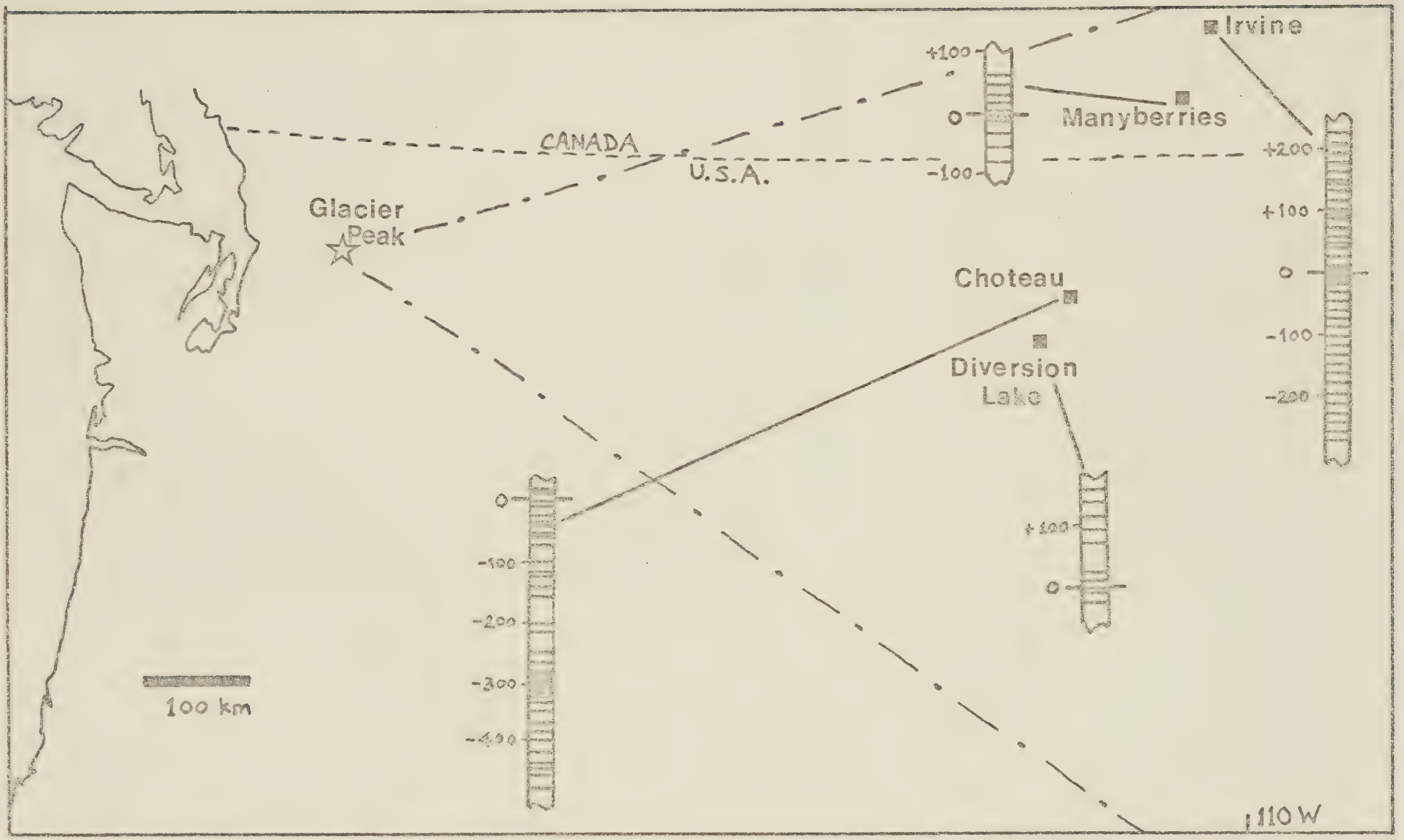
Irvine
+100
0
-100
Manyberries
+200
+100
0
-100
-200
CANADA
U.S.A.
Glacier
Peak
Choteau
Diversion
Lake
0
-100
-200
-300
-400
+100
0
100 km
110 W

5 m. thick and were sampled at more than 30 horizons each; the latter two are less than 2 m. thick, sampled at only 10 horizons each. The Manyberries and Diversion Lake data are therefore of a reconnaissance nature, insufficent to stand alone but hopefully of some use in making comparisons with the more thoroughly investigated Irvine and Choteau sites. The vertical extent of each section is indicated schematically in Figure 2-1 with the horizontal lines representing horizons sampled. The zero on the vertical scale represents the position of the Glacier Peak tephraat that locality.

2.2 Geological and Sampling Details

Three of the four sections studied contain a volcanic tephra originating from an eruption at Glacier Peak, Washington. This eruption has been dated at 12,750 ± 350 yrs. B.P. (Mudge, 1967) using snail shells from the ash bed at Diversion Lake. The tephra was identified at all three locations on the basis of its chemistry (Lemke et. al., 1975; Westgate, 1968), and is widely regarded as being the older of 2 ash-falls originating from Glacier Peak (Wilcox, 1969; Westgate et. al.,1970). However Westgate (Westgate and Evans, 1978) has discovered a third tephra in southeastern Alberta. This third tephra is undated and its stratigraphic relationship to the other two tephras is unknown, but it has a basically similar chemical composition and is therefore thought to have been erupted from Glacier Peak in the same general time interval as the other two ash falls. On the

basis of a chemical trend it seems likely that it is the oldest of the three (Westgate and Evans, 1978).

At all four sections paleomagnetic samples were collected using a rectangular brass channel as described in Chapter 1. As the geomagnetic features of interest in this study were relatively large compared to experimental error, it was decided to examine as many individual horizons as possible rather than concentrating on reducing noise by replicate sampling. To this end collection was restricted almost exclusively to one independently oriented sample per horizon. It was generally possible however, to cut and measure two or more individual cubic specimens from each sample. Averaging the results from these specimens helps reduce noise arising from any distortion of the sediment during sampling, and the measuring process in the laboratory.

The Irvine section is located in southeastern Alberta, approximately 10 km north of the town of Irvine (Lsd 4, sec 28, Tp 12, R 2, W 4; 50.1° N, 110.3° W). The sequence sampled is a near vertical, 5 metre thick, road cut exposure consisting entirely of horizontally bedded lacustrine silts (and some minor sands), probably of supraglacial origin. The marker horizon used was the undated Glacier Peak tephra discussed above -- at this locality it forms a white, clearly visible layer about 2 cm thick, located approximately in the middle of the section. A total of 35 horizons were

sampled at 15 cm intervals, from 228 cm above the tephra to 270 cm below it.

The Choteau section is located some 250 km southwest of the Irvine section (NE 1/4, SW 1/4, sec 8, Tp 24N, R 3W, New Rockport Colony, Teton County; 47.8° N 112.0° W). The tephra at this locality is approximately 1 cm thick and lies 25 cm below the upper boundary of a thick sequence of glacio-lacustrine sediments. This sequence is overlain by a different depositional unit about 1.3 meters in thickness which contains the much younger Mazama tephra (approx. 6600 yrs. old (Lemke et al., 1975)). The entire section is exposed on the nearly vertical wall of a 400 m. long landslide scarp. Lemke et al. describe this section in detail and indicate the presence of two depositional breaks in the lacustrine sediment below the Glacier Peak tephra. The positions of these depositional breaks are shown in Figure 2-2b. Lemke et al. argue that the lacustrine sediment beneath the lower depositional break was probably laid down during an earlier glaciation (Bull Lake Glaciation), which implies an age greater than 70,000 years. The paleomagnetic results discussed below are of some importance in this context, since they do not concur with this interpretation. Samples were collected at 40 horizons ranging from 11 cm above the Glacier Peak tephra to 468 cm below it. The average vertical distance between horizons was 15 cm, but a zone of interest was subsequently resampled on a more detailed basis.

The Manyberries section is located approximately 80 km southwest of the Irvine section, about 1 km south of the village of Manyberries, Alberta (Lsd 14, sec 13, Tp 5, R 6, W 4; 49.4° N, 110.7° W). It consists of a meter thick sequence of horizontally bedded lacustrine sands, silts, and clays enclosing a horizontal band of white tephra approximately 3 cm thick. This sequence is part of a 10 meter vertical stream cut escarpment described by Westgate (1968). The lacustrine sediment overlies about 1 meter of sand and fine gravel with inclusions of till, and this in turn overlies a brown basal till. Above the lacustrine sequence lies a meter of late glacial sand and fine gravel, and alluvial sediment then extends to the top of the bluff. The tephra has been shown, on the basis of chemistry, to be of Glacier Peak origin, and identical to that found at Diversion Lake, and hence can be assigned an age of about 12,700 years (Westgate and Evans, 1978). Paleomagnetic specimens were obtained from 10 horizons in the lacustrine sequence ranging from 60 cm above the tephra to 80 cm below. The vertical distance between horizons was typically about 18 cm.

The Diversion Lake section is located roughly 50 km southwest of Choteau, on the shore of Diversion Lake, Sun River, Montana (NW1/4, SW1/4, sec 36, Tp 22 N, R 9 W; 47.6° N, 112.7° W). Considerable digging into the side of the shallow embankment at the edge of the lake exposed about 2

meters of lacustrine silts with interbedded sands and gravels and a band of white tephra about 2 cm thick. As discussed above, this tephra is thought to be the same as that found near Manyberries and Choteau, and has an age of 12,750 ± 350 C-14 years (Mudge, 1967). Ten horizons were sampled from 26 cm below the tephra, to 154 cm above it. The presence of gravel beds in the sequence made uniform sampling impossible, however a typical distance between horizons was 20 cm. A geological description of this locality is given by Lemke et. al. (1975).

2.3 Measurements and Results

Remanence directions were measured using a Shonstedt model SSM-1 slow spinner magnetometer. Whenever possible (in roughly 80% of all cases) 2 or more individual specimens per horizon were measured. Five pilot specimens were subjected to stepwise A.F. demagnetization in fields up to 180 mT. A typical median destructive field (MDF) was found to be about 20 mT. In all but one case a relatively large angular shift took place on the first A.F. treatment (10 mT), suggesting the removal of a soft component of magnetization most likely picked up in the laboratory. Smaller shifts (roughly 10°) were then observed for successively higher A.F. treatments, until eventually directional instability set in, anywhere between 30 and 80 mT. All remaining specimens were therefore demagnetized at 10 and 20 mT. A complete archive of all the measurements is given in Appendix 2. Table 2-1 summarizes the more important features. As with the pilot specimens,

average angular shifts between 10 and 20 mT were significantly smaller than those between NRM and 10 mT for all four sections. For three of the sections within-site scatter is slightly smaller at 10 mT than at 20 mT, but the Diversion Lake data is more highly grouped after a 20 mT treatment. During laboratory storage (3 years) some of the Irvine specimens acquired a rather hard secondary magnetization which could not always be eliminated by 10 mT. In view of these observations, it was decided that the most appropriate treatments were 10 mT for the Choteau and Manyberries sections, and 20 mT for the Irvine and Diversion Lake sections. However it is stressed that this choice does not alter any essential feature of the conclusions drawn below. The results are illustrated in the form of declination and inclination magnetograms in Figure 2-2(a-d).

2.4 Discussion

In order to assess the statistical significance of the fluctuations in remanence direction apparent in the magnetograms, the serial correlation test of Beran and Watson (1967) was applied to each of the four data sequences. As can be seen in Table 2-1, three of the sequences easily pass the test, indicating strongly that sequential geomagnetic field behavior has been recorded. The failure of the Manyberries sequence suggests that any geomagnetic oscillations which may have occurred were of sufficiently small amplitude to be obscured by noise associated with sampling and/or the acquisition of magnetic

Fig. 2-2: Paleomagnetic results from the

a) Irvine section, Alberta (triangles = QV samples).

b) Choteau section, Montana (asterisks = QP samples).

c) Diversion Lake section, Montana.

d) Manyberries section, Alberta.

These magnetograms are plotted on different scales to provide maximum clarity compatible with page size. Stratigraphic elevations are positive (negative) above (below) each local tephra. Declination is positive east of north, and inclination is positive downward.

a) Irvine

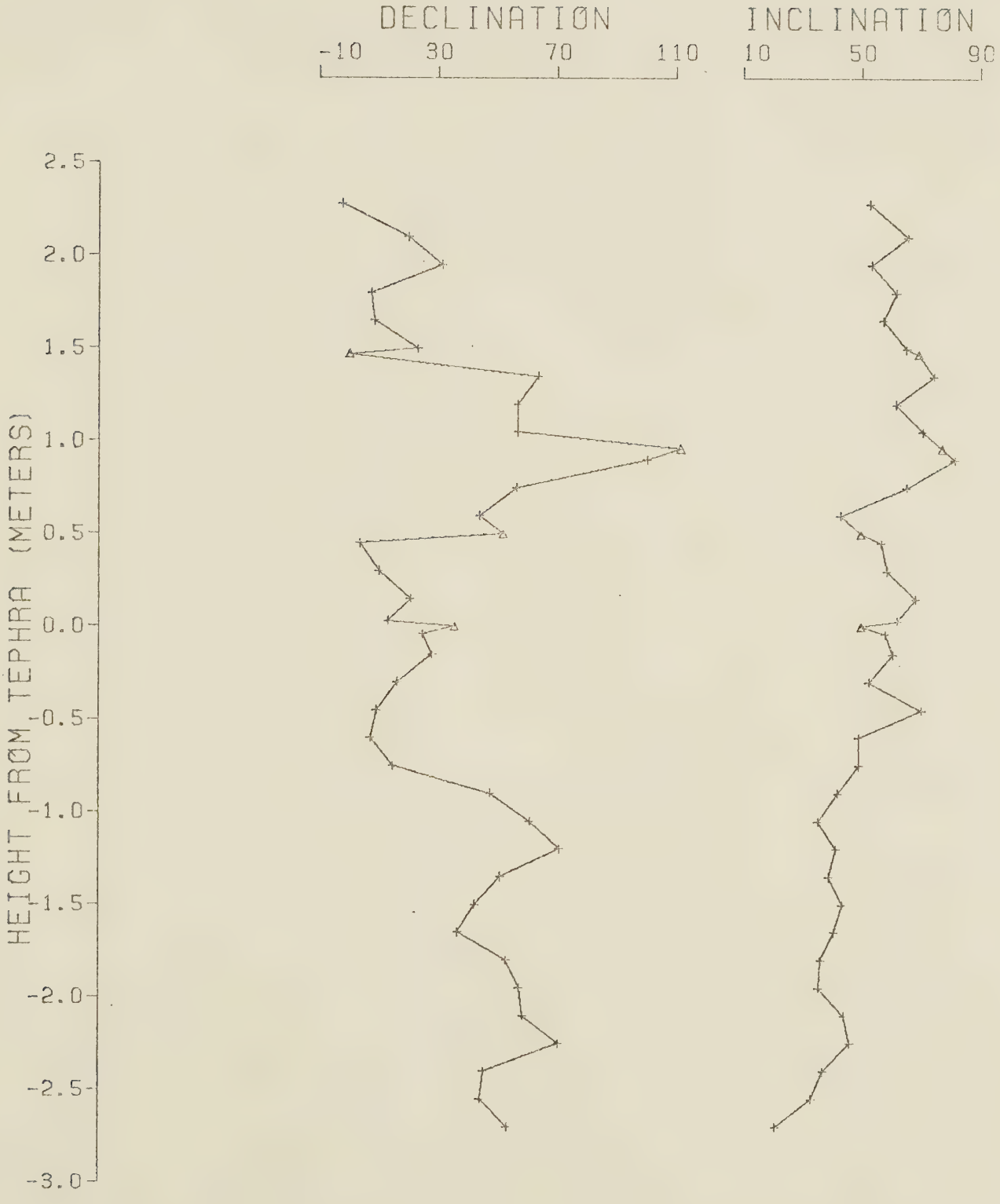
DECLINATION
-10
30
70
110
INCLINATION
10
50
90
HEIGHT FROM TEPHRA (METERS)
2.5
2.0
1.5
1.0
0.5
0.0
-0.5
-1.0
-1.5
-2.0
-2.5
-3.0

b) Choteau

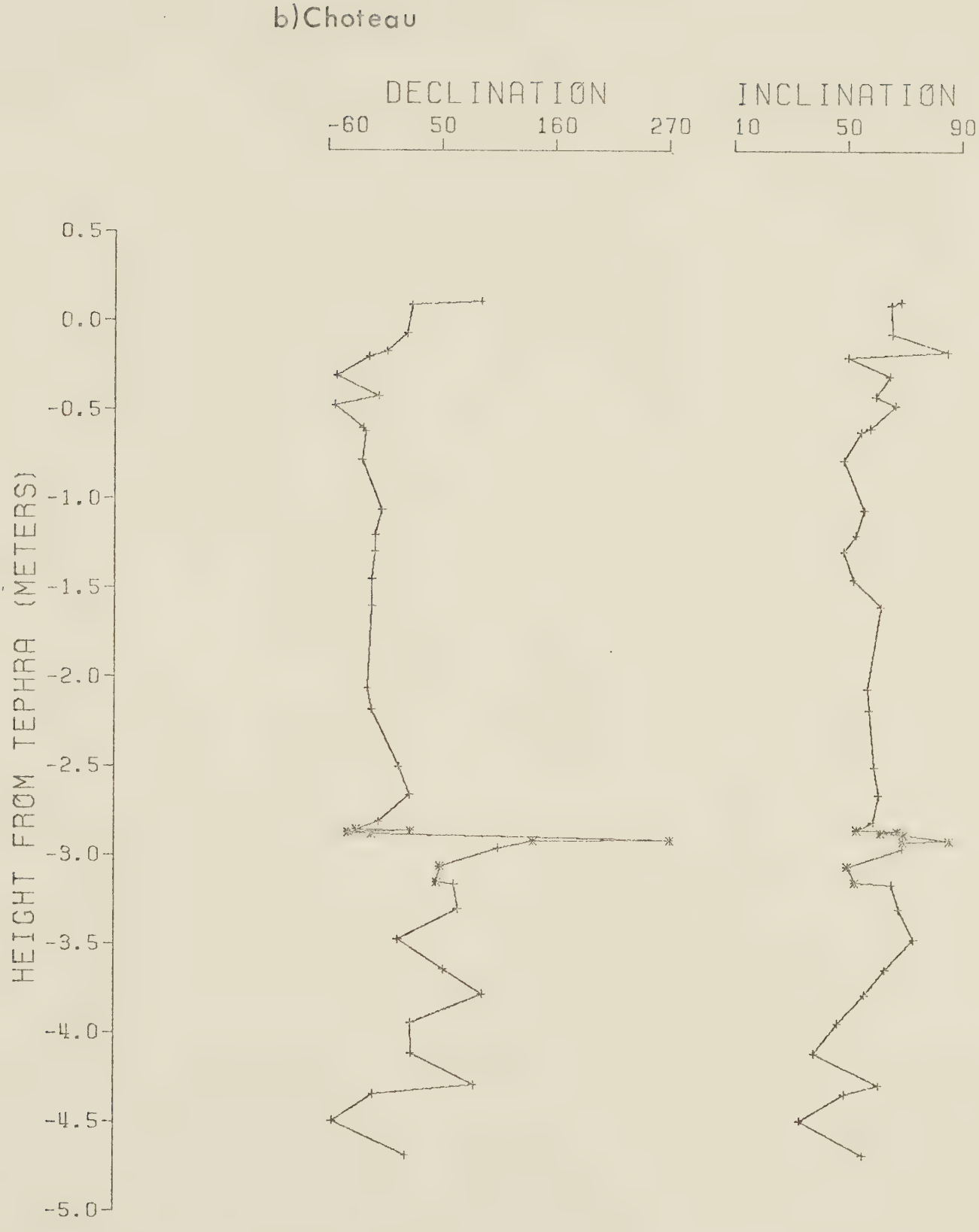
DECLINATION
-60
50
160
270
INCLINATION
10
50
90
HEIGHT FROM TEPHRA (METERS)
0.5
0.0
-0.5
-1.0
-1.5
-2.0
-2.5
-3.0
-3.5
-4.0
-4.5
-5.0

c)Diversion Lake

d) Manyberries

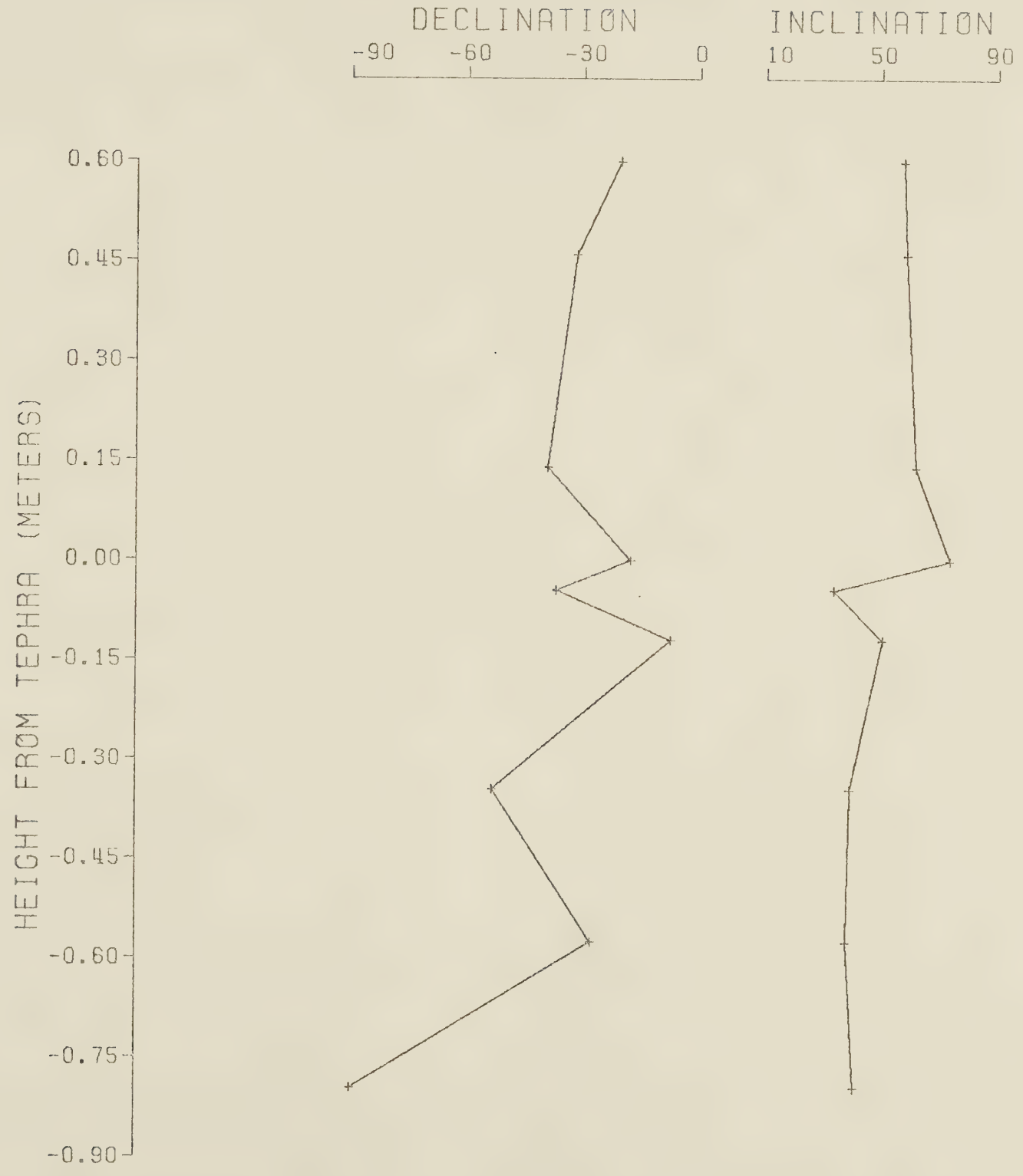

Table 2-1

Summary of Horizon Mean Data

	Irvine	Choteau	Diversion Lake	Manyberries
Stratigraphic thickness (m)	4.98	4.79	1.80	1.40
Number of horizons	35	40	10	10
Mean angular shift				
0-10mT	14.5°	5.0°	9.7°	15.7°
10-20mT	6.2°	2.5°	4.1°	10.2°
Mean α_{63}				
NRM	6.6°	4.6°	3.4°	6.8°
10mT	6.9°	5.1°	3.7°	5.9°
20mt	7.6°	5.5°	2.6°	7.4°
Mean Intensity				
NRM	6.7	7.0	4.9	4.8
'Cleaned'	2.2	6.2	2.9	3.9
Beran-Watson Test				
Serial Correlation Index	6.3	4.2	2.5	0.15
Sig. Level	>99%	>99%	>99%	None

Notes:

1. α_{63} is the standard error of the mean ($\sim 81(kN)^{-\frac{1}{2}}$) where k is Fisher's (1953) precision parameter and N is the number of specimens per horizon.
2. Magnetic intensities are given in units of 10^{-3}A/m.

remanence. Nevertheless acquisition of apparently meaningful geomagnetic records from 3 more or less contemporaneous sections made the prospects for correlation attractive.

It was initially felt that the unusually large declination swing discovered above the tephra at Irvine (Fig. 2-2a) would be recognizable if found at other localities. A similar feature is, in fact, visible on the Choteau magnetogram (Figure 2-2b). The comparison is better illustrated by plotting the appropriate data on a stereonet (Figure 2-3a). It is seen that an open loop having the same clockwise sense, similar magnitude, and occupying the same part of the stereonet is recorded at both sites. The reality of this loop is confirmed by the four QV horizons which represent a profile displaced about 3 meters laterally from the main profile and collected a year later. Some additional samples were also collected at Choteau (QP horizons) and they too are displayed in Figure 2-3a. The data points on each loop do not correlate on a one to one basis, however this is not surprising for two reasons. First, because of the distance between the two sites (250 km), slight differences in the secular variation patterns are to be expected, even in the absence of experimental error (e.g. see historical data from London and Paris, Fig. 1-2). Secondly, the sampling interval at Choteau is much finer than that at Irvine due tc subsequent resampling in the vicinity of the loop. In particular, the five southerly and westerly points on the Choteau plot span less than 10 cm

Fig. 2-3: Stereographic plots of paleomagnetic results from Choteau (dots) and Irvine (triangles). Open circles correspond to triangles in Fig. 2-2a and asterisks in Fig. 2-2b.

a) Details of the secular variation loop (see text) recorded at both sites. Choteau data from -394 cm to -266 cm, Irvine data from +45 cm to +165 cm.

b) Comparison of parts of (a) using a sliding 10 cm averaging window to smooth the densely sampled Choteau data. Stratigraphic intervals are: Choteau -330 cm to -250 cm; Irvine +105 cm to +165 cm.

c) Vectorial averages and their circles of 95% confidence for the stratigraphic intervals immediately above and below the secular variation loop illustrated in (a) and (b). Stratigraphic intervals are given in cm. The sequences of numbers in square brackets give the average declination and inclination, the number of horizons involved, the precision parameter (k), and the circle of 95% confidence in degrees.

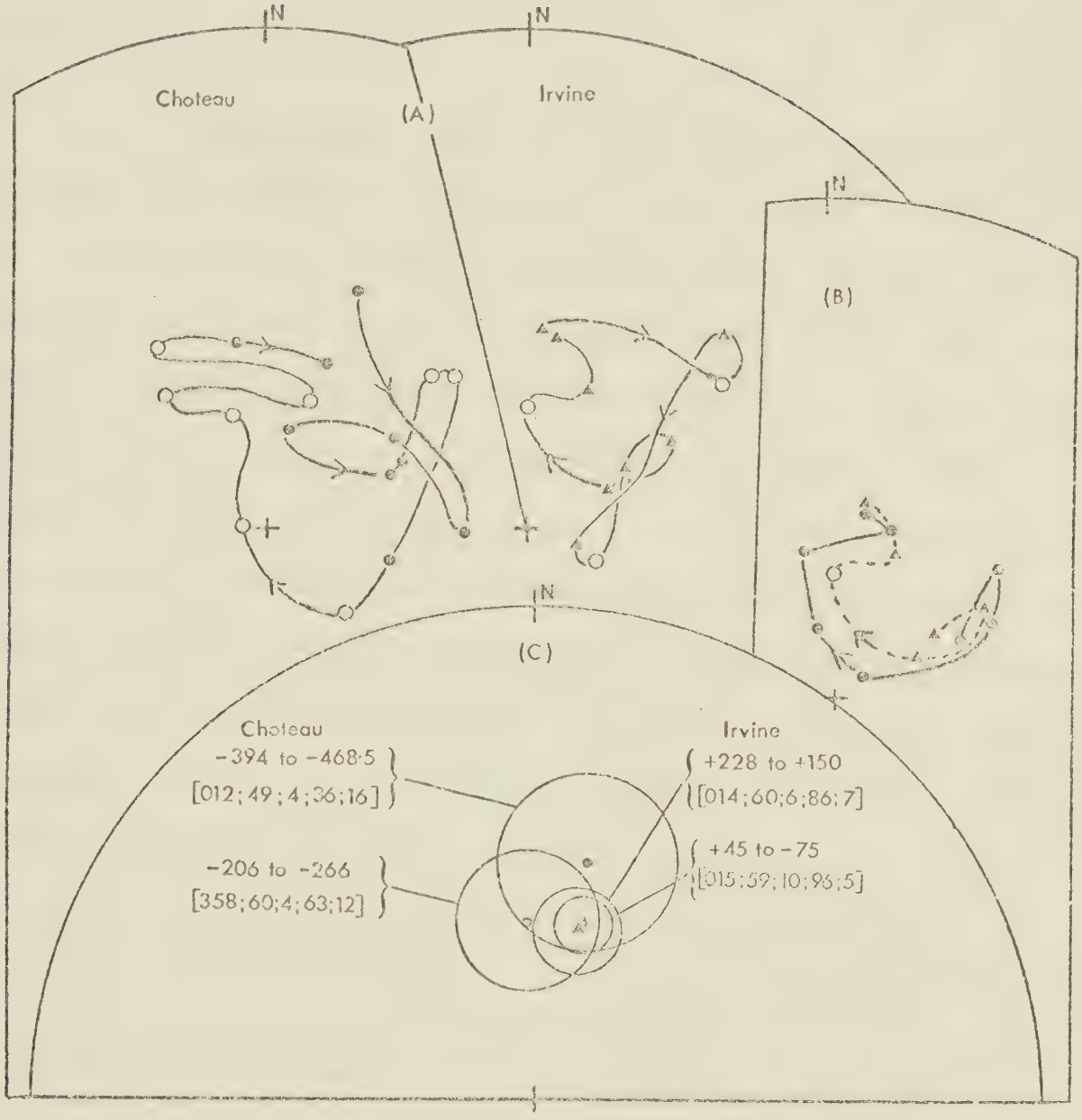
N
N
Choteau
(A)
Irvine
N
(B)
N
(C)
Choteau
-394 to -468·5
[012;49;4;36;16]
-206 to -266
[358;60;4;63;12]
Irvine
+228 to +150
[014;60;6;86;7]
+45 to -75
[015;59;10;96;5]

whereas the sample spacing at Irvine is essentially 15 cm throughout. A more appropriate comparison between the loops is illustrated in Fig. 2-3b after the densely sampled portion of the Choteau data was smoothed using a sliding 10 cm averaging window.

Mean directional vectors for zones immediately above and below the declination swing at both sites are plotted in Fig. 2-3c. Magnetic vectors near the base of the Choteau sequence were very scattered (N=6, D=007, I=+55, k=8) but a subset of these produced a much better grouping (N=4, D=012, I=+49, k=36), and it is this latter group which is represented in the figure. Data at both sites appear to be considerably less scattered above the declination swing than below. Mean directions above the swing are not only statistically indistinguishable from one another, but also exhibit the same westerly trend (Figs. 2-2a, b), although lack of outcrop curtails the Irvine data.

It is concluded that the loops recorded at the two localities result from the same geomagnetic feature and are therefore contemporaneous. The geological implications of this conclusion are interesting. The fact that the loop at Irvine is above the tephra, whereas at Choteau it is below, proves that the tephras are not the same, and that Irvine is the older, as suggested by chemical data (Westgate and Evans, 1978). Furthermore, unless one resorts to an inordinately large gap of some 50,000 to 60,000 years

between these two Glacier Peak ash falls, the correlation rules out the possibility that sediments below -240 cm at Choteau represent the much older Bull Lake Glaciation as inferred by Lemke et al. (1975).

The absence of any marked geomagnetic features at Diversion Lake (Fig. 2-2c), and the lack of any coherent sequential behavior at Manyberries limits the potential usefulness of these data. However as the chemical arguments for correlation of the tephra at Diversion Lake, Manyberries, and Choteau are quite strong (Westgate and Evans, 1978), it is expected that there should be some agreement between the magnetic results from each sequence. Compare first the data from Choteau and Diversion Lake. Unfortunately, geological conditions were such that nearly all samples collected at Choteau were from below the tephra whereas at Diversion Lake the majority came from above the tephra (Fig. 2-1). At Choteau, above the secular variation loop discussed earlier, directions are steadily west of north until the uppermost 30 cm or so are reached (Fig. 2-2b), where a rapid easterly swing takes place. Thus it is important to restrict comparison to the narrow zone of sampling overlap at the two localities. This is done in Figure 2-4. Despite the small number of horizons represented the overall agreement is reasonable, and if attention be restricted to the horizons immediately adjacent to the tephra the agreement is excellent.

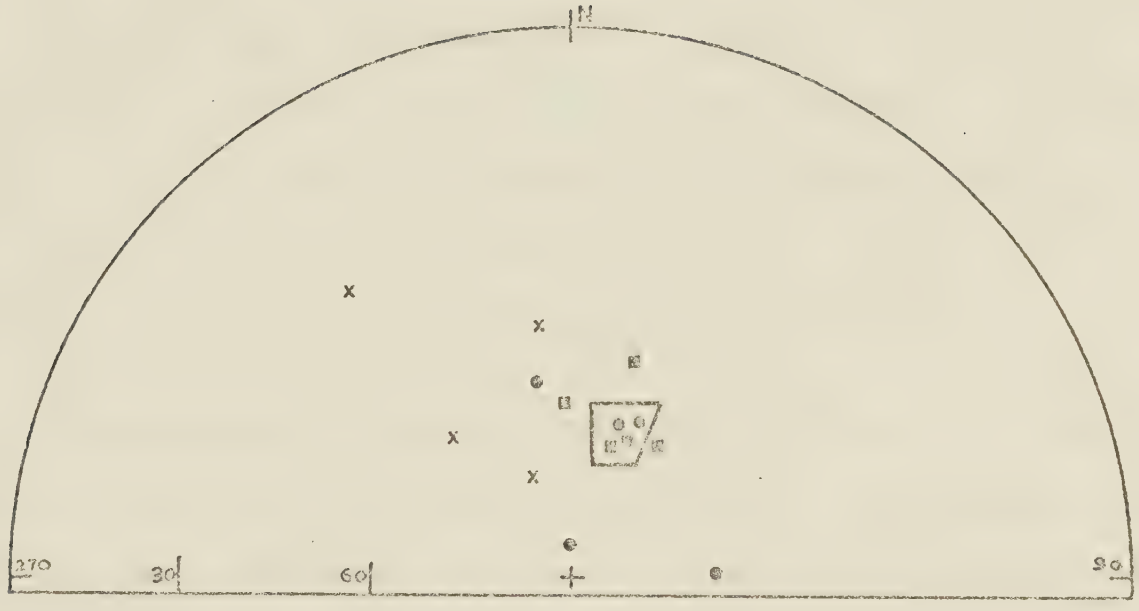

Fig. 2-4: Comparison of paleomagnetic vectors for certain stratigraphic intervals at Choteau (dots), Diversion Lake (squares), and Manyberries (crosses); see text. The box encloses the horizons immediately above and below the tephra at Choteau and Diversion Lake. Stereographic projection.

The Manyberries data is now considered. As at Choteau (below the tephra) declinations are mostly to the west and as the ash is approached an easterly swing is observed (Fig. 2-2d), but directions immediately adjacent to the ash do not agree with the Choteau - Diversion Lake results. In fact westerly decinaticns are reestablished above the tephra. It appears that either the Manyberries data has somehow suffered a systematic bias, or that the tephra at this site is not precisely equivalent in time to those found at Choteau and Diversion Lake, despite the chemical evidence. However, the Manyberries results are very scattered and fail the serial correlation test, therefore it is felt it is premature to draw any firm conclusions from them.

No geomagnetic reversal is present during the time span represented by all four data sets. This is consistent with other recent evidence which casts considerable doubt on the reality of the so-called Gothenburg Event (Thompson, 1976; Sukroo et al., 1978) as a genuine geomagnetic reversal. It is also interesting to speculate on what sort of geomagnetic behavior gave rise to the feature observed at Irvine and Choteau. The fact that is takes the form of a clockwise open loop, is reminiscent of the historical secular variation patterns recorded at many observatories. The loop discussed here however, is much larger. In the light of current knowledge concerning the geomagnetic field and secular variation it seems probable that this disturbance resulted from the rapid enhancement of some non-dipole feature in the

outermost core. The effect of such features can be of limited regional extent (Harrison and Ramirez, 1975) and if one were to drift westward past a point on the earth's surface (see Chapter 3), a clockwise loop would be described, similar to that observed in the paleomagnetic data discussed here.

Finally, it is perhaps worthwhile to note that the above interpretation implies a time scale on the order of a few centuries for the observed geomagnetic loop to have occurred. This immediately puts constraints on the deposition rates at the Irvine and Choteau sections and such information should be of considerable interest to geologists engaged in unravelling the Quaternary history of this region.

CHAPTER 3

Late Quaternary Paleomagnetic Results from Southern British Columbia

3.1 Introduction

Since the beginning of the study of magnetization in recent sediments, interesting periodicities in the behavior of the geomagnetic field have been noticed (Johnson et al., 1948; Nagata et al. 1949; Mackereth 1971; Creer 1974; Creer et al. 1976; Opdyke et al. 1972). It has, in fact, become generally accepted that the study of these periodicities is critical to the understanding of the physical mechanisms underlying geomagnetic secular variation. Variations in declination and inclination have been examined in detail by many authors, but unfortunately in most cases the two directional elements have not been studied simultaneously. Where it has been possible to examine the two dimensional oscillatory behavior of paleomagnetic directions, a strong tendency towards looping has often been observed (Nagata et al. 1968; Denham 1974) as in the case of the well-known London and Paris historical records. The importance of this looping as a source of information concerning the drift of the non-dipole field with respect to the mantle, was first pointed out by Runcorn (1959) and is discussed in detail by Skiles (1970). In essentially all cases of practical interest the motion of the non-dipole focus past any point on the earth's surface will generate an elliptical loop in the geomagnetic vector at that point. In a normally

polarized field, the sense of the loop, looking along the vector, will be clockwise if the motion is westward, and counterclockwise if the motion is eastward.

Previous studies have generally attempted to establish the presence of either looping or periodic variation in declination or inclination simply from visual inspection. However, high noise levels, combined with the presence of more than one frequency in some data sets, renders visual analysis inadequate. In such cases, the application of more sophisticated methods of spectral analysis is desirable. Denham (1975), outlines the particular method of spectral analysis best suited to paleomagnetic data. The method involves mapping the data onto the complex plane about the appropriate norm, and then analysing the resulting complex time series by means of the so-called maximum entropy method(MEM) of spectral analysis. The use of Burg's (1967, 1968) maximum entropy spectral estimator was suggested because of its superiority over other techniques in dealing with short, relatively noisy data sets. The advantage of the complex representation of the data is that all the directional information is contained in a single time series. As a result, one can determine not only the power at a given frequency, but also the tendency towards clockwise or counterclockwise looping at that frequency (for illustrations see chapter 4).

In this chapter, paleomagnetic data from a sedimentary

sequence in southern British Columbia are reported which constitute a time series of ancient geomagnetic directions spanning some 9000 years. Fourier and the above MEM analysis is undertaken, and the implications of the resulting spectra are discussed.

3.2 Geological and Sampling Details

Paleomagnetic specimens were collected from a stream cut escarpment on the edge of Bessette Creek several hundred yards from Riggins Road approximately 10 km east of Lumby, B.C. (50° 17' 55" N, 118° 51' 45" W). The set of paleomagnetic results obtained from these specimens will henceforth be referred to as the Riggins Road data. The portion of the outcrop sampled (Fig. 3-1), consisted of dark, organic rich floodplain sediments containing four radiocarbon dated horizons and two tephras (Westgate and Fulton 1975). Two of the dates were obtained from detrital peat and the other two were from wood. The peat dates are not used in the calculation of deposition rate as both are considerably older than their stratigraphic position, relative to the wood dated horizons, would indicate. The tendency for detritus dates to be "too old" is not uncommon, whereas the wood, having retained its integrity, is less likely to have suffered a long pre-depositional history. Neither of the two tephras present have been independently dated.

The lowermost wood dated horizon is at the base of the

section (31200 ± 900 yrs B.P.). The younger horizon is 4.50 meters above this and is dated at 25300 ± 320 yrs B.P., giving an average deposition rate at 13 ± 2 yrs/cm. It is worth pointing out that the discrepancies between the various dates are not large -- a linear regression using all four dates yields a deposition rate of 10 yrs/cm. Based on extrapolation of the estimated deposition rate, the age of the youngest specimens is 22100 yrs B.P. The oldest specimens were taken at the base of the section (31200 yrs B.P.). With the exception of the two coarse sandy beds approximately 20 cm. in thickness near the top of the section, the sediment is remarkably uniform in character and there is no evidence of any major change in depositional environment during the time span sampled.

Specimens were collected by pressing small plastic boxes into the vertical face of the outcrop. The boxes were oriented using a Brunton compass-clinometer, then removed and tightly capped to prevent dessication. Two independently oriented specimens were collected from each of 37 stratigraphic horizons. The boxes were 2 cm. square in cross section and thus each specimen spans some 2 to 3 decades; the horizon spacing is close to 19 cm which represents about 250 years.

3.3 Measurements and Results

The direction and intensity of the natural remanent

magnetization of each specimen was measured using a Digico balanced fluxgate magnetometer system. Eight pilot specimens were then subjected to stepwise A.F. demagnetization in fields up to 40 mT peak value, and a typical median destructive field was found to be about 20 mT. The remanence directions varied by less than 10 degress until A.F. treatment exceeded 15 mT, beyond which some specimens became unstable. Consequently, 10 mT was chosen as an appropriate field for A.F. cleaning of the remaining specimens. This treatment resulted in systematic movement away from the present field at the sampling locality, suggesting removal of small secondary components of recent origin. Prior to cleaning, intensities ranged from 2×10^{-1} to 5×10^{-3} A/m with an average of 6×10^{-2} A/m. A complete list of results is given in Appendix 3. In figure 3-1 individual cleaned remanence directions, along with the vector mean for each horizon, are illustrated in terms of declination and inclination magnetograms.

The mean angular discrepancy between the pairs of specimens at each horizon is $5.9^{o} \pm 4.4^{o}$ (s.d.). Although this is the only measure of scatter that can be obtained directly from the data, a few more widely recognized and potentially more descriptive statistical parameters may be obtained indirectly, provided one makes some simplifying assumptions about the noise present. The statistical parameter generally used to describe the scatter in paleomagnetic directions is Fisher's "k" (Fisher, 1953), given

Fig. 3-1: Individual specimen directions and horizon means after A.F. cleaning at 10 mT. All significant stratigraphic features in the portion at the section sampled are indicated. The white regions, which make the up most of the stratigraphic diagram, at the left, consist of dark floodplain silt.

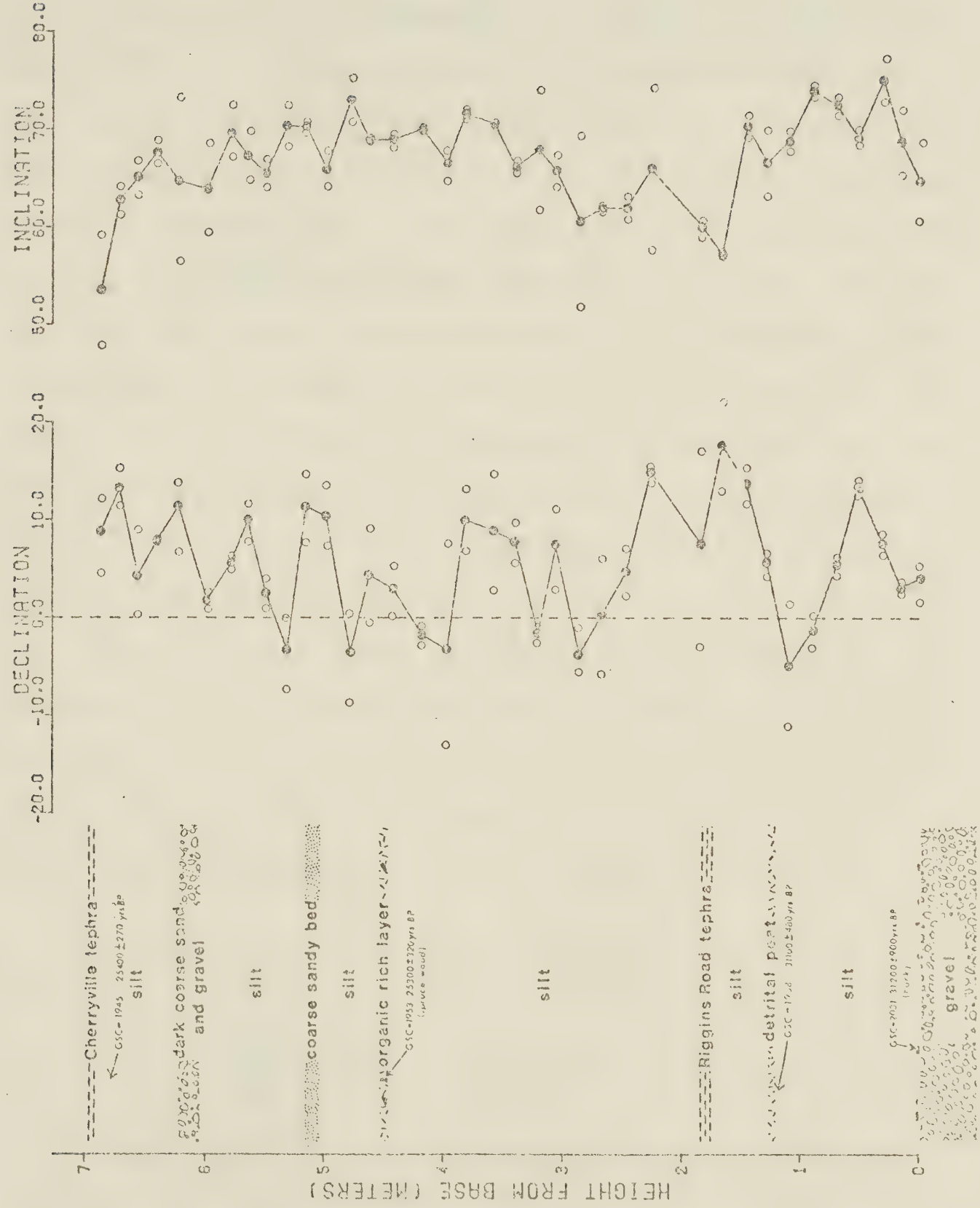
INCLINATION
50.0
60.0
70.0
80.0
DECLINATION
-20.0
-10.0
0.0
10.0
20.0
HEIGHT FROM BASE (METERS)
0
1
2
3
4
5
6
7
Cherryville tephra
GSC-1945 2540±270 yrs BP
silt
dark coarse sand and gravel
silt
coarse sandy bed
silt
organic rich layer
GSC-1933 25300±320 yrs BP
(spruce wood)
silt
Riggins Road tephra
silt
detrital peat
GSC-1708 3110±140 yrs BP
silt
GSC-2021 31200±900 yrs BP
(wood)
gravel

by:

$$k=(N-1)/(N-R)$$

where N=the number of paleomagnetic directions, and R is their vector sum. Unfortunately this estimate is poor when N is small. Obviously one cannot use all 74 remanence directions directly to obtain k since directional variation between horizons is to be expected due to geomagnetic secular variation. An indirect estimate of k can, however, be obtained using information from all 37 horizons if one assumes that the noise distribution at each horizon is the same. This assumption is reasonable when one considers the uniform character of the sediment being sampled throughout the section, as well as the fact that the same orientation procedure was used for all specimens. It is apparent from the above formula that to obtain k, an estimate of R is required. To illustrate how this estimate is obtained, consider the following derivation where x(i), y(i), and z(i) denote the 3 components of the ith remanence vector, V(i), and V(i)•V(j) denotes the dot product of the 2 vectors.

$$R^2 = \left(\sum_i^N x(i)\right)^2 + \left(\sum_i^N y(i)\right)^2 + \left(\sum_i^N z(i)\right)^2$$

$$= \sum_{ij}^{NN} x(i)x(j) + \sum_{ij}^{NN} y(i)y(j) + \sum_{ij}^{NN} z(i)z(j)$$

$$= \sum_{ij}^{NN} \Big(x(i)x(j) + y(i)y(j) + z(i)z(j) \Big)$$

$$= \sum_{ij}^{NN} v(i)\cdot v(j) = N^2 \langle v(i)\cdot v(j) \rangle$$

In the final line of the derivation $\langle V(i) \cdot V(j) \rangle$ denotes the average of all possible dot products for all 74 remanence vectors assuming that all time dependent signals, which would cause real variation between horizons, are absent. As these signals will, in fact, always be present in the data, one cannot determine $\langle V(i) \cdot V(j) \rangle$ exactly, however a reasonable estimate of this quantity can be obtained by calculating the dot product for each pair of vectors at each horizon, and then averaging the results for all 37 horizons. Having obtained this estimate, R is given by;

$$R = N\,\mathrm{sqrt}(\langle V(i) \cdot V(j) \rangle)$$

and therefore the best estimate of k can be obtained using the formula given earlier.

Using the above technique, the best estimate of k for the data discussed here is 244[1]. The quantity analogous to the standard deviation for a normal distribution is given by theta63 = 81/sqrt(k) degrees, and is called the circular standard deviation (Irving,1964)[2]. Given the above value for k, the circular standard deviation for the Riggins Road data is 5.2°, which corresponds to a standard error of the mean of 3.6°. The parameters k and theta63 are, of course, only

---

[1] The standard two-tier analysis (Watson and Irving, 1957) yields k=246.

[2] The circular standard deviation differs from the normal standard deviation in that 63% (as opposed to 68%) of all deviations from the "true value" are smaller than this quantity.

meaningful if the distribution of errors associated with the directional measurements is Fisherian (Fisher, 1953). Another statistical parameter often quoted in paleomagnetic literature, which is not based on any particular probability distribution, is the angular standard deviation given by arcos(R/N) (Wilson, 1959). For the present data, the angular standard deviation and the circular standard deviation are numerically the same to the accuracy quoted. The scatter in the data is most likely due to uncertainty involved in orienting the plastic cubes, combined with minor distortion of the sediment which may occur during sampling.

The Beran and Watson (1967) statistical test for serial correlation (Epp et al. 1971) indicates that the probability of sequential ordering in the sequence of mean directions is greater than 99%, and this implies that at least some of the oscillations apparent in the magnetograms (Fig. 3-1) represent real temporal fluctuations in the paleomagnetic field, the significance of which is discussed below.

3.4 Discussion

The overall mean direction for the entire sequence is D=005.8°, I=+67.6° (N=37, k=329, alpha95=1.4°) which differs significantly from the present geomagnetic vector at the sampling site (D=022.2°, I=+72.6°). However, the observed mean inclination is virtually identical to that of an axial dipole (+67.5°). The mean of the 37 virtual geo-

magnetic poles (VGP's) (Fig. 3-2) lies at 023.1° W, 86.3° N (N=37, K=125, A95=2.1°, arcos(R/N)=7.2°), and is statistically distinct from the earth's rotation axis. This pole, although "right handed", is not "far sided" which is of interest in connection with Wilson's well known offset dipole model (Wilson, 1970, 1971, 1972). However, too much weight cannot be placed on this comparison because the 9000 years represented at Riggins Road may be inadequate to fully average out secular variation and thus obtain a reliable paleomagnetic pole (for a recent review of this problem see McElhinny and Merrill, 1975).

The internal consistency, significant difference from the present local field, and high degree of serial correlation combine to strongly suggest that the Riggins Road data represent a reliable geomagnetic record. It is therefore interesting to note that there is no indication of any large angular shifts which could be correlated with the geomagnetic excursion reported from Lake Mungo, Australia (30,780-28,140 years B.P.; Barbetti and McElhinny 1972), or that from Mono Lake, California (25000-24000 yr B.P.; Denham and Cox, 1971; Liddicoat and Coe, 1975). This either implies that some (or all) of the sedimentation and/or magnetization dates are in error, or that such excursions result from the spatially restricted effects of specific non-dipole sources as envisaged by Harrison and Ramirez (1975) and discussed in Chapter 1. Harrison and Ramirez show that if one models the source of such an excursion as a small magnetic dipole

Fig. 3-2: Virtual geomagnetic poles (VGP's) for all 37 horizons with their mean and its circle of 95% confidence. IGRF indicates the pole calculated from the 1965 International Geomagnetic Reference Field, and PF indicates the pole corresponding to the present field vector at the sampling site. The arrow on the perimeter indicates the longitude of the sampling site. Equal area projection.

located near the core-mantle boundary, then the regional extent of the magnetic disturbance at the earth's surface is surprisingly small (radius of influence is approximately 40° at latitude 30°). Such an explanation is not consistent with the fact that large apparently correlative excursions have been observed in the Gulf of Mexico (Freed and Healy, 1975) and in the Indian Ocean (Opdyke et. al., 1974). One plausible explanation which seems to be consistent with the facts, would be that these excursions are the result of a drifting non-dipole disturbance located along a line of latitude slightly south of the equator. Such a disturbance could quite possibly affect the three areas mentioned and yet have no effect at latitude 50° north (Riggins Road location).

The absence of any unusual geomagnetic behavior, such as excursions, combined with a reasonably accurate knowledge of time spacing between specimens invites the use of some form of spectral analysis. Initially the declinations and inclinations were analysed seperately. Equal spacing between the horizons was assumed, and both the maximum entropy and fast Fourier transform techniques were applied. For both methods, the resulting declination spectrum is dominated by 2 peaks, one at a period of about 2000 years and the other at about 900 years; and the inclination spectrum is dominated by a single peak at approximately 5000 years. The maximum entropy and Fourier results are shown in figures 3-3 and 3-4 respectively. In order to obtain an acceptable

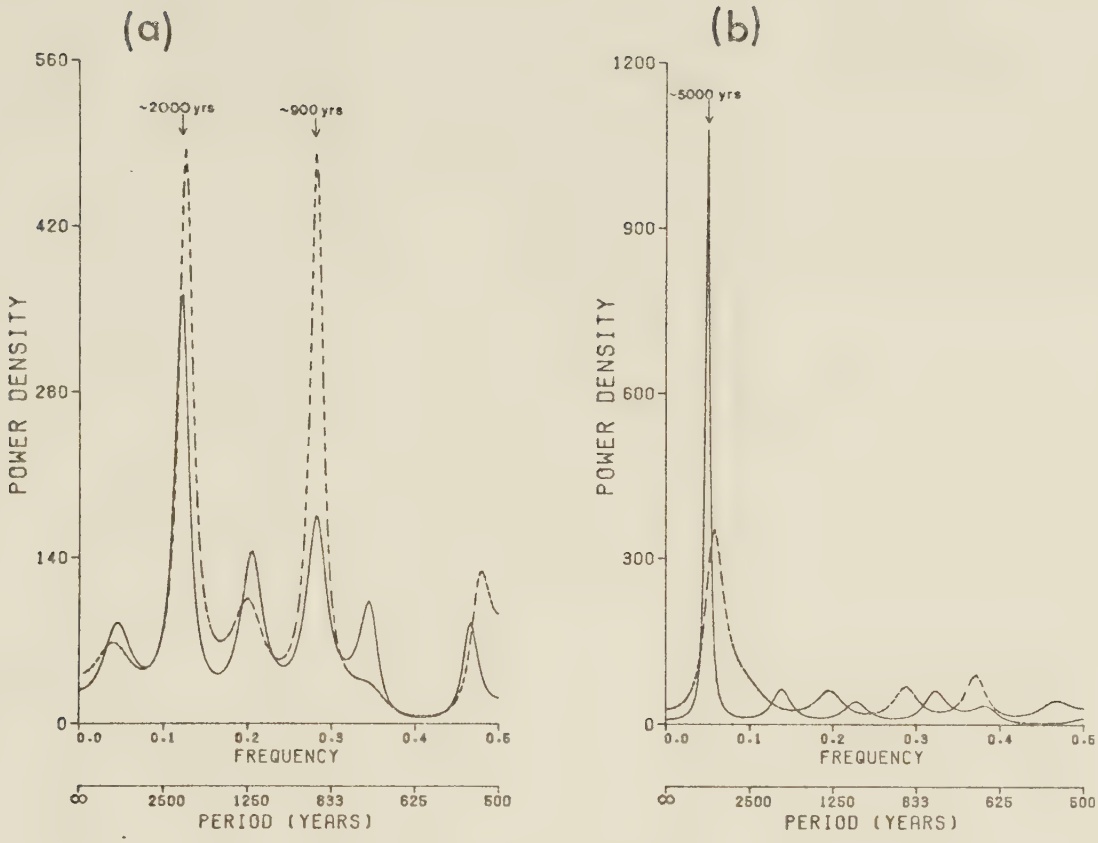

Fig. 3-3: Maximum entropy power spectra. In the plot the dashed line represents the spectrum before interpolation, whereas the solid line is the spectrum after interpolation. The declination spectra are shown in (a), the inclination spectra in (b). The units associated with the ordinate for each plot can be thought of as $(\text{degrees})^2$/unit frequency since the amplitude of oscillation (in degrees) associated with a given peak is equal to the square root of the area under the peak.

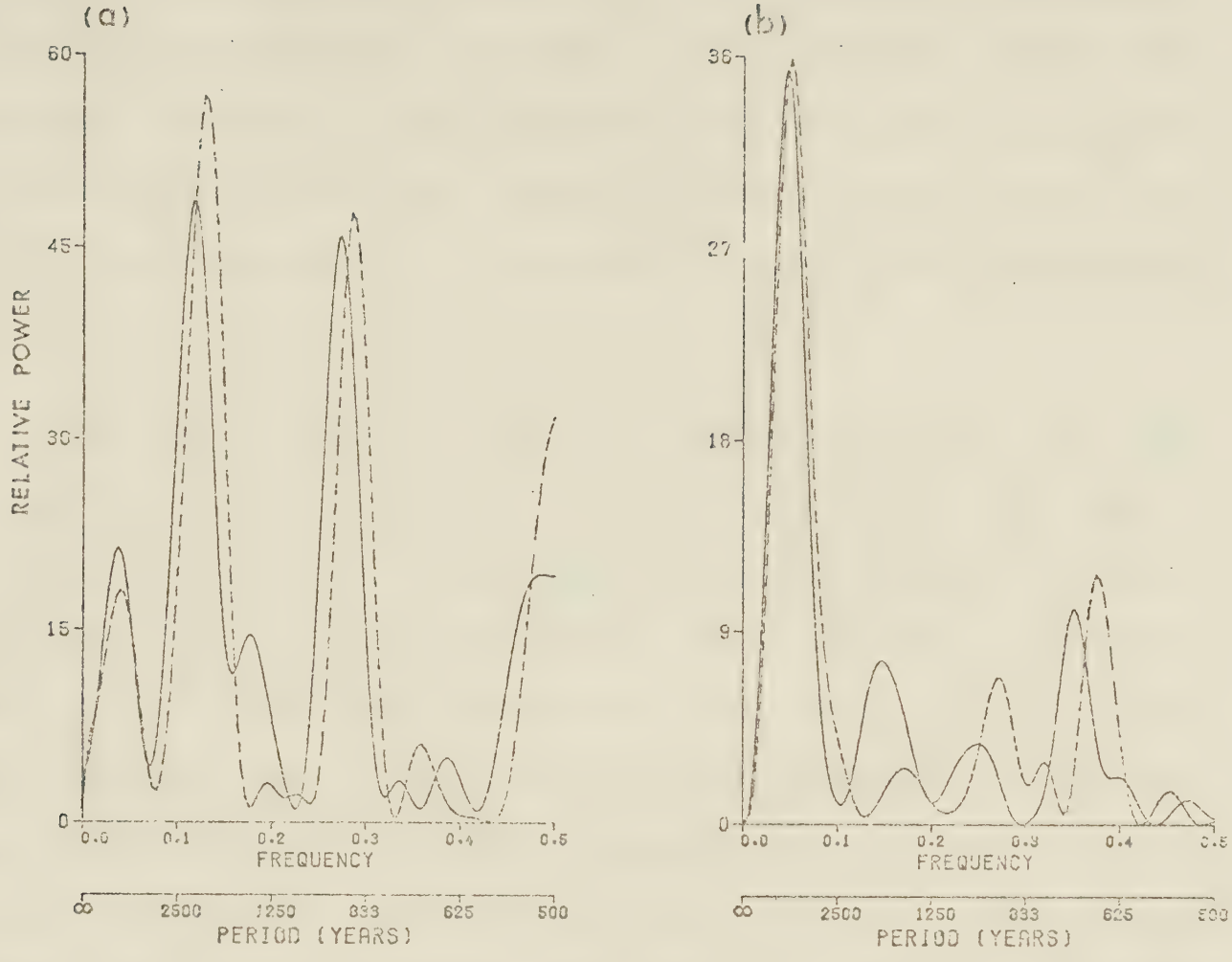

Fig. 3-4: Fourier spectra after application of a Hanning window. The dashed line shows the spectra before interpolation and the solid line shows the spectra after interpolation. The declination spectra are shown in (a), the inclination spectra in (b). The units associated with the ordinate for each plot are proportional to amplitude squared.

spectrum using the Fourier transform technique it was necessary to apply a Hanning window to the data consequently reducing the effective length of an already short time series. Because of this drawback, and since MEM is regarded as a superior technique, especially where short, noisy data sets are concerned, it alone will be used in all subsequent analyses.

The average spacing between horizons is 19.0 cm. (250 yrs), but 2 gaps greater than 25 cm. exist in the record, indicating that the assumption of uniform temporal spacing is only a fair approximation at best. In order to improve the initial spectral estimates, the data was therefore interpolated to a uniform sampling interval of 19.0 cm., prior to spectral analysis (interpolation was performed on each cartesian coordinate using natural cubic spline functions (Greville 1967)). The resulting spectra are also shown in Figs. 3-3 and 3-4. The "900 year" peak in the declination spectrum appears much smaller after interpolation, leaving only one dominant peak at 2000 years. The single peak in the inclination spectrum has been somewhat enhanced by interpolation. The reader should bear in mind at this point that the plots in figures 3-3 and 3-4 are power density plots, hence power is equivalent to the area under a peak rather than its height (Lacoss 1971).

The presence of a spectral peak at 2000 years is intriguing for two reasons. Firstly, oscillations of similar

period have been previously noted by other authors (Creer et al 1976; Yukutake 1962); secondly, 2000 years is close to the time associated with one full cycle of the so-called westward drift of the non-dipole field using the mean drift rate calculated from historical data, (Yukutake 1962; Bullard et al. 1950; Adam et al. 1964). If this 2000 year periodicity is indeed a product of westward drift then it should be associated with clockwise looping of the geomagnetic vector as described above. Obviously some knowledge concerning the presence or absence of looping in the Riggins Road data is of fundamental importance, and the analysis is therefore pursued further.

Denham (1975) has suggested a method of spectral analysis which yields information concerning the degree and sense of looping, in addition to the power, at any given frequency. Briefly the method involves analysing both the declination and inclination information simultaneously as a complex time series. Spectra obtained from complex series are often asymmetrical in that a peak in the "positive frequency" half of the spectrum is not the same size as its counterpart in the "negative frequency" half. The greater the degree of asymmetry at a given frequency, the more circular is the looping at that frequency. In general, looping at arbitrary frequency, f, is elliptical with the length of the semi-major axis given by;

$$| \text{sqrt}(P(f)) + \text{sqrt}(P(-f)) |$$

and that of the semi-minor by;

$$| \text{sqrt}(P(f)) - \text{sqrt}(P(-f)) |$$

where P(f) denotes the power associated with a spectral peak centered on f. The sense of the looping depends on the sign of P(f)-P(-f). A more complete description of the technique can be found in Denham's (1975) paper.

In order to generate the appropriate complex series the sequence of interpolated directions was first mapped onto an angular equidistant polar projection centered on the vectorial mean of the data. Each direction was then converted to a complex number (x+iy) using the transformations $x=r\cos\theta$, $y=r\sin\theta$, where r=distance (in degrees) from the center of the projection θ=azimuth (measured clockwise on the polar projection), and i=sqrt(-1). As the maximum entropy routine used to compute the spectra shown in Fig. 3-6 (Anderson 1974), was originally designed to analyse real data only, some minor modifications were necessary before analysing the complex time series. A FORTRAN listing of the routine used in analysing complex data for this chapter and chapter 4 is given in appendix 5.

Before discussing the spectrum obtained from this analysis, it is important to point out that the ability of the maximum entropy technique to provide a good spectral estimate for a given data set, relies on the choice of the correct number of terms for the prediction error filter (PEF). Analysis of the present data using many different PEF lengths showed that filters ranging from 11 to 20 terms gave

similar spectra. Experimentation with synthetic data containing known frequencies (see Chapter4), but having a similar length and signal/noise ratio as the present data, indicated that the best representation of the true spectrum was obtained using PEF lengths within the above range. A more objective criterion for choosing the correct filter length has recently been put forward by Ulrych and Bishop (1975), who suggest that the optimum filter length is that which minimizes what they refer to as the "final prediction error" (FPE). A plot of FPE versus filter length is given in figure 3-5. The position of the first minimum is somewhat surprising, since a two term filter would be much too short to resolve any appreciable detail. Application of this criterion synthetic data indicated that in order to obtain meaningful spectra the first minimum in the FPE had to be ignored, however the next most pronounced minimum did, in fact, seem to be a reliable indicator of the correct filter length. The second most pronounced minimum in Fig. 3-5 appears at 13, hence this was the PEF length used in the final analysis of the data. The resulting spectrum is given in Fig. 3-6 and is clearly dominated by 3 major peaks. One of these strongly suggests clockwise looping at a period of 1900 years, whereas the other two are indicative of elliptical counterclockwise motion at a period of about 5000 years. In the shorter period region of the spectrum the power present is spread over a wide range of frequencies, and neither clockwise nor counterclockwise motion appears to

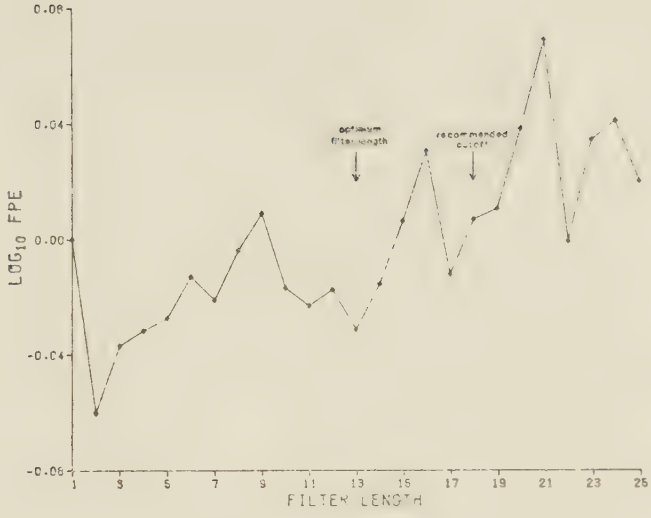

Fig. 3-5: Plot of FPE vs. prediction error filter length. Ulrych and Bishop (1975) have suggested that a cutoff of N/2 in the filter length be imposed when using this criterion (N = number of data points). For the present data N = 37, hence FPE values for filter length greater than 18 are not considered.

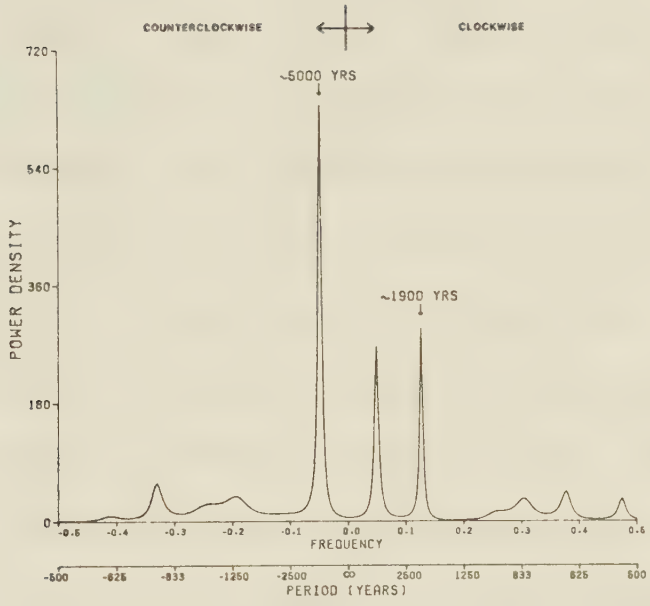

Fig. 3-6: Spectrum of the complex time series. Power (in degrees^2) associated with a given peak is equivalent to the area under the peak. Power in the positive frequency half of the spectrum is indicative of clockwise looping whereas counterclockwise power resides in the negative frequency half of the spectrum.

dominate.

The spectral peaks at 5000 years appear reasonably sharp, but their actual widths cover an extensive range of periods conservatively estimated as extending from 7500 years to 4000 years. In other words, the period of oscillation represented by these peaks is not significantly different from the 6000 year period discovered by Opdyke et al (1971) in sediments from the Aegean Sea. The similarity becomes more convincing when one considers that in both data sets the oscillation is primarily a feature of the inclination. These authors suggest that this periodic variation may be due to a counterclockwise circular motion of the geomagnetic dipole axis. Our data definitely imply counterclockwise motion of the pole, but of about half the 12° amplitude suggested by Opdyke et al. (1971).

The spectral peak at 1900 years covers a range of periods from about 2100 years to about 1800 years. The high degree of clockwise power associated with this peak strongly suggests that it represents the period associated with one full cycle of the westward drift of the non-dipole field. If this interpretation is correct, then it implies that at least some features of the non-dipole field are relatively stable for periods of 2000 years or more, and that the phenomenon of westward drift was in existence some 30,000 years ago.

CHAPTER 4

Spectral Analysis of Synthetic Data

4.1 Introduction

In the previous chapter MEM analysis revealed three spectral peaks in the time sequence from the Riggins Road section (Fig. 3-6). The amplitudes (obtained by numerical integration) and frequencies (f) are 2.7° at f=-0.05, 1.8° at f=0.05, and 1.6° at f=0.14. Considering the rather high noise level (standard error of the mean = 3.6°) one is justified in questioning the ability of the maximum entropy technique to yield reliable information concerning this motion. An experimental MEM study by Chen and Stegen (1974) using a real time sequence of length 24, containing a single sinusoid and random noise, revealed that "acceptable" spectra could not be obtained for noise levels greater than 80%. In view of this rather discouraging result it seems that if one is to place any confidence in the "2000 year" spectral peak discussed earlier, it is essential to enquire whether or not the maximum entropy technique can consistently identify low amplitude motion in the presence of noise similar to that encountered in the Riggins Road data.

In this chapter sequences of synthetic paleomagnetic data are generated containing superimposed looping motions of known frequencies in addition to random noise. Spectral analysis is then performed on each sequence in order to

determine under what conditions "acceptable" spectra can be obtained using the maximum entropy technique.

The synthetic data are generated by a FORTRAN IV program written by the author, called "wrtfreq". Details concerning user input are provided along with a listing in Appendix 4. Basically the program produces an elliptical periodic signal of a given frequency, simply by incrementing the following function:

$$F(t)=A\exp(2\pi ift)+B\exp(-2\pi ift)$$

where t=time, f=frequency, i=sqrt(-1), B=clockwise amplitude, and A=counterclockwise amplitude. The semi-major and semi-minor axes of the resulting ellipse are given by A+B and |A-B| respectively. The sense of the ellipse is clockwise if B>A and counterclockwise if B<A.

In order to approximate the type of noise appropriate to magnetic remanence vectors each vector in the synthetic sequence is rotated from its original direction by a randomly chosen angle θ. Care is taken to ensure that θ is chosen from a noise distribution which is, to a sufficient approximation, Fisherian. Assuming Fisher's "k" is not too small (k>3 is sufficient) then the probability that a given direction will be observed at an angle greater than θ' from the true direction is given by the following formula (Watson and Irving, 1957).

$$\text{Prob}(\theta>\theta')=\exp\{-k(1-\cos(\theta'))\}$$

A subroutine named GGEXP currently exists in the IMSL

library[1] which generates random deviates "x" with the following distribution:

$$\text{Prob}(x>x')=\exp(-x'/m)$$

where m is a constant specified by the user. Using this routine the appropriate angular deviations are generated by setting xm equal to 1/k and choosing θ from the formula $\theta=\cos^{-1}(1-x)$. After rotating a given vector away from its original direction by an amount θ it is then rotated azimuthally by another randomly chosen angle ϕ. In order that the noise distribution be azimuthally symmetric ϕ is chosen from a uniform noise distribution in the interval $(0,2\pi)$, using the IMSL routine GGUB.

Long sequences (10000 points) of pure noise (no periodic signal present) have been generated using the procedure decribed above and submitted to the "chi squared" test for a Fisher distribution (Watson and Irving, 1957). The results indicate that the noise is indeed Fisherian at a confidence level greater than 97%. It is important to mention however, that short sequences (40 points) of noise produced by this routine sometimes deviate significantly from a Fisherian distribution. Fortunately the IMSL noise generating routines all require as input a "seed" integer (range 1 to 2147483647) which uniquely determines the "noise" output. In other words the subroutines will always

---

[1] International Mathematical and Statistical Library

produce the same string of "random" numbers if the same seed integer is provided each time one of the routines is called. The above problem can therefore be effectively eliminated by using only "pre-tested" seed integers; that is, seed integers which have previously resulted in the production of Fisherian noise. After generating and testing approximately 50 noise sequences of length 40 using randomly selected seed integers, 10 of these integers were found to produce noise which is Fisherian at a confidence level of greater than 75%. These 10 integers have been retained, and utilized in the production of all synthetic data sequences studied in this chapter (these integers are listed immediately following the listing of wrtfreq in Appendix 4).

4.2 MEM Spectra for Varying Ellipticities

To illustrate the type of periodic motion implied by various kinds of spectra, several relatively clean (low noise level) sequences of data containing looping frequencies of varying ellipticity, have been generated and analysed using the complex MEM technique. This exercise also serves as a useful test against possible programming errors in the MEM routine, as the true spectra of such clean data are easily predictable.

The resulting power density plots are presented along with polar projections of the 4 synthetic data sets in figure 4-1. The complete absence of counterclockwise power

Fig. 4-1: MEM spectra for signals of varying ellipticity

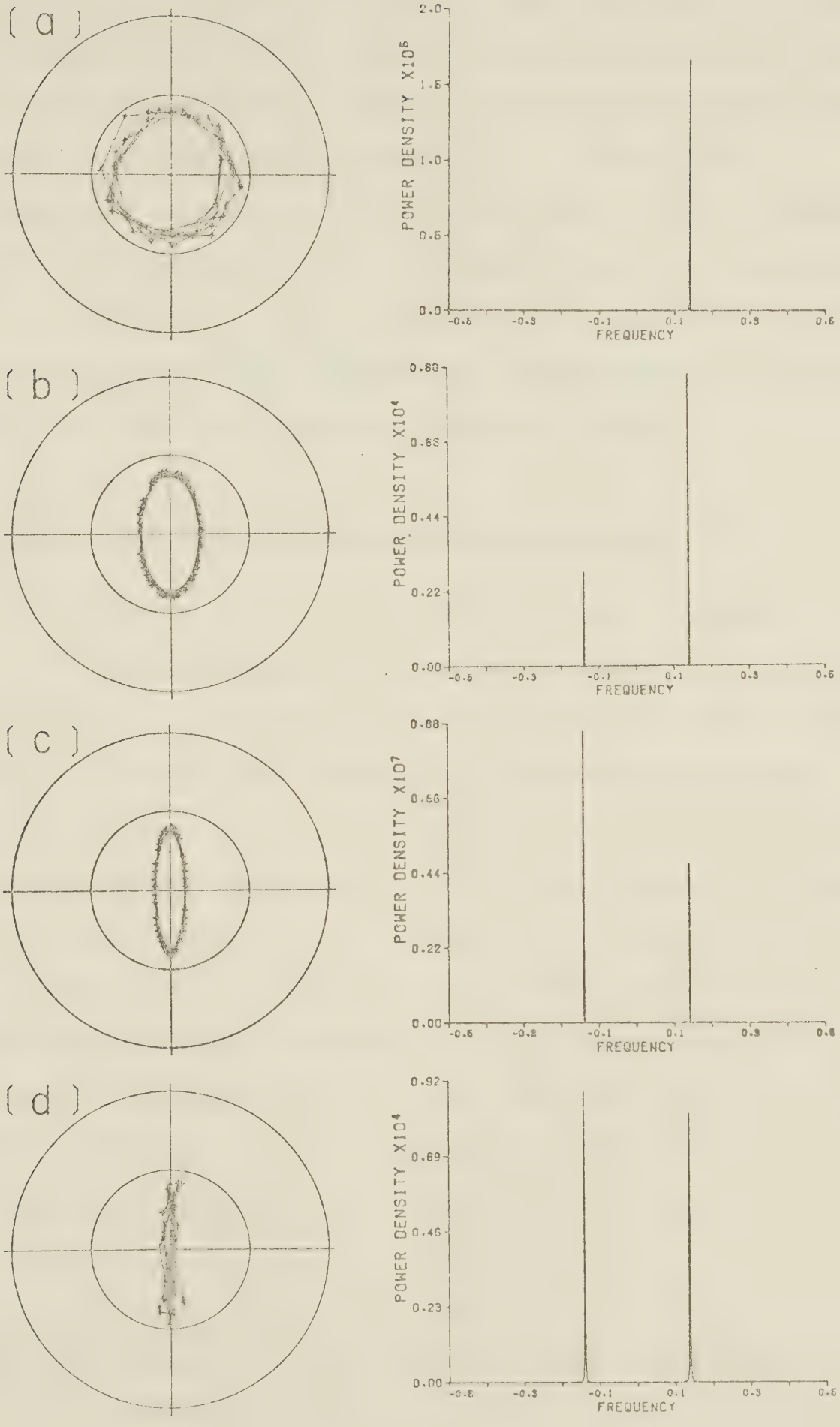
(a)
2.0
1.5
1.0
0.5
0.0
POWER DENSITY X10⁵
-0.5
-0.3
-0.1
0.1
0.3
0.5
FREQUENCY
(b)
0.88
0.66
0.44
0.22
0.00
POWER DENSITY X10⁴
-0.5
-0.3
-0.1
0.1
0.3
0.5
FREQUENCY
(c)
0.88
0.66
0.44
0.22
0.00
POWER DENSITY X10⁷
-0.5
-0.3
-0.1
0.1
0.3
0.5
FREQUENCY
(d)
0.92
0.69
0.46
0.23
0.00
POWER DENSITY X10⁴
-0.5
-0.3
-0.1
0.1
0.3
0.5
FREQUENCY

in the spectrum associated with circular clockwise looping is demonstrated in figure 4-1a. The spectrum of a 2:1 clockwise ellipse is shown in figure 4-1b where clockwise power outweighs counterclockwise power by a factor of 9. The spectrum in figure 4-1c represents that of a 3:1 counterclockwise ellipse (ratio of counterclockwise to clockwise power is 25 to 9). Finally, figure 4-1d shows the spectrum resulting from a simple linear oscillation where, of course, counterclockwise and clockwise power are equal.

4.3 MEM Spectra for Varying Signal to Noise Ratios

As the noise in a paleomagnetic time sequence will often be large compared to the relevant signals present, it is important to have some indication of the limits under which the complex MEM technique can perform successfully. In this section an attempt is made to determine the smallest signal detectable in a paleomagnetic time sequence of fixed length (n=40)[1] containing a noise level typical of real data. The synthetic data sets originally generated for this purpose each contain 3 superimposed circular looping motions of different frequencies but of the same amplitude (angular radius). Two of the signals are of clockwise sense at frequencies of 0.05 and 0.31 and the third is counterclock-

---

[1] This is similar to the length of the Riggins Road data (n=37).

wise at a frequency of 0.14. The presence of 3 frequencies as opposed to one in the synthetic data provides a check as to whether or not the "detectability" of a signal is a function of its frequency, as well as its amplitude. The angular standard deviation of the noise added to the data is fixed at (5/sqrt(2))°. This noise level is considered appropriate since 5° is a typical standard error for a single paleomagnetic specimen, and 2 specimens per horizon is regarded as an optimum sampling scheme (Watson and Irving, 1957). This noise level is also very similar to that found in the Riggins Road sequence, where 2 specimens per horizon were collected.

Ten distinct synthetic data sets were generated containing signals of amplitude 1.0° and noise of the level indicated above, using ten pre-tested seed integers. The same ten seed integers were then used in the production of ten more data sets containing signals of amplitude 1.5°. This procedure was continued until a total of 50 data sets were produced with signal amplitudes of 1.0°, 1.5°, 2.0°, 2.5°, and 3.0°. The power density spectra of the first 5 data sets at amplitudes 1.0°, 2.0°, and 3.0° are shown in figure 4-2. One can see that all of the spectra shown at amplitudes 2° and 3° are reasonably good whereas 4 out of 5 of the spectra at amplitude 1° are definitely unacceptable. It should be mentioned at this point, that in obtaining all of the spectra discussed in this section, and henceforth in this chapter, the FPE criterion was utilized in choosing the

Fig. 4-2: Power density spectra for synthetic data containing signals of varying amplitude and a constant noise level (see text). NR"n" denotes the particular noise realization at a given amplitude.

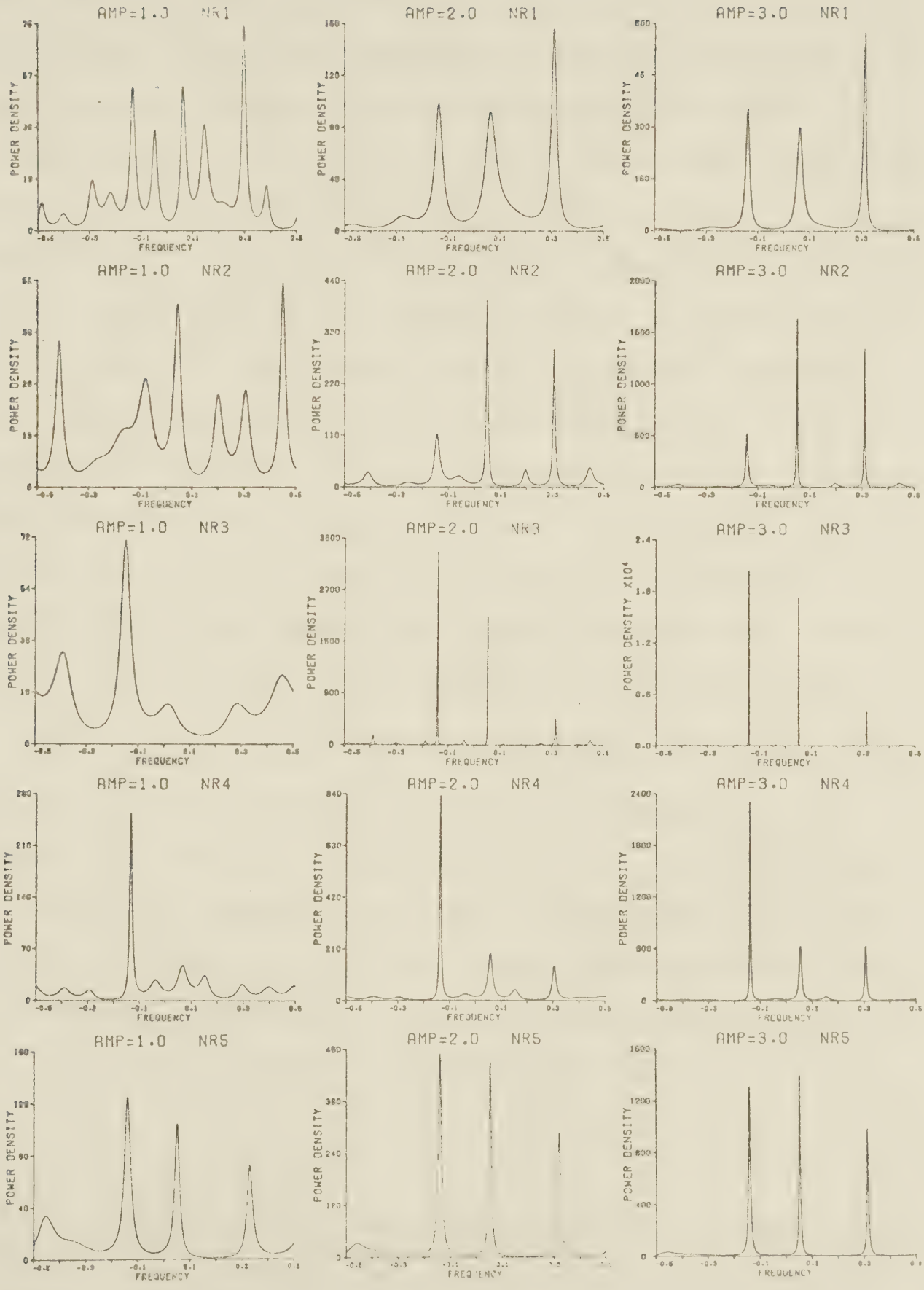
AMP=1.0 NR1
AMP=2.0 NR1
AMP=3.0 NR1
AMP=1.0 NR2
AMP=2.0 NR2
AMP=3.0 NR2
AMP=1.0 NR3
AMP=2.0 NR3
AMP=3.0 NR3
AMP=1.0 NR4
AMP=2.0 NR4
AMP=3.0 NR4
AMP=1.0 NR5
AMP=2.0 NR5
AMP=3.0 NR5
POWER DENSITY
POWER DENSITY X10⁴
FREQUENCY

optimum prediction error filter length. It is important to note however, that in using this criterion on a large number of synthetic data sets similar to those described above, it was found that occasionally an FPE minimum would occur at a filter length which was far too low to produce a spectrum with acceptable resolution. An acceptable spectrum could generally be obtained in such a case by using the filter length where the next FPE minimum occured. Since PEF lengths of less than 6 were found never to produce spectra of sufficient resolution when analysing noisy data, an arbitrary lower limit of 6 was imposed each time the FPE criterion was used. An upper cutoff of n/2 (n=number of data points) was also imposed as suggested by Ulrych and Bishop (1975). The filter lengths (FL) used in calculating spectra for the above synthetic data sets are given in Table 4-1.

An obvious method of judging the "acceptability" of synthetic spectra, such as those in figure 4-2, is to compare the heights of the "true" spectral peaks with those of the ever present "spurious" peaks[1]. The power density ratio of the smallest true peak to the largest spurious peak is therefore chosen as a numerical indicator of the quality of a particular spectrum. Such a ratio will be referred to

---

[1] If a prediction error filter length of M is used when employing the MEM technique, M-1 peaks will be present in the resulting spectrum, regardless of the true spectral content of the data.

here as an RTS (ratio of true to spurious) value. RTS values for all 50 synthetic data sets are represented graphically in figure 4-3). These values are also listed in Table 4-1. When examining this data one can generally regard spectra with an RTS value of less than 2 to be unacceptable since an observer who is not aware of the number of "true" peaks present (as is the case with real data) will find such spectra very difficult to interpret. This being the case, figure 4-3 indicates that attempting to identify signals of amplitude less than 2° using the complex MEM technique in noise of the level indicated above, would not be advisable. One should bear in mind however, that any conclusions concerning the limitations of the complex MEM technique drawn on the basis of the above results, may be overly pessimistic due to the requirement that 3 signals be identified at a given amplitude rather than one.

As mentioned earlier, the presence of 3 signals in the synthetic data provides a rough check as to whether of not the rate of signal deterioration with decreasing amplitude is influenced by frequency. A slight trend towards improved signal recovery at lower frequencies is, in fact, apparent but the effect of this trend on the observed power density is small compared with the effects of varying filter length and signal to noise ratio.

In an attempt to assess the performance of the complex MEM technique under less adverse, and perhaps more realistic

Fig. 4-3: Semi-log plot of RTS versus amplitude for synthetic data containing 3 superimposed periodic signals.

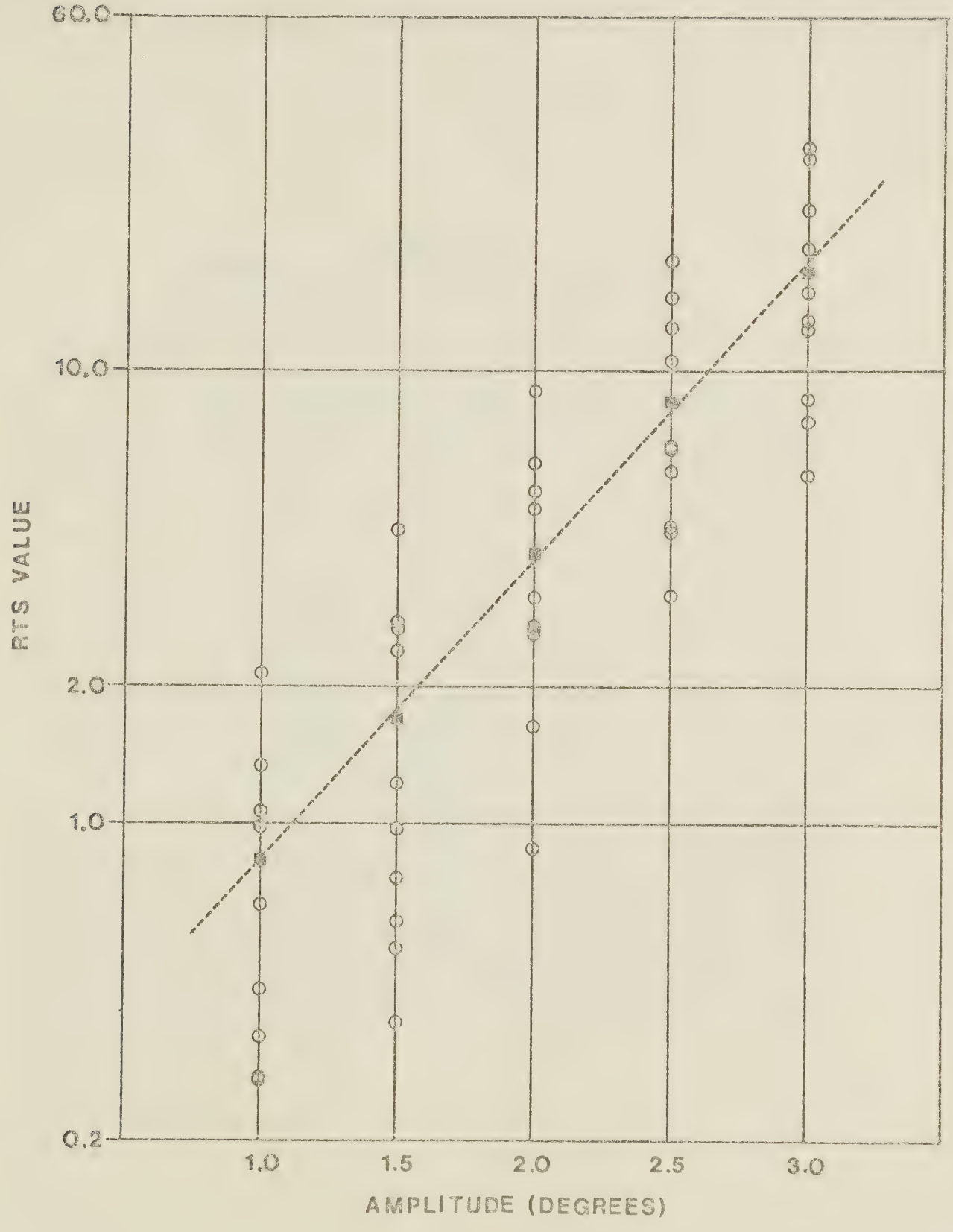
60.0
10.0
2.0
1.0
0.2
RTS VALUE
1.0
1.5
2.0
2.5
3.0
AMPLITUDE (DEGREES)

Table 4-1
Summary of Results for Synthetic
Data Containing 3 Periodic Signals

AMPLITUDE	1.0°		1.5°		2.0°		2.5°		3.0°	
	RTS	FL	RTS	FL	RTS	FL	RTS	FL	RTS	FL
NR1	1.35	12	2.78	12	5.39	07	10.5	07	18.6	07
NR2	.277	09	.533	09	2.66	10	6.02	10	12.3	10
NR3	.434	06	.622	13	2.70	18	14.4	19	29.6	19
NR4	.664	10	1.21	07	3.14	10	6.66	10	13.0	10
NR5	2.16	06	4.42	06	9.00	06	17.3	06	31.2	06
NR6	.984	08	2.39	08	4.98	08	4.51	11	7.84	11
NR7	.339	16	.759	16	1.63	16	5.23	16	5.91	16
NR8	.274	18	.968	18	2.75	18	6.78	18	15.0	18
NR9	--	08	.363	08	.874	08	4.50	11	8.70	11
NR10	1.05	06	2.74	10	6.23	10	12.5	10	22.9	10
AVERAGE	.837	10	1.68	11	3.94	11	8.84	12	16.5	12

conditions, another series of synthetic data sets were generated identical to the first, except this time containing only one periodic signal, at a frequency of 0.14. The results are summarized in the same manner as above; first graphically in figure 4-4, and then in table form (Table 4-2). Examination of figure 4-4 reveals that in typical paleomagnetic noise of the level described earlier, one can be reasonably certain of recovering a single periodic signal with an amplitude as low as 1.5°. In other words, the lowest allowable signal to noise ratio that can be present if one wishes to obtain a reasonable spectrum, given a data sequence of about 40 points, is approximately 0.42.

These results appear to conflict with those of Chen and Stegen (1974) who were able to obtain "acceptable" spectra in only 6 out of 10 runs with a signal to noise ratio of 2.5. The disagreement is more apparent than real however, for 2 reasons. The first is that the time sequences used by Chen and Stegen were only 24 points long as opposed to the 40 point sequences used here. The second, and probably more important reason however, is that the definition of "acceptable spectra" used by Chen and Stegen, although not clearly defined in their paper, appears to be considerably

Fig. 4-4: Semi-log plot of RTS versus amplitude for synthetic data containing only one periodic signal.

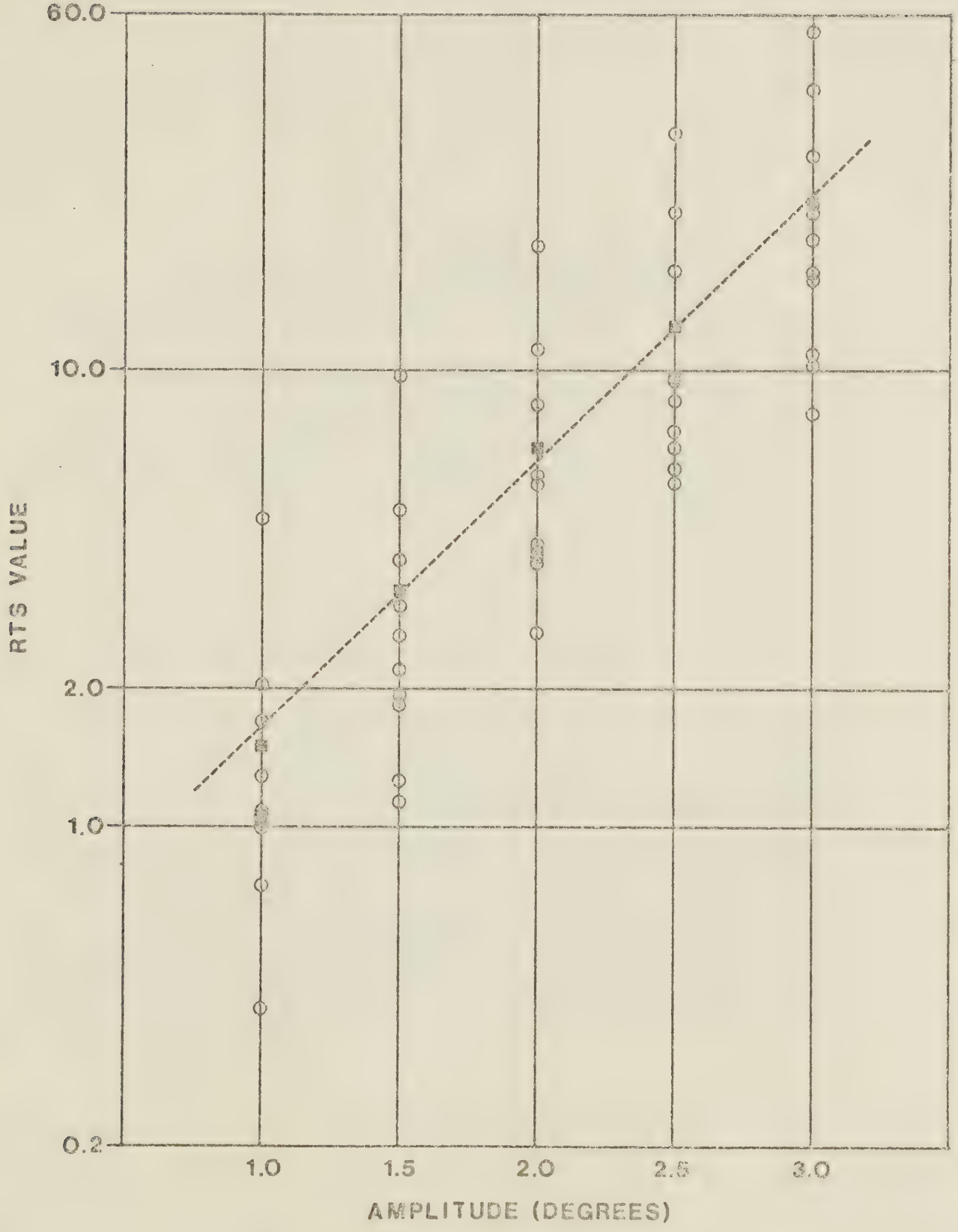
60.0
10.0
2.0
1.0
0.2
RTS VALUE
1.0
1.5
2.0
2.5
3.0
AMPLITUDE (DEGREES)

Table 4-2
Summary of Results for Synthetic
Data Containing One Periodic Signal.

AMPLITUDE	1.0°		1.5°		2.0°		2.5°		3.0°	
	RTS	FL	RTS	FL	RTS	FL	RTS	FL	RTS	FL
NR1	1.06	08	1.94	08	3.87	08	7.29	08	22.4	06
NR2	.749	07	1.85	08	4.24	08	8.61	08	15.9	08
NR3	1.69	09	3.91	09	8.37	09	16.4	09	29.7	09
NR4	.992	16	2.62	16	5.96	16	6.12	07	10.3	07
NR5	4.72	09	9.80	09	18.7	09	33.1	09	55.0	09
NR6	2.07	12	5.01	12	11.0	12	22.1	12	40.6	12
NR7	.402	08	1.12	08	2.69	08	5.69	08	10.8	08
NR8	1.07	07	1.37	10	4.00	10	9.47	10	19.4	10
NR9	1.30	09	2.21	09	3.91	09	6.82	09	8.17	15
NR10	1.07	09	3.04	09	5.68	09	9.87	09	16.2	09
AVERAGE	1.51	09	3.29	10	6.82	10	12.5	09	22.8	09

more conservative than that used in this chapter[1].

The best estimate for the angular standard deviation associated with the noise in the Riggins Road data was found to be 3.6°. Taking the amplitude of the "2000 year" oscillation discussed in Chapter 3 to be 1.6° gives a signal to noise ratio of 0.44. The analysis of synthetic data described above therefore implies that the "2000 year" oscillation observed at Riggins Road, is real but lies very near the lower limit of the complex MEM technique.

4.4 The Effect of Noise on Apparent Ellipticity

One important conclusion drawn in Chapter 3 is that the power density spectrum of the Riggins Road data is indicative of counterclockwise elliptical motion of the geomagnetic vector at a period of approximately 5000 years. The assertion that the motion is counterclockwise rests on the fact that the counterclockwise amplitude associated with the signal is larger than the clockwise amplitude by approximately 0.8°. Considering the noise level present in the Riggins Road data one is justified in challenging the significance of this difference.

To obtain some indication of the fluctuations in

---

[1] Spectra with RTS values as low as 2 have been generally regarded as "acceptable".

apparent amplitude that one might expect in the spectra of noisy data such as that encountered at Riggins Road, 10 synthetic data sequences were generated, each containing a single linear oscillation in addition to noise of the same level used in the previous section. In each sequence the total amplitude of the oscillation was 5° (i.e. clockwise amplitude=2.5° and counterclockwise amplitude=2.5°) and the frequency was 0.05. Spectra were obtained for each of the data sets and numerical integration was performed to obtain the apparent clockwise and counterclockwise amplitudes associated with the signal present. The results are presented in Table 4-3.

Considerable fluctuation is evident in the amplitudes shown, the average standard deviation being approximately 15% of the true amplitude. Also evident is a slight tendency for the amplitudes to be too large. This trend is most likely a consequence of setting the integration limits too far apart when calculating the area under the spectral peaks (the limits used were .03 and .08 for both positive and negative frequencies). The RMS deviation of the differences (clockwise amp. minus counterclockwise amp.) from their true mean of zero is 0.37°, and the maximum value is 0.57°. As the difference value associated with the "5000 year" spectral peaks in the Riggins Road data is 0.8°, it is highly unlikely that the apparent counterclockwise sense associated with this periodic motion, is purely a result of noise in the data.

Table 4-3
Summary of Results for Synthetic Data Containing a Single Linear Oscillation of Amplitude 5.0°

NOISE REALIZATION	COUNTER-CLOCKWISE AMPLITUDE	CLOCKWISE AMPLITUDE	DIFFERENCE	FILTER LENGTH
NR1	2.64°	2.10°	-0.54°	07
NR2	2.77°	2.32°	-0.45°	19
NR3	2.68°	2.52°	-0.16°	20
NR4	2.96°	2.52°	-0.44°	15
NR5	2.80°	3.01°	0.21°	11
NR6	3.16°	2.69°	-0.47°	11
NR7	2.44°	3.01°	0.57°	20
NR8	2.52°	2.46°	-0.06°	19
NR9	2.72°	2.75°	0.03°	10
NR10	3.05°	3.33°	0.28°	14
AVERAGE	2.77°	2.67°	-0.10°	15
RMS ERROR	0.35°	0.39°	0.37°	

4.5 Simulation of the Riggins Road Data

As stated in section 4.3, given the noise level present in the Riggins Road time sequence, along with its limited length of 37 points, a signal with amplitude equal to that of the so called "2000 year" oscillation found in the Riggins Road data, is probably the smallest signal that one could hope to identify with reasonable certainty using the complex MEM technique. One must keep in mind that section 4.3 is designed to explore the limits under which the MEM technique can perform successfully, rather than to accurately simulate any real data set. For this reason there are several differences between the synthetic time sequences used in that section and the Riggins Road sequence. In view of the rather borderline nature of the "2000 year" spectral peak, these differences may be important enough to alter any interpretation as to the significance of that peak, based on the results of section 4.3. In this section an attempt is made to produce synthetic data sets which simulate the Riggins Road data as closely as possible.

Ten synthetic data sets of length 37 were generated containing signals similar to those thought to exist in the Riggins Road sequence (amp. 2.67° at freq.=-0.05, amp. 1.84° at f=0.05, and amp. 1.63° at f=0.14). The angular standard deviation of the noise added to the data was set at 3.6°. The synthetic sequences were also produced with the same unequal spacing in time (elevation) as the Riggins Road

data, and interpolation was performed prior to spectral analysis as in the case of the real data.

Spectral density plots for the ten data sequences are shown in figure 4-5. Numerical integration was carried out to determine the amplitudes associated with each of the 3 peaks, in each spectrum. These results, along with the RTS values and PEF lengths for each spectrum, are presented in table 4-4. If one judged the spectra purely on the basis of RTS value, then 8 out of 10 spectra could qualify as acceptable (RTS > 2). Most readers however, would likely agree on the basis of visual examination of the power density plots, that data sets 5 through 8 give unacceptable spectra. From these results it is concluded that, given the signal to noise conditions present in the Riggins Road data, the chances of extracting, in recognizable form, the signals discussed in Chapter 3 through spectral analysis is between 60% and 80%, assuming the signals are in fact real.

One method of assessing whether the spectral peaks found in the Riggins Road data are real or spurious is to compare the spectral densities of the largest spurious peaks found in the synthetic data sets, with those of the "true" spectral peaks found in the real data. To carry out this exercise properly, it was necessary to recalculate the power density spectra for each data set using a PEF length equal to that used in analysing the Riggins Road data. This is because the power density of any spectral peak obtained

Fig. 4-5: Power density spectra for simulated Riggins Road data

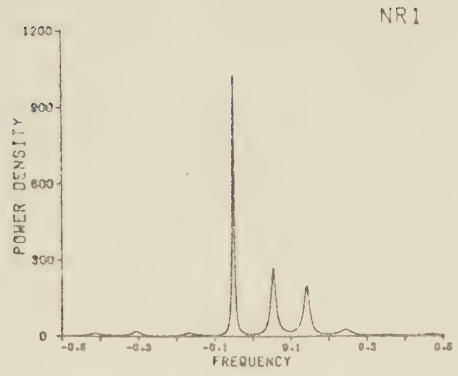
NR1
POWER DENSITY
FREQUENCY

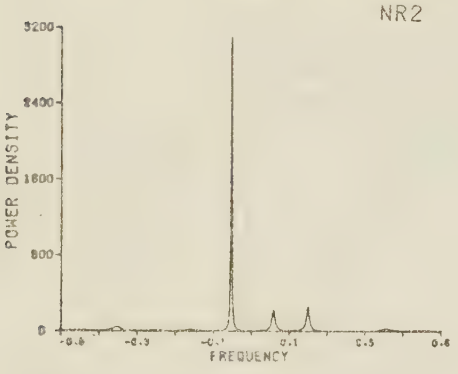
NR2
POWER DENSITY
FREQUENCY

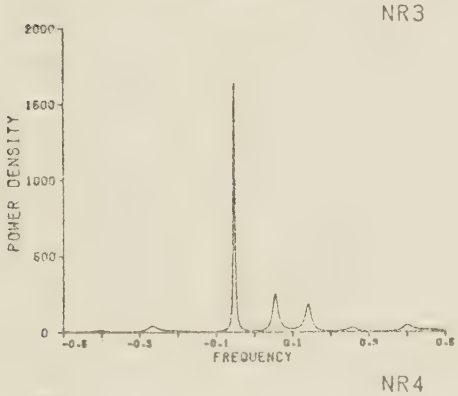
NR3
POWER DENSITY
FREQUENCY

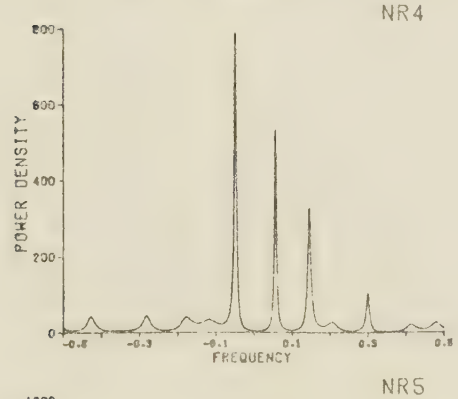
NR4
POWER DENSITY
FREQUENCY

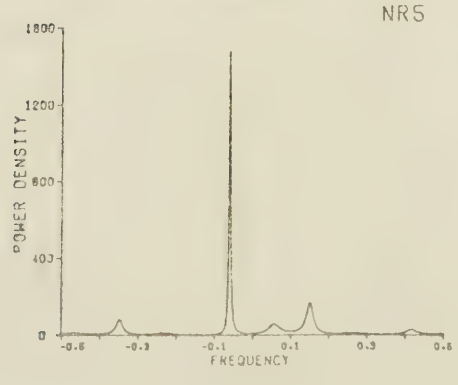
NR5
POWER DENSITY
FREQUENCY

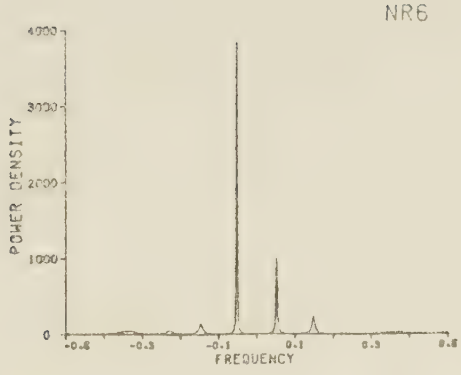
NR6
POWER DENSITY
FREQUENCY

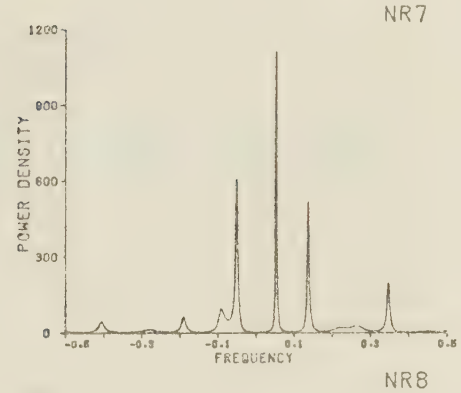
NR7
POWER DENSITY
FREQUENCY

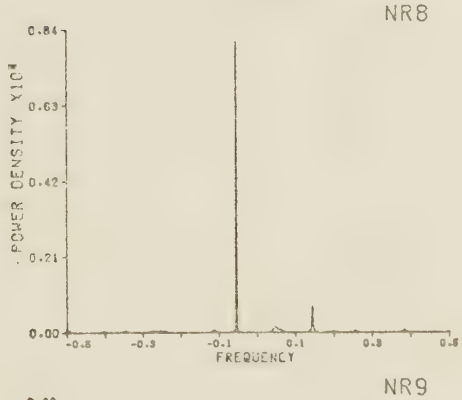
NR8
POWER DENSITY X10⁴
FREQUENCY

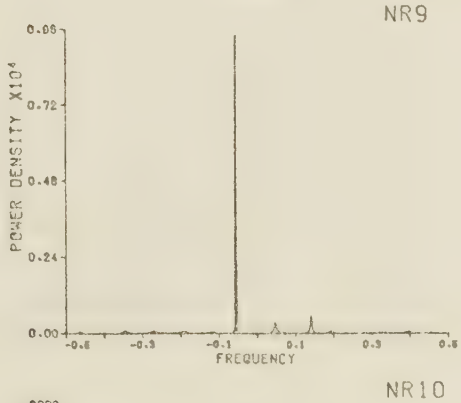
NR9
POWER DENSITY X10⁴
FREQUENCY

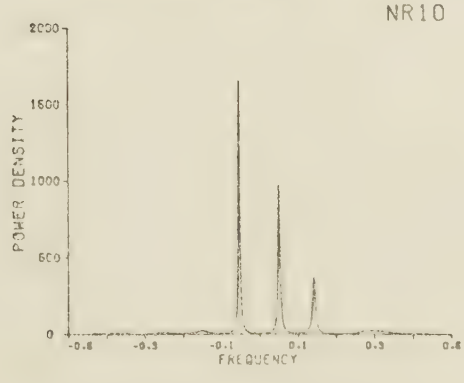
NR10
POWER DENSITY
FREQUENCY

Table 4-4
Summary of Results for Simulated Riggins Road Data
(unit of amplitude is degrees)

NOISE REALIZATION	RTS	AMPLITUDE (f=-0.05)	AMPLITUDE (f=+0.05)	AMPLITUDE (f=1.4)	FILTER LENGTH
NR1	7.45	2.87	2.36	2.14	10
NR2	4.71	3.54	1.85	1.87	11
NR3	4.07	3.34	2.38	2.09	10
NR4	3.17	2.82	2.16	2.11	13
NR5	0.73	3.17	1.53	2.08	09
NR6	1.59	3.36	2.34	1.72	12
NR7	2.64	2.68	2.26	2.07	14
NR8	2.04	2.75	1.84	1.83	17
NR9	3.75	3.13	2.02	2.05	17
NR10	15.65	3.17	2.83	2.09	11
AVERAGE	4.58	3.08	2.16	2.00	12.4
RMS ERROR		0.30	0.36	0.14	

Fig. 4-6: Histogram of power densities of spurious peaks. The height of the smallest 'real' peak claimed in the Riggins Road data (269) is indicated. The best-fit log-normal curve yields a value of chi-squared of 4.75 (see text).

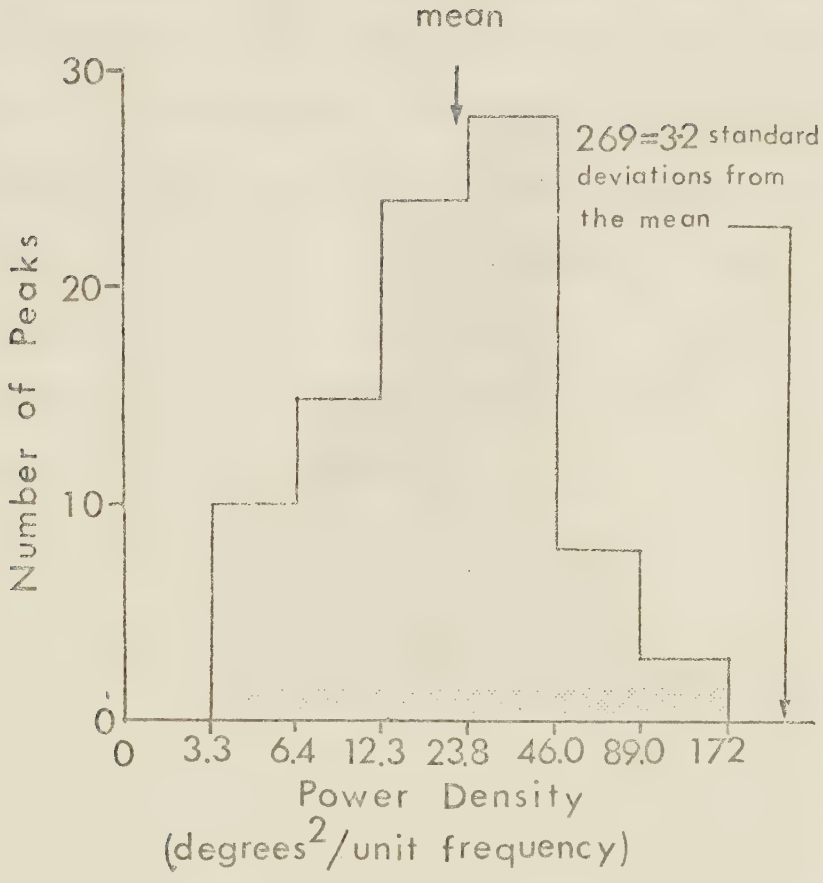
mean
269=3.2 standard deviations from the mean
30
20
10
0
Number of Peaks
0
3.3
6.4
12.3
23.8
46.0
89.0
172
Power Density
(degrees^2/unit frequency)

using MEM varies strongly as a function of filter length. Upon examination of the spectra for all 10 synthetic data sets calculated using a filter length of 13, only 3 spurious peaks (out of a total 120) were found to have power densities greater than 100 deg^2 per unit frequency, the largest of these having a height of 171 deg^2 per unit frequency. The distribution of power densities for the spurious peaks is illustrated in figure 4-6. The shortest of the 3 peaks found in the Riggins Road sequence (the clock-wise peak at period of 5000 yrs.) has a power density of 269 deg^2 per unit frequency. If one assumes that the distribution in figure 4-6 is log-normal[1], then these results indicate that the probability of such a peak occurring by accident is less than 1%.

---

[1] The power density values pass the chi-squared test for such a distribution (see appendix 6).

CHAPTER 5

Summary and Conclusions

Paleomagnetic results from 5 stratigraphic sequences have been reported. Four of these are discussed in Chapter2 and concern the time interval 12000 to 13000 years B.P. The motivation behind this work was two-fold; first to seek evidence corroborating the existence of the so-called Gothenburg event (Morner et al., 1970), and second to explore the feasibility of using paleomagnetic signatures for stratigraphic correlation. No evidence for a geomagnetic reversal was found but this was not totally unexpected as more recent evidence (Thompson, 1976; Sukroo et al., 1978) indicates that the Gothenburg event, if it existed at all, was more likely a non-dipole excursion of limited regional extent rather than a global polarity reversal. An enhanced clockwise loop in remanence direction was however observed, and it is felt that this is indicative of some unusually intense non-dipole feature drifting westward past the sampling locality. It is tempting to equate this disturbance with that which initiated the Gothenburg "event" in Sweden, but until further evidence is presented supporting the existence of the Swedish excursion, such a conclusion could only be regarded as speculation. The existence of the loop was established at two localities some 250 km apart. This correlation was of considerable significance geologically in that it established a stratigraphic relationship between two volcanic tephras which had previously been unknown (Westgate

and Evans, 1978).

In Chapter 3 a single 9000 year paleomagnetic sequence is discussed in detail. No geomagnetic excursions are found, although two have been documented for the time span represented by the data (22000 to 31000 yrs B.P.). The absence of the Lake Mungo excursion at the sampling locality is regarded as evidence supporting the spacially restricted nature of such phenomena (Harrison and Ramirez, 1975). The absence of the Mono Lake excursion is somewhat more puzzling as it was discovered only about 1200 km from Riggins Road. It therefore appears that either a large depositional break is present in the section, or the dates at Riggins Road and/or Mono Lake are in error, or that the Mono Lake excursion did not occur at the time claimed. The latter hypothesis is supported by Verosub (1976) who was unable to detect the excursion in a contemporaneous sequence only 300 km from Mono Lake.

Spectral analysis (using the MEM technique) reveals the presence of two types of periodic looping motion in the Riggins Road data. The highly elliptical counterclockwise looping with a period of roughly 5000 years may be indicative of eastward drift of some portion of the non-dipole field, or of a counterclockwise circular motion of the geomagnetic dipole axis as suggested by Opdyke et al. (1971). The circular clockwise looping motion of period 1900 years indicates the presence of westward drift of the non-

dipole field. As mentioned in Chapter1, there is presently considerable uncertainty regarding the long term stability of the westward drift thus any evidence concerning its existence in past is of considerable importance. If one accepts the interpretation that the 1900 year period represents one full cycle of the drift, then the results of Chapter 3 not only demonstrate the existence of westward drift some 30000 years ago, but give an estimate of the drift rate for that time interval as well (0.19°/yr).

In Chapter 4 the complex MEM technique was investigated by means of synthetic data sets in an effort to assess the validity of the results of Chapter 3. Some interesting conclusions were arrived at. The most important of these, is that the three principal peaks in the spectrum are not simply products of the noise present in the data, and therefore almost certainly represent real geomagnetic phenomena. Furthermore the sense of the periodic signals as inferred from the Riggins Road spectum is statistically significant. In spite of the above however, the findings of this chapter strongly suggest that the signal to noise conditions under which the Riggins Road results were obtained are marginal (especially where the "1900 year" peak is concerned). In other words, anyone wishing to verify the presence of the above signals using a different paleomagnetic data set, would be well advised to either reduce noise by collecting more samples per horizon, or collect a longer data sequence. Due to the marginal character of the Riggins Road sequence,

the presence of shorter period (less than 1900 yrs.) oscillatory motion of the geomagnetic vector with an amplitude similar to, or less than that of the 1900 year oscillation, cannot be ruled out.

Apart from the results concerning the Riggins Road data, this chapter has also demonstrated the impressive power of the complex MEM technique. The fact that it enables one to identify both the frequency and sense of looping signals in the presence of noise levels twice that of the signal amplitude, makes it an ideal tool for analysing the type of time sequences encountered in paleomagnetism.

REFERENCES

Adam, N. V., Benkova, N. P., Orlov, V. P., and Tyurmina, L.O., 1964. Western drift of the geomagnetic field, Geomag. Aeron., 4, 434-441.

Anderson, N., 1974. On the calculation of filter coefficients for maximum entropy spectral analysis. Geophys., 39, 69-72.

Barbetti, M., and McElhinny, M., 1972. Evidence of a geomagnetic excursion 30,000 yr BP, Nature, 239, 327-330.

Beran, R. J., and Watson, G S., 1967. Testing a sequence of unit vectors for serial correlations, J. geophys. Res., 72, 5655-5659.

Bucha, V., Taylor, R. E., Berger, R., and Haury, E. M., 1970. Geomagnetic intensity: changes during the past 3000 years in the western hemisphere, Science, 168, 111.

Bullard, E. C., Freedman, C., Gellman, H., and Nixon, J., 1950. The westward drift of the earth's magnetic field, Phil. Trans. R. Soc, Lond. A, 243, 67-92.

Burg, J. P., 1967. Maximum entropy spectral analysis, paper presented at the 37th Annual Meeting, Soc. explor. Geophys. Oklahoma City, October 31.

Burg, J. P., 1968. A new analysis technique for time series data, paper presented at Advanced Study Institute on Signal Processing NATO, Enshede, Netherlands, August.

Burlatskaya, S. P., Nechayva, T. B., and Petrova, G. N., 1965. The westward drift of the secular variation of magnetic inclination and variations of the earth's magnetic moment according to archeomagnetic data, Amer. Geophys. Union English ed., 6, 380.

Burlatskaya, S. P., Nechayva, T. B., and Petrova, G. N., 1968. Characteristics of secular variations of the geomagnetic field as indicated by world archeomagnetic data, Amer. Geophys. Union English ed., 12, 754.

Cain, J. L., and Hendricks, S.J., 1968. The geomagnetic secular variation 1900 - 1965, N.A.S.A. Technical Note TN D-4527, Washington, D.C.

Chen, W. Y., and Stegen, G. R., 1974. Experiments with maximum entropy power spectra of sinusoids, J. Geophys. Res., 79, 3019-3022.

Cox, A., and Doell, R. R., 1960. Review of paleomagnetism, Geol. Soc. Amer. Bull. 71, 647-768.

Creer, K. M., 1974. Geomagntic variations for the interval 7000-25,000 yr BP as recorded in a core of sediment from station 1474 of the Black Sea cruise of 'Atlantis II', Earth planet. Sci. Lett., 23, 34-42.

Creer, K. M., Gross, D. L., and Lineback, J. A., 1976. Origin of regional geomagnetic variations recorded by Wisconsinan and Holocene sediments from Lake Michigan, U. S. A., and Lake Windermere, England, Geol. Soc. Am. Bull., 87, 531-540.

Denham, C. R., 1974. Counter-clockwise motion of paleomagnetic directions 24,000 years ago at Mono Lake, California, J. Geomagn. Geoelect., 26, 487.

Denham, C. R., 1975. Spectral analysis of paleomagnetic time series, J. geophys. Res., 80, 1897-1901.

Denham, C. R., and Cox, A., 1971. Evidence that the Laschamp polarity event did not occur 13,300-30,400 years ago, Earth planet. Sci. Lett., 13, 181-190.

Epp, R. J., Tukey, J. W., and Watson. G. S., 1971. Testing unit vectors for correlation, J. Geophys. Res., 76, 8480-8483.

Fisher, R. A., 1953. Dispersion on a sphere, Proc. Roy. Soc. London, A, 217, 295-305.

Freed, W. K., and Healy, N., 1974. Excursions of the Pleistocene geomagnetic field recorded in Gulf of Mexico sediments, Earth Planet. Sci. Lett., 24, 99-104.

Gaitar-Puertas, C., 1953. Variacion secular del campo geomagnetico, Observ. del Elso, Memo No. 11.

Greville, T. N. E., 1967. spline functions, interpolaton, and numerical quadrature, Mathematical methods for digital computers, Vol. II, pp. 156-168, ed. Ralston, A., and Wilf, H. S., J. Wiley, New York.

Harrison, C. G. A., and Ramirez, E., 1975. Areal coverage of spurious reversals of the earth's magnetic field, J. Geomagn. Geoelect., 27, 139.

Irving, E., 1964. Paleomagnetism and its Application to Geological and Geophysical Problems, 399 pp., John Wiley, New York.

Harwood, J. M., and Malin, S. R. C., 1976. Present trends in the earth's magnetic field, Nature, 259, 469-471.

Hide, R., and Malin, S. R. C., 1970. Novel correlations between global features of the earth's gravitational and magnetic fields, Nature, 225, 605.

Jacobs, J. A., 1975. The Earth's core, 253 pp., Academic Press, New York.

Johnson, E. A., Murphy, T., and Torreson, O. W., 1948. Prehistory of the earth's magnetic field, Terr. Magn, atmos. Elec., 53, 349-372.

Kawai, N., and Hirooka, K., 1967. Wobbling motion of the geomagnetic dipole field in historic time during the last 2000 years, J. Geomag. Geolec., 19, 217.

Lacoss, R. T., 1971. Data adaptive spectral analysis methods, Geophys., 36, 661-675.

Lemke, R. W., Mudge, M. R., Wilcox, R. E., and Powers, H. A., 1975. Geologic setting of the Glacier Peak and Mazama ash-bed markers in west-central Montana, United States Geological Survey, Bulletin 1395-H, 31 pp.

Liddicoat, J. C., and Coe, R. A., 1975. Mono Lake 24,000 year BP geomagnetic excursion: additional data, EOS Trans. Am. geophys. Un., 56, 978.

Mackereth, F. H., 1971. On the variation in direction of the horizontal component of remanent magnetization in lake sediments, Earth planet. Sci. Lett., 12, 332-338.

McDonald, K. L., and Gunst, R. H., 1968. Recent trends in the earth's magnetic field, J. Geophys. Res., 73, 2057-2067.

McElhinny, M. W., 1973, Paleomagnetism and Plate Tectonics, 386 pp., Cambridge University Press, New York.

McElhinny, M., and Merrill, R. T., 1975. Geomagnetic secular variation over the past 5 m.y., Rev. Geophys. Space Phys., 13, 687-708.

Molyneux, L., 1971. A complete result magnetometer for measuring the remanent magnetization of rocks, Geophys, J. R. astr. Soc., 24, 429-433.

Morner, N-A., Lanser, J. P., and Hospers, J., 1971. Late Weichselian palaeomagnetic reversal, Nature phys. Sci., 234, 173-174.

Morner, N-A., and Lanser, J. P., 1974. Gothenburg Magnetic "Flip", Nature, 251, 408-409.

Mudge, M. R., 1967. Surficial geologic map of the Sawtooth Ridge quadrangle, Teton and Lewis and Clark Countries, Montana, United States Geological Survey, Geologic Quadrangle Map GQ-610.

Murthy, G. S., 1969. Paleomagnetic Studies in the Canadian Shield, unpublished PhD thesis, University of Alberta.

Nagata, T., Hirao, K., and Yoshikawa, H., 1949. Remanent magnetism in 'Pleistocene' deposits - Paleomagnetism in Japan, J. Geomagn. Geoelect., 1, 52-58.

Opdyke, N. D., Ninkovich, D., Lowrie, W., and Hays, J. D., 1972. The paleomagnetism of two Aegean deep-sea cores, Earth Planet. Sci. Lett., 14, 145-159.

Opdyke, N. D., Shackleton, N. J., and Hays, J. D., 1974. The details of a magnetic excursion as seen in a piston core from the southern Indian Ocean (abs.), EOS, Am. Geophys. Union Trans., 55, 237.

Runcorn, S. K. 1959. On the theory of the geomagnetic secular variation, Ann. Geophys., 15, 87-92.

Skiles, D. D., 1970. A method of inferring the direction of drift of the geomagnetic field from paleomagnetic data, J. Geomagn, Geoelect., 22, 441-462.

Sukroo, J. C. Christoffel, D. A., Vella, P., and Topping, W. W., 1978. Rejecting evidence of Gothenberg geomagnetic reversal in New Zealand, Nature, 271, 650.

Tarkhov, Y. N., 1965. Some results of archeomagnetic investigations in the western USSR, Geomag. Aeron., 5, 97.

Thompson, R., and Berglund, B., 1976. Late Weichselian geomagnetic 'reversal' as a possible example of the reinforcement syndrome, Nature, 263, 490-491.

Ulrych, T. J., and Bishop, T. N., 1975. maximum entropy spectral analysis and autoregressive decomposition, Rev. Geophys, Space Phys., 13, 183-200.

Verosub, K. L., 1976. The Mono Lake excursion as seen from Clear Lake, California (abs.), EOS, Am. Geophys. Union Trans., 57, 909.

Verosub, K. L., and Banerjee, S. K., 1977. Geomagnetic excursions and their paleomagnetic record, Rev. Geophys. Space Phys., 15, 145-155.

Watson, G. S., and Irving, E., 1957. Statistical methods in rock magnetism, Mon. Not. R. astr. Soc., Geophys. Suppl., 7, 289-300.

Westgate, J. A., 1968. Surficial geology of the Foremost-Cypress Hills area, Alberta, Research Council of Alberta, Bull. 22, 121 pp.

Westgate, J. A., and Evans, M. E., 1978. Compositional variability of Glacier Peak tephra and stratigraphic significance (in press)

Westgate, J. A., and Fulton, R. J., 1975. Tephrostratigraphy of Olympia interglacial sediments in south-central British Columbia, Canada, Can, J. Earth. Sci., 12, 489-502.

Westgate, J. A., Smith, D. G. W., and Tomlinson, M., 1970. Late Quatemary tephra layers in southwest Canada. In Early man and environments in northwest North America. Edited by R. A. Smith and J. W. Smith. Proceeding of the Second Annual Paleoenvironmental Workshop, University of Calgary Archeological Association, The Student's Press, Calgary, Alberta, pp 13-34.

Wilcox, R. E., 1969. Airfall deposits of two closely spaced eruptions in late glacial time from Glacier Peak Volcano, Washington, Geological Society of America, Abstracts with Programs, 1, 88-89.

Wilson, R. L., 1959. Remanent magnetism of late Secondary and early Tertiary British rocks, Phil. mag., 4, 750-755.

Wilson, R. L., 1970. Permanent aspects of the earth's non-dipole magnetic field over Upper Tertiary Times, Geophys. J. R. astr. Soc., 19, 417-438.

Wilson, R. L., 1971. Dipole offset - the time-average paleomagnetic field over the past 25 million years, Geophys. J. R. astr. Soc., 22, 491-504.

Wilson, R. L., 1972. Paleomagnetic differences between normal and reversed field sources, and the problem of far-sided and right-handed pole positions, Geophys. J. R. astr. Soc., 28, 295-304.

Yukutake, T., 1962. The westward drift of the magnetic field of the earth, Bull. Earthq. Res. Inst., 40, 1-65.

Yukutake, T., 1967. The westward drift of the earth's magnetic field in historic times, J. Geomagn. Geoelect., 19, 103-116.

Yukutake, T., and Tachinaka, H., 1969. Separation of the earth's magnetic field into drifting and standing parts, Bull. Earthquake Res. Inst. Tokyo, 47, 65-97.

APPENDIX 1

Description of Sampling Techniques

Essentially all specimens from the four sites discussed in Chapter 2 were collected by driving a rectangular 3-sided brass channel into the vertical face of the outcrop. Care was taken to ensure that a sufficient portion of the channel was exposed after emplacement so that its orientation could be measured. Orientation was defined by three angles -- one called the "strike" was the horizontal bearing of the sides of the of the channel -- another, the "dip", was the angle of the top edge below the horizontal (measured in the vertical plane) -- the third, called the "roll", was roughly equivalent to the rotation of the channel about its long axis, but more precisely was the dip of the top of the rear face (also measured in the vertical plane). A clockwise roll (i.e. top of the rear face dipping to the right) was defined as positive. Measurements were taken with a Brunton compass-clinometer and were accurate to roughly one degree.

Prior to removal of the channel from the sediment, a flat steel chisel was driven into the outcrop sliding along the top (open) face so that sediment in the channel would be enclosed on all four sides. Both the chisel and the brass channel were then gripped together and pulled from the outcrop simultaneously. To force the sample out of the channel a rectangular brass piston was placed behind the sediment and attached to a rod inserted through a hole in the rear face of the channel. Employing a device designed by

John Westgate, the channel was held in a stationary position while sufficient pressure was applied to the piston rod to force the sediment out. Once removed, the rectangular sample was marked to preserve its orientation then immediately sprayed with laquer to prevent it from drying out and crumbling. The samples were generally long enough so that 2 to 4 individual cubic specimens could be cut from each. These specimens were sequentially labelled A, B, C, ... where A would be the one closest to the end of the sample at the outer face of the outcrop.

As mentioned earlier the above method was used extensively in collecting the data analysed in Chapter 2, and although reasonably sucessful, the technique had two major disadvantages. Firstly the process of cutting the rectangular samples into cubes was extremely time consuming and sometimes impossible as the sediment would generally crumble if not handled properly. Secondly most samples were significantly compressed while being extruded from the brass channel, causing distortion of the sediment sufficient to affect the magnetic remanence. Visual examination of samples in the field both before and after extrusion revealed that most of the compression was taken up in the centimeter of sediment closest to the brass piston. For this reason, remanence directions obtained from the so-called A specimens (see above) are not considered in the analysis of paleomagnetic data in Chapter 2.

In an attempt to avoid the above two problems a somewhat simpler sampling scheme was devised to collect the data presented in Chapter 3. In place of the brass channel transparent plastic cubes, roughly two centimeters on a side, were either pressed or gently tapped into the vertical face of the outcrop. Once in place, the vertical position of the sample was measured and recorded as in the previous method; the orientation procedure however, was somewhat different. The strike in this case was defined as the horizontal bearing of the rear face of the cube. The dip, although defined the same as previously, was measured by holding the Brunton flush against the rear face in a vertical plane perpendicular to the face. The roll was obtained in the same manner as before. Measurements were accurate to within 2° or 3°. After removal from the outcrop, excess sediment was carefully scraped away so that the sample was flush with the open side of the cube. The cube was then capped (each had its own tightly fitting lid), marked to preserve its orientation, and labelled with a felt pen. In the laboratory, the samples were simply measured while still in the cubes (the plastic cubes were totally non-magnetic) avoiding the weeks of work associated with cutting up the "brass channel specimens". As it was not necessary to force the sediment out of its container as was done previously, distortion was minimized as well. The one disadvantage of the newer scheme was that each oriented sample yielded only a single specimen for magnetic

measurement. For this reason at least two independently oriented samples were collected per horizon as opposed to only one when the brass channel was used.

APPENDIX 2

The data used in Chapter 2 is listed here in the following seven-column format:

column 1 -- specimen name

column 2 -- specimen mass in grams

column 3 -- vertical distance above tephra in cm

column 4 -- A.F. demagnetization field in mT

column 5 -- magnetic moment in amp m^2

column 6 -- declination

column 7 -- inclination

Irvine Section

QZI01A	12.66	228.0	0.0	1.445E-07	299.3	19.5
QZI01A	12.66	228.0	10.0	6.460E-08	318.4	39.2
QZI01A	12.66	228.0	20.0	3.446E-08	342.5	44.4
QZI01B	11.60	228.0	0.0	8.961E-08	15.6	52.6
QZI01B	11.60	228.0	10.0	5.431E-08	0.8	53.2
QZI01B	11.60	228.0	20.0	3.871E-08	357.6	52.9
QZH01A	12.31	210.0	0.0	1.393E-07	300.5	17.4
QZH01A	12.31	210.0	10.0	3.597E-08	316.0	40.6
QZH01A	12.31	210.0	20.0	2.508E-08	348.3	60.7
QZH01B	11.68	210.0	0.0	7.746E-08	31.6	53.7
QZH01B	11.68	210.0	10.0	3.696E-08	19.2	65.6
QZH01B	11.68	210.0	20.0	2.728E-08	20.0	65.8
QZH01B	11.68	210.0	30.0	2.093E-08	25.0	65.6
QYG01A	13.44	195.0	0.0	1.277E-07	303.4	27.6
QYG01A	13.44	195.0	10.0	5.075E-08	347.5	48.9
QYG01A	13.44	195.0	20.0	3.256E-08	15.2	50.7
QYG01B	12.31	195.0	0.0	8.362E-08	28.3	50.9
QYG01B	12.31	195.0	10.0	4.449E-08	34.6	56.2
QYG01B	12.31	195.0	20.0	3.326E-08	31.3	53.4
QZG01A	12.32	180.0	0.0	1.020E-07	338.3	39.8
QZG01A	12.32	180.0	10.0	3.930E-08	2.0	62.2
QZG01A	12.32	180.0	20.0	2.922E-08	16.2	60.1
QZG01B	12.06	180.0	0.0	7.350E-08	14.9	56.0
QZG01B	12.06	180.0	10.0	3.494E-08	11.2	59.3
QZG01B	12.06	180.0	20.0	2.517E-08	7.5	61.8
QYF01A	13.55	165.0	0.0	1.040E-07	314.7	36.7
QYF01A	13.55	165.0	10.0	4.148E-08	345.3	60.9
QYF01A	13.55	165.0	20.0	2.819E-08	7.4	65.3
QYF01B	12.24	165.0	0.0	7.470E-08	28.5	57.4
QYF01B	12.24	165.0	10.0	3.763E-08	13.1	59.5

QYF01B	12.24	165.0	20.0	2.782E-08	8.5	57.5
QZF01B	12.77	150.0	0.0	8.387E-08	24.9	49.4
QZF01B	12.77	150.0	10.0	5.104E-08	19.4	57.6
QZF01B	12.77	150.0	20.0	3.402E-08	25.5	60.0
QZF01C	12.87	150.0	0.0	1.050E-07	18.5	55.0
QZF01C	12.87	150.0	10.0	4.925E-08	19.8	68.1
QZF01C	12.87	150.0	20.0	3.694E-08	19.9	70.6
QVD01B	12.94	147.0	0.0	7.742E-08	38.3	68.4
QVD01B	12.94	147.0	2.5	6.853E-08	34.8	68.9
QVD01B	12.94	147.0	5.0	6.107E-08	34.4	70.8
QVD01B	12.94	147.0	10.0	4.479E-08	38.1	72.6
QVD01B	12.94	147.0	20.0	3.889E-08	25.1	75.1
QVD01B	12.94	147.0	30.0	2.452E-08	32.0	69.1
QVD01B	12.94	147.0	40.0	1.860E-08	49.8	75.6
QVD01C	12.76	147.0	0.0	7.235E-08	8.0	59.1
QVD01C	12.76	147.0	5.0	5.667E-08	356.8	63.9
QVD01C	12.76	147.0	10.0	4.327E-08	349.4	65.9
QVD01C	12.76	147.0	20.0	2.973E-08	347.0	61.7
QYE01B	13.10	135.0	0.0	7.607E-08	50.1	59.0
QYE01B	13.10	135.0	10.0	4.005E-08	77.9	70.9
QYE01B	13.10	135.0	20.0	2.943E-08	84.4	66.7
QYE01C	12.32	135.0	0.0	7.375E-08	30.7	57.5
QYE01C	12.32	135.0	10.0	3.948E-08	25.3	65.5
QYE01C	12.32	135.0	20.0	3.418E-08	21.1	78.0
QZE01A	13.52	120.0	0.0	1.399E-07	303.6	25.1
QZE01A	13.52	120.0	10.0	3.961E-08	323.0	54.8
QZE01A	13.52	120.0	20.0	2.716E-08	354.6	63.1
QZE01B	12.61	120.0	0.0	6.988E-08	25.1	50.1
QZE01B	12.61	120.0	10.0	3.129E-08	49.2	64.7
QZE01B	12.61	120.0	20.0	2.330E-08	57.0	61.8
QYD01A	12.92	105.0	0.0	8.816E-08	305.1	29.7
QYD01A	12.92	105.0	10.0	3.562E-08	34.6	66.1
QYD01A	12.92	105.0	20.0	3.086E-08	71.9	59.6
QYD01B	12.24	105.0	0.0	7.429E-08	39.3	61.8
QYD01B	12.24	105.0	10.0	4.795E-08	52.4	68.3
QYD01B	12.24	105.0	20.0	3.406E-08	56.9	70.8
QYD01B	12.24	105.0	30.0	2.553E-08	64.5	66.7
QYD01B	12.24	105.0	40.0	2.026E-08	347.5	63.8
QYD01B	12.24	105.0	60.0	1.187E-08	270.1	64.5
QYD01B	12.24	105.0	80.0	9.611E-09	52.1	78.2
QYD01B	12.24	105.0	100.0	4.620E-09	57.0	69.5
QYD01B	12.24	105.0	140.0	6.499E-09	309.1	2.3
QYD01B	12.24	105.0	180.0	1.405E-09	13.1	23.6
QVC01A	12.69	96.0	0.0	6.654E-08	66.0	76.3
QVC01A	12.69	96.0	2.5	6.042E-08	74.6	76.8
QVC01A	12.69	96.0	5.0	5.480E-08	74.6	77.8
QVC01A	12.69	96.0	10.0	4.345E-08	88.9	80.1
QVC01A	12.69	96.0	20.0	3.335E-08	94.8	77.6
QVC01A	12.69	96.0	30.0	2.628E-08	118.7	81.3
QVC01A	12.69	96.0	40.0	2.248E-08	89.3	80.9
QVC01A	12.69	96.0	50.0	1.935E-08	94.5	79.9
QVC01A	12.69	96.0	60.0	1.607E-08	68.5	76.4
QVC01B	13.22	96.0	0.0	7.044E-08	66.6	77.7
QVC01B	13.22	96.0	2.5	6.156E-08	81.7	79.4

QVC01B	13.22	96.0	5.0	5.422E-08	89.1	80.9
QVC01B	13.22	96.0	10.0	4.202E-08	100.6	77.4
QVC01B	13.22	96.0	20.0	3.092E-08	111.7	77.3
QVC01B	13.22	96.0	30.0	2.592E-08	115.3	73.1
QVC01B	13.22	96.0	40.0	1.961E-08	133.6	72.8
QVC01B	13.22	96.0	50.0	1.417E-08	141.9	69.2
QVC01B	13.22	96.0	60.0	1.164E-08	107.3	73.6
QZD01A	13.49	90.0	0.0	9.802E-07	99.2	-3.0
QZD01A	13.49	90.0	10.0	7.109E-08	91.1	17.9
QZD01A	13.49	90.0	20.0	3.128E-08	88.8	49.5
QZD01B	12.97	90.0	0.0	5.208E-08	15.8	36.1
QZD01B	12.97	90.0	10.0	3.719E-08	72.2	81.1
QZD01B	12.97	90.0	20.0	2.246E-08	100.5	81.8
QYC01A	13.42	75.0	0.0	8.287E-08	300.8	33.8
QYC01A	13.42	75.0	10.0	2.703E-08	6.3	74.8
QYC01A	13.42	75.0	20.0	2.047E-08	58.3	74.1
QYC01A	13.42	75.0	30.0	1.472E-08	91.4	79.5
QYC01B	12.91	75.0	0.0	5.875E-08	37.9	62.1
QYC01B	12.91	75.0	10.0	2.910E-08	66.8	70.6
QYC01B	12.91	75.0	20.0	2.266E-08	74.7	67.4
QYC01C	11.75	75.0	0.0	5.890E-08	25.7	49.1
QYC01C	11.75	75.0	10.0	2.910E-08	44.3	64.5
QYC01C	11.75	75.0	20.0	2.098E-08	41.8	61.6
QZC01A	13.30	60.0	0.0	1.143E-07	290.1	12.3
QZC01A	13.30	60.0	10.0	3.312E-08	344.1	46.4
QZC01A	13.30	60.0	20.0	2.241E-08	356.2	72.9
QZC01A	13.30	60.0	30.0	1.712E-08	358.5	68.5
QZC01B	12.95	60.0	0.0	6.130E-07	90.9	12.3
QZC01B	12.95	60.0	10.0	5.249E-08	66.6	33.0
QZC01B	12.95	60.0	20.0	3.368E-08	57.0	41.1
QZC01C	13.26	60.0	0.0	7.046E-08	22.5	49.6
QZC01C	13.26	60.0	10.0	3.547E-08	25.5	52.8
QZC01C	13.26	60.0	20.0	2.627E-08	30.5	43.8
QVB01B	13.25	50.0	0.0	4.488E-08	48.3	53.0
QVB01B	13.25	50.0	2.5	3.771E-08	58.1	48.8
QVB01B	13.25	50.0	5.0	2.960E-08	58.5	52.2
QVB01B	13.25	50.0	10.0	2.259E-08	57.4	53.4
QVB01B	13.25	50.0	20.0	1.626E-08	51.9	49.9
QVB01B	13.25	50.0	30.0	1.371E-08	57.2	56.0
QYB01A	13.53	45.0	0.0	9.648E-08	301.1	36.2
QYB01A	13.53	45.0	10.0	2.940E-08	347.4	75.3
QYB01A	13.53	45.0	20.0	2.174E-08	16.2	83.7
QYB01A	13.53	45.0	30.0	1.393E-08	13.4	81.9
QYB01B	12.95	45.0	0.0	6.253E-08	13.0	54.7
QYB01B	12.95	45.0	10.0	3.289E-08	0.0	60.7
QYB01B	12.95	45.0	20.0	2.323E-08	3.7	56.9
QZB01A	13.76	30.0	0.0	1.254E-07	314.7	17.4
QZB01A	13.76	30.0	10.0	3.913E-08	341.8	38.6
QZB01A	13.76	30.0	20.0	2.212E-08	355.8	40.4
QZB01B	13.63	30.0	0.0	6.808E-08	15.2	49.3
QZB01B	13.63	30.0	10.0	3.091E-08	12.9	55.9
QZB01B	13.63	30.0	20.0	2.207E-08	10.2	58.8
QYA01C	12.99	15.0	0.0	8.391E-08	12.9	61.0
QYA01C	12.99	15.0	10.0	4.873E-08	17.2	64.4

QYA01C	12.99	15.0	20.0	3.601E-08	16.4	63.5
QYA01C	12.99	15.0	30.0	2.867E-08	19.1	63.3
QYA01C	12.99	15.0	40.0	2.262E-08	18.1	66.2
QYA01C	12.99	15.0	60.0	1.592E-08	16.1	48.9
QYA01C	12.99	15.0	80.0	1.308E-08	34.4	49.7
QYA01C	12.99	15.0	100.0	8.013E-09	42.0	62.1
QYA01C	12.99	15.0	140.0	5.693E-09	63.8	70.2
QYA01C	12.99	15.0	180.0	2.289E-09	334.0	30.4
QYA01D	12.52	15.0	0.0	6.607E-08	23.1	62.6
QYA01D	12.52	15.0	10.0	3.945E-08	16.1	55.8
QYA01D	12.52	15.0	20.0	2.023E-08	27.8	73.8
QYA01D	12.52	15.0	30.0	1.104E-08	8.2	55.7
QYA01D	12.52	15.0	40.0	1.197E-08	14.1	51.7
QYA01D	12.52	15.0	60.0	8.190E-10	7.6	49.0
QYA01D	12.52	15.0	80.0	5.990E-10	319.6	56.8
QYA01D	12.52	15.0	100.0	5.410E-10	326.9	40.3
QYA01D	12.52	15.0	140.0	3.340E-10	80.0	41.5
QYA01D	12.52	15.0	180.0	6.860E-10	278.2	-3.9
QZA01A	13.23	3.0	0.0	7.478E-08	28.9	40.9
QZA01A	13.23	3.0	10.0	2.742E-08	30.5	45.6
QZA01A	13.23	3.0	20.0	1.656E-08	20.7	44.7
QZA01B	12.60	3.0	0.0	8.588E-08	356.5	63.5
QZA01B	12.60	3.0	10.0	5.035E-08	10.0	64.4
QZA01B	12.60	3.0	20.0	3.331E-08	13.2	62.4
QZA01B	12.60	3.0	30.0	2.667E-08	10.1	65.8
QZA01B	12.60	3.0	40.0	2.072E-08	5.6	64.8
QZA01B	12.60	3.0	60.0	1.201E-08	350.1	54.9
QZA01B	12.60	3.0	80.0	5.054E-09	341.4	9.5
QVA01B	12.61	0.0	0.0	1.261E-07	34.0	44.2
QVA01B	12.61	0.0	2.5	9.848E-08	30.3	50.8
QVA01B	12.61	0.0	5.0	8.088E-08	31.6	51.1
QVA01B	12.61	0.0	10.0	5.567E-08	30.7	52.7
QVA01B	12.61	0.0	20.0	3.705E-08	17.3	56.2
QVA01C	13.21	0.0	0.0	7.907E-08	19.4	49.9
QVA01C	13.21	0.0	5.0	5.214E-08	24.0	56.6
QVA01C	13.21	0.0	10.0	3.723E-08	25.1	55.4
QVA01C	13.21	0.0	20.0	3.205E-08	49.2	41.7
QZJ01A	13.39	-4.0	0.0	1.067E-07	305.3	23.5
QZJ01A	13.39	-4.0	10.0	4.300E-08	351.6	57.3
QZJ01A	13.39	-4.0	20.0	1.816E-08	19.3	55.0
QZJ01B	13.07	-4.0	0.0	8.408E-08	14.5	49.6
QZJ01B	13.07	-4.0	10.0	4.828E-08	22.4	58.3
QZJ01B	13.07	-4.0	20.0	3.490E-08	24.9	58.3
QYJ01B	12.97	-15.0	0.0	8.015E-08	31.3	51.8
QYJ01B	12.97	-15.0	10.0	5.940E-08	28.7	55.5
QYJ01B	12.97	-15.0	20.0	3.698E-08	30.2	55.1
QYJ01C	12.89	-15.0	0.0	8.092E-08	18.3	59.7
QYJ01C	12.89	-15.0	10.0	4.524E-08	12.1	62.4
QYJ01C	12.89	-15.0	20.0	3.133E-08	25.0	66.4
QZK01A	14.18	-30.0	0.0	8.842E-08	311.5	31.5
QZK01A	14.18	-30.0	10.0	4.523E-08	310.7	48.4
QZK01A	14.18	-30.0	20.0	1.932E-08	347.1	52.9
QZK01B	13.66	-30.0	0.0	7.721E-08	16.8	50.2
QZK01B	13.66	-30.0	10.0	3.995E-08	21.4	51.1

QZK01B	13.66	-30.0	20.0	2.837E-08	16.3	52.9
QYK01A	12.79	-45.0	0.0	8.231E-08	9.2	51.8
QYK01A	12.79	-45.0	10.0	5.071E-08	7.5	60.5
QYK01A	12.79	-45.0	20.0	3.298E-08	355.3	57.8
QYK01B	12.88	-45.0	0.0	7.709E-08	3.9	68.5
QYK01B	12.88	-45.0	10.0	3.664E-08	353.0	72.0
QYK01B	12.88	-45.0	20.0	2.815E-08	9.3	70.6
QZL01A	13.76	-60.0	0.0	1.051E-07	310.8	21.2
QZL01A	13.76	-60.0	10.0	4.062E-08	338.1	48.1
QZL01A	13.76	-60.0	20.0	3.477E-08	355.7	51.7
QZL01B	12.75	-60.0	0.0	8.072E-08	9.4	55.2
QZL01B	12.75	-60.0	10.0	4.177E-08	10.5	53.8
QZL01B	12.75	-60.0	20.0	2.930E-08	7.3	49.4
QYL01A	13.31	-75.0	0.0	1.301E-07	300.9	31.3
QYL01A	13.31	-75.0	10.0	5.590E-08	347.8	53.1
QYL01A	13.31	-75.0	20.0	3.964E-08	3.0	53.4
QYL02A	13.16	-75.0	0.0	1.583E-07	289.2	9.4
QYL02A	13.16	-75.0	10.0	4.936E-08	322.4	41.0
QYL02A	13.16	-75.0	20.0	3.418E-08	20.2	48.1
QYL02B	13.69	-75.0	0.0	7.064E-08	21.7	66.0
QYL02B	13.69	-75.0	10.0	4.177E-08	18.2	40.3
QYL02B	13.69	-75.0	20.0	3.693E-08	15.0	49.5
QYL02B	13.69	-75.0	30.0	2.487E-08	52.1	56.3
QYL02B	13.69	-75.0	40.0	2.311E-08	27.4	52.8
QYL02B	13.69	-75.0	60.0	1.074E-08	8.0	34.3
QYL02B	13.69	-75.0	80.0	1.191E-08	24.7	42.1
QYL02B	13.69	-75.0	100.0	7.525E-09	61.3	37.6
QYL02B	13.69	-75.0	140.0	4.494E-09	44.4	37.5
QYL02B	13.69	-75.0	180.0	6.706E-09	1.3	63.4
QZM01B	13.08	-90.0	0.0	4.147E-08	49.5	26.9
QZM01B	13.08	-90.0	10.0	3.298E-08	55.9	31.5
QZM01B	13.08	-90.0	20.0	1.858E-08	51.7	32.0
QZM01C	13.26	-90.0	0.0	6.230E-08	27.8	42.4
QZM01C	13.26	-90.0	10.0	3.296E-08	44.1	53.0
QZM01C	13.26	-90.0	20.0	2.386E-08	42.2	52.6
QYM01A	13.23	-105.0	0.0	4.624E-08	298.0	9.2
QYM01A	13.23	-105.0	10.0	1.064E-08	26.4	12.3
QYM01A	13.23	-105.0	20.0	1.607E-08	60.3	12.8
QYM01B	13.37	-105.0	0.0	5.286E-08	44.2	36.0
QYM01B	13.37	-105.0	10.0	2.684E-08	59.6	39.8
QYM01B	13.37	-105.0	20.0	1.884E-08	61.1	35.6
QZN01B	13.33	-120.0	0.0	5.954E-08	55.2	29.3
QZN01B	13.33	-120.0	10.0	2.664E-08	74.9	34.3
QZN01B	13.33	-120.0	20.0	1.905E-08	70.0	33.9
QZN01C	13.55	-120.0	0.0	6.815E-08	43.3	41.4
QZN01C	13.55	-120.0	10.0	3.344E-08	67.9	53.0
QZN01C	13.55	-120.0	20.0	2.279E-08	72.4	49.7
QYN01B	13.41	-135.0	0.0	4.801E-08	40.7	23.0
QYN01B	13.41	-135.0	10.0	4.008E-08	53.3	25.2
QYN01B	13.41	-135.0	20.0	2.724E-08	54.2	25.1
QYN01C	13.67	-135.0	0.0	6.637E-08	34.8	41.4
QYN01C	13.67	-135.0	10.0	3.381E-08	47.5	48.0
QYN01C	13.67	-135.0	20.0	2.367E-08	46.6	53.5
QZO01A	13.43	-150.0	0.0	9.948E-08	42.6	41.3

QZO01A	13.43	-150.0	10.0	4.914E-08	49.3	53.8
QZO01A	13.43	-150.0	20.0	3.189E-08	52.3	47.8
QZO01B	13.77	-150.0	0.0	1.142E-07	35.2	36.8
QZO01B	13.77	-150.0	10.0	5.534E-08	53.4	42.0
QZO01B	13.77	-150.0	20.0	3.739E-08	42.7	43.9
QYO01A	13.23	-165.0	0.0	1.258E-07	301.4	2.6
QYO01A	13.23	-165.0	10.0	3.230E-08	0.2	12.6
QYO01A	13.23	-165.0	20.0	1.736E-08	36.6	15.6
QYO01B	13.95	-165.0	0.0	1.181E-07	18.6	26.2
QYO01B	13.95	-165.0	10.0	5.503E-08	36.6	35.3
QYO01B	13.95	-165.0	20.0	3.923E-08	37.0	41.2
QZP01A	13.13	-180.0	0.0	5.704E-08	21.8	3.9
QZP01A	13.13	-180.0	10.0	2.149E-08	54.0	4.5
QZP01A	13.13	-180.0	20.0	1.916E-08	52.7	5.3
QZP01B	13.10	-180.0	0.0	1.467E-07	20.2	-31.7
QZP01B	13.10	-180.0	10.0	2.904E-08	28.5	17.0
QZP01B	13.10	-180.0	20.0	2.014E-08	53.2	36.6
QZP01B	13.10	-180.0	30.0	1.782E-08	41.6	36.6
QZP01B	13.10	-180.0	40.0	1.093E-08	63.9	46.0
QYP01B	13.40	-195.0	0.0	8.265E-08	44.3	1.1
QYP01B	13.40	-195.0	10.0	3.345E-08	60.5	30.5
QYP01B	13.40	-195.0	20.0	2.230E-08	60.0	32.2
QYP01C	13.54	-195.0	0.0	1.007E-07	35.9	-4.5
QYP01C	13.54	-195.0	10.0	4.237E-08	30.5	20.2
QYP01C	13.54	-195.0	20.0	2.582E-08	55.0	39.8
QYP01C	13.54	-195.0	30.0	1.794E-08	61.0	41.3
QZQ01A	13.34	-210.0	0.0	8.445E-08	324.3	17.1
QZQ01A	13.34	-210.0	10.0	2.678E-08	10.8	37.1
QZQ01A	13.34	-210.0	20.0	1.660E-08	36.8	32.4
QZQ01B	13.53	-210.0	0.0	9.026E-08	33.6	37.9
QZQ01B	13.53	-210.0	10.0	3.584E-08	56.6	45.1
QZQ01B	13.53	-210.0	20.0	2.422E-08	58.9	44.8
QYQ01A	13.33	-225.0	0.0	8.819E-08	327.9	-44.9
QYQ01A	13.33	-225.0	10.0	2.737E-08	41.0	-9.8
QYQ01A	13.33	-225.0	20.0	2.543E-08	58.4	17.4
QYQ01B	13.59	-225.0	0.0	9.321E-08	64.1	-27.9
QYQ01B	13.59	-225.0	10.0	4.156E-08	69.8	28.3
QYQ01B	13.59	-225.0	20.0	3.201E-08	70.9	46.8
QYQ01B	13.59	-225.0	30.0	2.254E-08	73.3	50.1
QZR01A	13.38	-240.0	0.0	8.861E-08	4.3	15.9
QZR01A	13.38	-240.0	10.0	3.537E-08	28.3	18.8
QZR01A	13.38	-240.0	20.0	2.258E-08	36.1	16.6
QZR01B	13.39	-240.0	0.0	9.497E-08	29.6	30.6
QZR01B	13.39	-240.0	10.0	2.864E-08	47.1	33.1
QZR01B	13.39	-240.0	20.0	1.517E-08	47.8	25.6
QZR02B	13.31	-240.0	0.0	1.009E-07	59.2	30.1
QZR02B	13.31	-240.0	10.0	4.349E-08	65.3	39.1
QZR02B	13.31	-240.0	20.0	2.457E-08	66.2	37.4
QZR02D	13.45	-240.0	0.0	9.673E-08	34.6	43.7
QZR02D	13.45	-240.0	10.0	3.886E-08	19.7	53.8
QZR02D	13.45	-240.0	20.0	1.690E-08	7.2	55.9
QYR01A	13.90	-255.0	0.0	8.793E-08	320.2	-8.3
QYR01A	13.90	-255.0	10.0	1.953E-08	24.7	14.8
QYR01A	13.90	-255.0	20.0	1.764E-08	32.7	20.5

QYR01A	13.90	-255.0	30.0	1.483E-08	38.6	23.1
QYR01B	13.40	-255.0	0.0	9.529E-08	31.4	17.9
QYR01B	13.40	-255.0	10.0	3.356E-08	39.2	16.3
QYR01B	13.40	-255.0	20.0	1.460E-08	35.5	14.5
QYR01C	13.64	-255.0	0.0	7.015E-08	18.6	40.7
QYR01C	13.64	-255.0	10.0	2.900E-08	52.9	28.4
QYR01C	13.64	-255.0	20.0	1.751E-08	58.5	51.5
QYR01C	13.64	-255.0	30.0	9.099E-09	56.8	36.0
QYR01C	13.64	-255.0	40.0	1.094E-08	359.7	56.7
QYR01C	13.64	-255.0	60.0	6.548E-09	47.2	19.2
QYR01C	13.64	-255.0	80.0	5.198E-09	318.6	56.6
QYR01C	13.64	-255.0	100.0	8.605E-09	72.3	37.3
QYR01C	13.64	-255.0	140.0	4.208E-10	314.3	70.2
QYR01C	13.64	-255.0	180.0	4.579E-09	8.8	5.2
QZS01B	13.40	-270.0	0.0	9.943E-08	36.5	15.4
QZS01B	13.40	-270.0	10.0	3.862E-08	46.5	8.3
QZS01B	13.40	-270.0	20.0	2.036E-08	48.1	3.7
QZS01C	13.30	-270.0	0.0	1.061E-07	52.3	36.2
QZS01C	13.30	-270.0	10.0	4.605E-08	69.8	40.7
QZS01C	13.30	-270.0	20.0	3.842E-08	60.9	39.3

Choteau Section

QUF01B	12.86	11.0	0.0	6.523E-08	70.4	63.0
QUF01B	12.86	11.0	5.0	5.865E-08	80.4	67.2
QUF01B	12.86	11.0	10.0	5.237E-08	81.4	67.7
QUF01B	12.86	11.0	20.0	4.536E-08	104.8	55.6
QUF01C	13.13	11.0	0.0	6.242E-08	78.9	66.2
QUF01C	13.13	11.0	2.5	5.779E-08	89.4	68.8
QUF01C	13.13	11.0	5.0	5.436E-08	89.7	71.2
QUF01C	13.13	11.0	10.0	4.994E-08	95.5	69.6
QUF01C	13.13	11.0	20.0	4.162E-08	97.6	68.3
QUF01C	13.13	11.0	30.0	3.471E-08	108.6	69.6
QTU01A	12.29	9.0	0.0	6.752E-08	12.8	51.0
QTU01A	12.29	9.0	2.5	6.802E-08	9.7	50.7
QTU01A	12.29	9.0	5.0	6.570E-08	8.9	49.8
QTU01A	12.29	9.0	10.0	6.081E-08	8.0	49.1
QTU01A	12.29	9.0	20.0	5.169E-08	7.0	47.9
QTU01A	12.29	9.0	30.0	4.034E-08	5.1	47.7
QUE01A	12.71	-7.0	0.0	5.466E-08	22.3	59.4
QUE01A	12.71	-7.0	5.0	5.044E-08	24.0	62.9
QUE01A	12.71	-7.0	10.0	4.617E-08	21.8	65.4
QUE01A	12.71	-7.0	20.0	3.821E-08	27.9	67.3
QUE01B	12.64	-7.0	0.0	5.491E-08	23.6	60.8
QUE01B	12.64	-7.0	2.5	5.134E-08	22.7	64.7
QUE01B	12.64	-7.0	5.0	4.896E-08	20.6	65.1
QUE01B	12.64	-7.0	10.0	4.498E-08	17.3	65.6
QUE01B	12.64	-7.0	20.0	3.654E-08	24.2	66.5
QUE01B	12.64	-7.0	30.0	3.087E-08	19.7	66.6
QUD01A	11.92	-17.0	0.0	4.400E-08	-15.0	75.6
QUD01A	11.92	-17.0	10.0	4.224E-08	-37.4	73.3
QUD01A	11.92	-17.0	20.0	4.288E-08	-42.8	74.5
QUD01B	13.72	-17.0	0.0	6.723E-08	19.4	73.9

QUD01B	13.72	-17.0	10.0	5.809E-08	-2.3	85.1
QUD01B	13.72	-17.0	20.0	5.886E-08	-12.6	81.4
QTA01A	11.83	-20.0	0.0	6.367E-11	343.0	50.0
QTA01A	11.83	-20.0	10.0	5.222E-08	344.7	50.4
QTA01A	11.83	-20.0	20.0	4.481E-08	344.2	49.0
QTA01B	11.46	-20.0	0.0	6.308E-08	342.2	49.7
QTA01B	11.46	-20.0	10.0	5.423E-08	340.4	50.3
QTA01B	11.46	-20.0	20.0	4.445E-08	338.4	49.3
QUC01B	13.47	-30.5	0.0	6.380E-08	-42.5	71.3
QUC01B	13.47	-30.5	10.0	4.899E-08	-53.9	65.9
QUC01B	13.47	-30.5	20.0	3.687E-08	-60.5	67.0
QUC01C	13.50	-30.5	0.0	6.846E-08	-35.9	71.7
QUC01C	13.50	-30.5	10.0	5.601E-08	-48.7	63.6
QUC01C	13.50	-30.5	20.0	3.910E-08	-46.3	60.3
QTT01B	12.09	-42.0	0.0	5.721E-08	347.9	57.7
QTT01B	12.09	-42.0	5.0	5.304E-08	344.4	58.3
QTT01B	12.09	-42.0	10.0	4.961E-08	342.8	57.9
QTT01B	12.09	-42.0	20.0	4.707E-08	327.6	47.6
QTT01C	12.48	-42.0	0.0	5.532E-08	0.3	60.2
QTT01C	12.48	-42.0	2.5	5.433E-08	357.7	60.8
QTT01C	12.48	-42.0	5.0	5.360E-08	356.4	61.7
QTT01C	12.48	-42.0	10.0	4.812E-08	357.0	61.6
QTT01C	12.48	-42.0	20.0	4.076E-08	354.9	59.0
QTT01C	12.48	-42.0	30.0	3.471E-08	357.4	59.3
QUB01A	13.07	-47.0	0.0	5.101E-08	-53.3	64.3
QUB01A	13.07	-47.0	10.0	4.330E-08	-52.9	62.6
QUB01A	13.07	-47.0	20.0	4.286E-08	-54.6	58.8
QUB01B	12.20	-47.0	0.0	5.845E-08	-40.6	75.7
QUB01B	12.20	-47.0	10.0	4.751E-08	-52.7	66.9
QUB01B	12.20	-47.0	20.0	3.412E-08	-56.9	59.4
QUA01A	13.51	-60.0	0.0	5.563E-08	-0.5	74.0
QUA01A	13.51	-60.0	10.0	5.110E-08	-29.8	74.2
QUA01A	13.51	-60.0	20.0	4.340E-08	-31.2	77.9
QUA01B	13.81	-60.0	0.0	4.012E-08	-4.1	59.3
QUA01B	13.81	-60.0	10.0	4.762E-08	-25.6	58.1
QUA01B	13.81	-60.0	20.0	5.751E-08	-34.0	59.7
QTS01A	12.43	-62.0	0.0	5.618E-08	347.3	62.3
QTS01A	12.43	-62.0	10.0	4.769E-08	341.8	64.8
QTS01A	12.43	-62.0	20.0	4.029E-08	333.0	65.1
QTS01B	13.33	-62.0	0.0	5.227E-08	348.3	53.3
QTS01B	13.33	-62.0	10.0	4.400E-08	337.1	54.8
QTS01B	13.33	-62.0	20.0	3.598E-08	336.7	54.3
QTQ01A	12.43	-78.0	0.0	6.630E-08	337.1	50.0
QTQ01A	12.43	-78.0	5.0	6.053E-08	332.4	52.6
QTQ01A	12.43	-78.0	10.0	5.615E-08	326.4	52.1
QTQ01A	12.43	-78.0	20.0	4.678E-08	327.2	53.1
QTQ01B	12.53	-78.0	0.0	6.364E-08	-17.7	43.7
QTQ01B	12.53	-78.0	10.0	5.862E-08	-26.6	48.8
QTQ01B	12.53	-78.0	20.0	5.124E-08	-29.7	47.6
QTR01A	12.53	-106.0	0.0	5.486E-08	359.1	51.1
QTR01A	12.53	-106.0	5.0	4.883E-08	356.8	52.2
QTR01A	12.53	-106.0	10.0	4.492E-08	353.9	52.4
QTR01A	12.53	-106.0	20.0	3.895E-08	358.0	49.8
QTR01B	12.05	-106.0	0.0	4.486E-08	353.2	55.9

QTR01B	12.05	-106.0	2.5	4.236E-08	357.7	56.9
QTR01B	12.05	-106.0	5.0	4.098E-08	351.9	56.0
QTR01B	12.05	-106.0	10.0	3.936E-08	353.0	56.0
QTR01B	12.05	-106.0	20.0	3.237E-08	352.3	54.4
QTR01B	12.05	-106.0	30.0	2.714E-08	350.5	55.5
QTOB6A	13.95	-120.0	10.0	8.527E-08	-13.5	53.3
QTOB6A	13.95	-129.0	0.0	9.711E-08	-12.4	51.9
QTOB6A	13.95	-129.0	5.0	7.557E-08	-13.2	49.9
QTOB6A	13.95	-129.0	20.0	8.017E-08	-13.0	50.9
QTOB6A	13.95	-129.0	30.0	6.063E-08	-13.3	49.3
QTOB6B	12.42	-129.0	0.0	8.040E-08	-13.9	53.4
QTOB6B	12.42	-129.0	5.0	8.628E-08	-18.2	55.6
QTOB6B	12.42	-129.0	10.0	7.796E-08	-13.5	49.1
QTOB6B	12.42	-129.0	20.0	6.847E-08	-13.6	50.2
QTOB6B	12.42	-129.0	30.0	4.915E-08	-18.5	52.0
QTOB5A	11.83	-145.0	0.0	7.071E-08	-9.3	54.7
QTOB5A	11.83	-145.0	10.0	5.821E-08	-14.5	49.0
QTOB5A	11.83	-145.0	20.0	5.934E-08	-16.4	49.0
QTOB5B	11.54	-145.0	0.0	7.025E-08	-6.0	53.8
QTOB5B	11.54	-145.0	10.0	5.938E-08	-16.5	52.4
QTOB5B	11.54	-145.0	20.0	5.430E-08	-17.3	50.5
QTOB4A	12.08	-160.0	0.0	6.427E-08	-5.3	72.3
QTOB4A	12.08	-160.0	10.0	5.627E-08	-13.4	62.3
QTOB4A	12.08	-160.0	20.0	5.000E-08	-14.6	57.3
QTOB4B	12.15	-160.0	0.0	5.698E-08	-17.2	68.3
QTOB4B	12.15	-160.0	10.0	4.852E-08	-16.5	61.9
QTOB4B	12.15	-160.0	20.0	4.479E-08	-19.4	61.6
QTOB2A	12.94	-206.0	0.0	1.140E-07	-14.5	59.4
QTOB2A	12.94	-206.0	5.0	7.857E-08	-20.5	58.4
QTOB2A	12.94	-206.0	10.0	9.031E-08	-18.7	57.8
QTOB2A	12.94	-206.0	20.0	7.946E-08	-25.3	56.2
QTOB2A	12.94	-206.0	30.0	6.910E-08	-24.3	57.2
QTOB2B	13.07	-206.0	0.0	1.053E-07	-17.1	56.8
QTOB2B	13.07	-206.0	5.0	9.866E-08	-20.7	55.9
QTOB2B	13.07	-206.0	10.0	9.569E-08	-20.9	55.8
QTOB2B	13.07	-206.0	20.0	7.883E-08	-23.2	56.5
QTOB2B	13.07	-206.0	30.0	7.014E-08	-25.6	55.6
QTOB2C	13.76	-206.0	0.0	1.099E-07	-16.6	58.7
QTOB2C	13.76	-206.0	5.0	1.110E-07	-20.5	59.0
QTOB2C	13.76	-206.0	10.0	9.890E-08	-19.9	58.9
QTOB2C	13.76	-206.0	20.0	8.592E-08	-23.5	56.2
QTOB2C	13.76	-206.0	30.0	7.179E-08	-21.2	58.5
QTOB1B	10.43	-218.0	0.0	4.111E-08	-8.9	59.5
QTOB1B	10.43	-218.0	10.0	3.572E-08	-18.4	59.2
QTOB1B	10.43	-218.0	20.0	2.731E-08	-19.7	61.6
QTOB1C	10.71	-218.0	0.0	4.185E-08	-30.2	59.4
QTOB1C	10.71	-218.0	10.0	3.499E-08	-14.6	56.6
QTOB1C	10.71	-218.0	20.0	1.939E-08	-19.4	53.0
QTP01B	10.79	-250.0	0.0	6.245E-08	356.0	58.8
QTP01B	10.79	-250.0	5.0	5.878E-08	358.6	62.0
QTP01B	10.79	-250.0	10.0	5.345E-08	356.4	62.9
QTP01B	10.79	-250.0	20.0	4.429E-08	356.2	65.8
QTP01C	11.61	-250.0	0.0	8.237E-08	23.0	56.0
QTP01C	11.61	-250.0	2.5	7.937E-08	20.1	56.3

QTP01C	11.61	-250.0	5.0	7.577E-08	21.0	56.3
QTP01C	11.61	-250.0	10.0	6.891E-08	20.6	55.6
QTP01C	11.61	-250.0	20.0	5.813E-08	19.9	56.4
QTP01C	11.61	-250.0	30.0	5.018E-08	19.8	55.9
QTO01A	12.17	-266.0	0.0	1.409E-07	183.7	67.4
QTO01A	12.17	-266.0	5.0	1.358E-07	183.9	68.8
QTO01A	12.17	-266.0	10.0	1.273E-07	184.7	69.5
QTO01A	12.17	-266.0	20.0	1.131E-07	183.2	69.9
QTO01B	10.93	-266.0	10.0	6.376E-08	20.4	61.4
QTO01B	10.93	-266.0	20.0	5.451E-08	20.6	62.4
QTN01B	11.26	-281.0	0.0	1.013E-07	-8.7	59.2
QTN01B	11.26	-281.0	10.0	1.202E-07	-9.9	58.1
QTN01B	11.26	-281.0	20.0	1.012E-07	-10.6	60.3
QTN01C	11.18	-281.0	0.0	1.131E-07	353.1	60.8
QTN01C	11.18	-281.0	2.5	1.116E-07	353.1	61.0
QTN01C	11.18	-281.0	5.0	1.071E-07	353.5	60.8
QTN01C	11.18	-281.0	10.0	1.024E-07	351.1	60.6
QTN01C	11.18	-281.0	20.0	9.024E-08	350.6	60.6
QTN01C	11.18	-281.0	30.0	7.822E-08	350.2	61.3
QPA02	7.34	-285.5	0.0	9.124E-08	-33.0	54.6
QPA02	7.34	-285.5	5.0	8.584E-08	-31.7	55.1
QPA02	7.34	-285.5	10.0	7.888E-08	-31.4	53.8
QPA02	7.34	-285.5	20.0	6.688E-08	-31.6	54.9
QPA02	7.34	-285.5	30.0	5.841E-08	-32.6	54.5
QPA02	7.34	-285.5	45.0	4.543E-08	-34.5	55.3
QPA01B	13.19	-286.0	0.0	9.231E-08	45.7	66.4
QPA01B	13.19	-286.0	10.0	7.622E-08	41.2	67.2
QPA01B	13.19	-286.0	20.0	6.603E-08	42.5	67.1
QPA01B	13.19	-286.0	30.0	5.567E-08	36.1	66.6
QPA01B	13.19	-286.0	45.0	4.684E-08	41.6	68.1
QPA01C	13.00	-286.0	0.0	8.945E-08	9.2	63.5
QPA01C	13.00	-286.0	10.0	7.641E-08	2.1	66.3
QPA01C	13.00	-286.0	20.0	6.638E-08	3.4	65.5
QPA01C	13.00	-286.0	30.0	5.817E-08	9.9	67.3
QPA01C	13.00	-286.0	45.0	4.697E-08	1.6	65.3
QPA03	7.96	-287.0	0.0	7.888E-08	-38.0	60.5
QPA03	7.96	-287.0	5.0	7.737E-08	-40.3	61.1
QPA03	7.96	-287.0	10.0	7.067E-08	-38.8	62.1
QPA03	7.96	-287.0	20.0	5.936E-08	-39.3	62.1
QPA03	7.96	-287.0	30.0	5.096E-08	-39.7	62.6
QPA03	7.96	-287.0	45.0	3.972E-08	-41.8	64.6
QPB03	8.26	-288.0	0.0	6.454E-08	-15.4	70.6
QPB03	8.26	-288.0	10.0	4.757E-08	-16.6	70.1
QPB03	8.26	-288.0	20.0	4.241E-08	-11.6	71.2
QPB03	8.26	-288.0	30.0	3.628E-08	-15.4	72.1
QPB03	8.26	-288.0	45.0	2.849E-08	-6.2	72.0
QPB02	8.44	-291.5	0.0	7.873E-08	-59.7	84.8
QPB02	8.44	-291.5	10.0	6.590E-08	-88.0	86.2
QPB02	8.44	-291.5	20.0	5.781E-08	-100.3	85.4
QPB02	8.44	-291.5	30.0	5.336E-08	-129.9	85.6
QPB02	8.44	-291.5	45.0	4.363E-08	-107.0	86.4
QPB01A	13.21	-292.0	0.0	6.549E-08	88.4	57.6
QPB01A	13.21	-292.0	10.0	6.131E-08	97.5	58.8
QPB01A	13.21	-292.0	20.0	5.335E-08	100.5	56.7

QPB01A	13.21	-292.0	30.0	4.683E-08	104.8	57.7
QPB01A	13.21	-292.0	45.0	3.825E-08	101.2	52.5
QPB01B	12.67	-292.0	0.0	8.658E-08	130.5	72.3
QPB01B	12.67	-292.0	10.0	7.814E-08	139.7	69.9
QPB01B	12.67	-292.0	20.0	7.107E-08	141.0	69.7
QPB01B	12.67	-292.0	30.0	6.065E-08	143.5	69.5
QPB01B	12.67	-292.0	45.0	4.927E-08	145.5	70.0
QTM01A	11.45	-296.0	0.0	1.344E-07	87.2	58.0
QTM01A	11.45	-296.0	5.0	1.290E-07	92.9	57.4
QTM01A	11.45	-296.0	10.0	1.239E-07	94.2	57.6
QTM01A	11.45	-296.0	20.0	1.122E-07	96.8	57.5
QTM01C	12.09	-296.0	0.0	1.598E-07	101.1	69.8
QTM01C	12.09	-296.0	2.5	1.566E-07	102.1	69.6
QTM01C	12.09	-296.0	5.0	1.522E-07	104.2	70.2
QTM01C	12.09	-296.0	10.0	1.463E-07	105.5	69.6
QTM01C	12.09	-296.0	20.0	1.312E-07	103.2	69.2
QTM01C	12.09	-296.0	30.0	1.161E-07	105.2	69.3
QPC01B	12.45	-306.0	0.0	1.337E-07	49.0	56.0
QPC01B	12.45	-306.0	10.0	1.133E-07	53.8	57.0
QPC01B	12.45	-306.0	20.0	1.133E-07	53.8	57.0
QPC01B	12.45	-306.0	30.0	9.726E-08	53.3	56.4
QPC01B	12.45	-306.0	45.0	8.028E-08	56.4	56.8
QPC01B	12.45	-306.0	60.0	6.236E-08	53.4	55.6
QPC01C	12.22	-306.0	0.0	1.323E-07	42.2	42.8
QPC01C	12.22	-306.0	10.0	1.179E-07	46.5	43.9
QPC01C	12.22	-306.0	20.0	1.051E-07	46.9	44.8
QPC01C	12.22	-306.0	30.0	9.119E-08	46.2	44.6
QPC01C	12.22	-306.0	45.0	7.399E-08	47.3	44.3
QPD01A	11.94	-315.0	0.0	2.025E-07	5.3	51.4
QPD01A	11.94	-315.0	10.0	1.848E-07	5.9	50.8
QPD01A	11.94	-315.0	20.0	1.636E-07	5.3	50.9
QPD01A	11.94	-315.0	30.0	1.451E-07	4.9	50.8
QPD01A	11.94	-315.0	45.0	1.222E-07	4.1	51.9
QPD01B	11.13	-315.0	0.0	1.889E-07	32.0	57.0
QPD01B	11.13	-315.0	10.0	1.710E-07	30.0	57.1
QPD01B	11.13	-315.0	20.0	1.510E-07	29.3	57.1
QPD01B	11.13	-315.0	30.0	1.387E-07	28.9	57.6
QPD01B	11.13	-315.0	45.0	1.098E-07	28.8	57.8
QPD01C	11.55	-315.0	0.0	1.858E-07	56.8	47.6
QPD01C	11.55	-315.0	10.0	1.678E-07	59.1	47.3
QPD01C	11.55	-315.0	20.0	1.476E-07	58.7	47.7
QPD01C	11.55	-315.0	30.0	1.317E-07	60.0	47.7
QPD01C	11.55	-315.0	45.0	1.067E-07	59.6	48.4
QTL01B	12.75	-316.0	0.0	2.613E-07	37.8	70.3
QTL01B	12.75	-316.0	5.0	2.546E-07	39.7	70.7
QTL01B	12.75	-316.0	10.0	2.432E-07	40.3	71.1
QTL01B	12.75	-316.0	20.0	2.128E-07	40.2	71.5
QTL01B	12.75	-316.0	30.0	1.867E-07	39.5	72.0
QTL01B	12.75	-316.0	45.0	1.540E-07	41.4	73.3
QTL01B	12.75	-316.0	60.0	1.185E-07	40.3	72.7
QTL01C	11.86	-316.0	0.0	2.376E-07	37.0	71.0
QTL01C	11.86	-316.0	10.0	2.205E-07	36.2	71.6
QTL01C	11.86	-316.0	20.0	1.914E-07	35.4	72.9
QTL01C	11.86	-316.0	30.0	1.714E-07	38.1	73.6

QTL01C	11.86	-316.0	45.0	1.373E-07	37.4	72.5
QTL01C	11.86	-316.0	60.0	1.052E-07	36.8	73.0
QTL01D	12.34	-316.0	0.0	2.157E-07	74.0	48.1
QTL01D	12.34	-316.0	5.0	2.134E-07	74.1	48.7
QTL01D	12.34	-316.0	10.0	2.039E-07	73.2	49.4
QTL01D	12.34	-316.0	20.0	1.791E-07	73.9	50.3
QTL01D	12.34	-316.0	30.0	1.554E-07	73.5	50.2
QTL01D	12.34	-316.0	45.0	1.271E-07	74.1	51.0
QTL01E	11.23	-316.0	0.0	2.219E-07	83.8	65.5
QTL01E	11.23	-316.0	5.0	2.131E-07	84.0	65.4
QTL01E	11.23	-316.0	10.0	2.009E-07	86.7	65.7
QTL01E	11.23	-316.0	20.0	1.773E-07	86.5	66.2
QTL01E	11.23	-316.0	30.0	1.569E-07	87.8	66.0
QTL01E	11.23	-316.0	45.0	1.286E-07	87.7	66.4
QTK01B	12.22	-330.0	0.0	1.189E-07	77.8	60.4
QTK01B	12.22	-330.0	10.0	1.088E-07	84.8	60.9
QTK01B	12.22	-330.0	20.0	9.934E-08	85.9	61.1
QTK01C	12.95	-330.0	0.0	1.325E-07	32.7	70.4
QTK01C	12.95	-330.0	10.0	1.187E-07	37.7	72.7
QTK01C	12.95	-330.0	20.0	1.074E-07	39.1	73.1
QTJ01C	12.70	-347.0	0.0	1.226E-07	19.2	72.5
QTJ01C	12.70	-347.0	5.0	1.174E-07	16.4	74.6
QTJ01C	12.70	-347.0	10.0	1.126E-07	15.4	75.5
QTJ01C	12.70	-347.0	20.0	1.002E-07	13.4	75.5
QTJ01D	12.69	-347.0	0.0	1.242E-07	3.5	72.0
QTJ01D	12.69	-347.0	2.5	1.201E-07	4.4	71.6
QTJ01D	12.69	-347.0	5.0	1.168E-07	4.7	71.8
QTJ01D	12.69	-347.0	10.0	1.114E-07	4.1	71.9
QTJ01D	12.69	-347.0	20.0	9.900E-08	0.9	71.9
QTJ01D	12.69	-347.0	30.0	8.788E-08	1.4	71.3
QTI01B	13.12	-364.0	0.0	4.208E-08	32.6	59.2
QTI01B	13.12	-364.0	10.0	3.158E-08	39.7	71.7
QTI01B	13.12	-364.0	20.0	2.682E-08	38.6	69.4
QTI01C	13.05	-364.0	0.0	3.600E-08	48.5	50.3
QTI01C	13.05	-364.0	10.0	2.608E-08	60.5	55.2
QTI01C	13.05	-364.0	20.0	3.000E-08	47.1	51.9
QTH01B	13.96	-378.0	0.0	7.533E-08	80.9	55.2
QTH01B	13.96	-378.0	10.0	6.788E-08	93.6	56.5
QTH01B	13.96	-378.0	20.0	6.152E-08	93.6	57.2
QTH01C	12.78	-378.0	0.0	6.218E-08	73.9	53.4
QTH01C	12.78	-378.0	10.0	5.779E-08	87.9	56.9
QTH01C	12.78	-378.0	20.0	4.991E-08	91.2	58.2
QTG01C	11.59	-394.0	0.0	2.449E-08	21.0	48.7
QTG01C	11.59	-394.0	5.0	1.794E-08	4.4	61.4
QTG01C	11.59	-394.0	10.0	1.521E-08	2.0	60.8
QTG01C	11.59	-394.0	20.0	1.289E-08	7.6	60.5
QTG01D	12.56	-394.0	0.0	3.282E-08	25.6	35.0
QTG01D	12.56	-394.0	5.0	2.110E-08	32.7	34.8
QTG01D	12.56	-394.0	10.0	1.578E-08	33.0	31.6
QTG01D	12.56	-394.0	20.0	1.556E-08	34.9	29.5
QTF01B	12.44	-411.0	0.0	1.295E-07	16.4	38.2
QTF01B	12.44	-411.0	5.0	1.236E-07	17.1	38.1
QTF01B	12.44	-411.0	10.0	1.168E-07	15.8	38.2
QTF01B	12.44	-411.0	20.0	1.033E-07	15.2	38.3

QTF01C	12.05	-411.0	0.0	1.168E-07	30.5	39.7
QTF01C	12.05	-411.0	2.5	1.150E-07	29.9	39.5
QTF01C	12.05	-411.0	5.0	1.114E-07	30.1	39.3
QTF01C	12.05	-411.0	10.0	1.073E-07	29.2	39.4
QTF01C	12.05	-411.0	20.0	9.323E-08	30.8	39.1
QTF01C	12.05	-411.0	30.0	8.549E-08	31.9	39.9
QTE01B	12.20	-429.0	0.0	5.166E-08	83.3	63.8
QTE01B	12.20	-429.0	10.0	6.574E-08	97.2	65.2
QTE01B	12.20	-429.0	20.0	5.584E-08	96.5	67.6
QTE01D	13.05	-429.0	0.0	5.553E-08	59.4	54.4
QTE01D	13.05	-429.0	10.0	4.267E-08	71.7	56.9
QTE01D	13.05	-429.0	20.0	3.489E-08	75.2	54.2
QTD01A	12.77	-434.0	0.0	8.445E-08	-33.7	7.3
QTD01A	12.77	-434.0	10.0	5.132E-08	-36.0	6.1
QTD01A	12.77	-434.0	20.0	4.829E-08	-34.8	6.8
QTD01B	14.01	-434.0	0.0	1.019E-07	-13.4	45.3
QTD01B	14.01	-434.0	10.0	8.758E-08	-14.3	49.8
QTD01B	14.01	-434.0	20.0	7.264E-08	-16.3	50.5
QTC01B	12.73	-449.0	0.0	4.444E-08	-33.0	35.3
QTC01B	12.73	-449.0	10.0	3.891E-08	-42.1	37.2
QTC01B	12.73	-449.0	20.0	3.543E-08	-46.8	37.9
QTC01C	12.57	-449.0	0.0	4.331E-08	-57.8	27.6
QTC01C	12.57	-449.0	10.0	3.392E-08	-64.9	29.7
QTC01C	12.57	-449.0	20.0	1.814E-08	-63.5	24.6
QTB01B	13.04	-468.5	0.0	6.846E-08	13.4	42.9
QTB01B	13.04	-468.5	5.0	5.907E-08	14.6	45.3
QTB01B	13.04	-468.5	10.0	5.430E-08	15.3	46.1
QTB01B	13.04	-468.5	20.0	4.595E-08	13.2	46.0
QTB01C	12.48	-468.5	0.0	6.215E-08	28.7	64.9
QTB01C	12.48	-468.5	2.5	5.949E-08	26.1	66.0
QTB01C	12.48	-468.5	5.0	5.400E-08	23.4	64.2
QTB01C	12.48	-468.5	10.0	4.957E-08	20.9	65.8
QTB01C	12.48	-468.5	20.0	4.244E-08	17.4	65.1

Manyberries Section

QWC01B	11.60	60.0	0.0	3.496E-08	327.3	60.7
QWC01B	11.60	60.0	2.5	3.229E-08	338.7	53.0
QWC01B	11.60	60.0	5.0	2.930E-08	338.1	53.6
QWC01B	11.60	60.0	10.0	2.646E-08	338.7	48.3
QWC01B	11.60	60.0	20.0	2.171E-08	335.8	42.3
QWC01B	11.60	60.0	30.0	1.739E-08	342.7	47.1
QWC01C	11.76	60.0	0.0	3.400E-08	283.3	65.9
QWC01C	11.76	60.0	5.0	2.947E-08	326.3	66.2
QWC01C	11.76	60.0	10.0	2.556E-08	341.4	66.9
QWC01C	11.76	60.0	20.0	2.234E-08	314.2	67.8
QWX01B	10.33	46.0	0.0	3.116E-08	307.2	60.0
QWX01B	10.33	46.0	5.0	2.637E-08	333.5	59.8
QWX01B	10.33	46.0	10.0	2.456E-08	329.6	60.1
QWX01B	10.33	46.0	20.0	2.092E-08	326.6	54.5
QWX01C	10.86	46.0	0.0	3.577E-08	300.6	56.7
QWX01C	10.86	46.0	5.0	3.151E-08	325.1	56.6
QWX01C	10.86	46.0	10.0	2.868E-08	326.9	57.3

QWX01C	10.86	46.0	20.0	2.351E-08	334.4	55.5
QWW01B	10.22	14.0	0.0	6.611E-08	299.5	63.2
QWW01B	10.22	14.0	5.0	3.615E-08	326.9	53.5
QWW01B	10.22	14.0	10.0	2.430E-08	314.7	48.0
QWW01B	10.22	14.0	20.0	1.872E-08	326.9	35.1
QWW01C	10.20	14.0	0.0	1.263E-07	325.2	18.5
QWW01C	10.20	14.0	5.0	4.054E-08	342.3	73.2
QWW01C	10.20	14.0	10.0	2.952E-08	337.3	75.3
QWW01C	10.20	14.0	20.0	1.989E-08	356.1	77.4
QWW01C	10.20	14.0	30.0	1.690E-08	188.0	77.0
QWA01A	8.52	0.0	0.0	1.776E-07	340.8	75.3
QWA01A	8.52	0.0	5.0	1.562E-07	354.0	73.9
QWA01A	8.52	0.0	10.0	1.300E-07	355.8	75.2
QWA01A	8.52	0.0	20.0	8.990E-08	349.1	77.1
QWA01B	8.54	0.0	0.0	3.143E-08	347.2	68.7
QWA01B	8.54	0.0	2.5	2.871E-08	351.0	68.6
QWA01B	8.54	0.0	5.0	1.602E-07	352.0	68.8
QWA01B	8.54	0.0	10.0	1.300E-07	350.3	69.8
QWA01B	8.54	0.0	20.0	9.204E-08	350.2	71.7
QWA01B	8.54	0.0	30.0	7.294E-08	355.3	73.0
QWA01B	8.54	0.0	40.0	5.823E-08	356.5	72.7
QWA02B	8.38	0.0	0.0	1.492E-07	304.3	74.7
QWA02B	8.38	0.0	5.0	1.260E-07	319.7	77.5
QWA02B	8.38	0.0	10.0	1.055E-07	321.0	78.3
QWA02B	8.38	0.0	20.0	7.523E-08	322.7	77.5
QWA02C	8.56	0.0	0.0	1.662E-07	324.3	77.0
QWA02C	8.56	0.0	5.0	1.430E-07	338.1	76.9
QWA02C	8.56	0.0	10.0	1.210E-07	337.4	76.7
QWA02C	8.56	0.0	20.0	8.605E-08	340.8	76.8
QWL01B	11.92	-4.5	0.0	4.070E-08	322.5	37.1
QWL01B	11.92	-4.5	5.0	3.388E-08	325.9	31.2
QWL01B	11.92	-4.5	10.0	3.354E-08	320.6	27.6
QWL01B	11.92	-4.5	20.0	2.906E-08	320.8	22.8
QWL01C	12.11	-4.5	0.0	3.707E-08	314.9	46.2
QWL01C	12.11	-4.5	2.5	3.453E-08	324.6	45.2
QWL01C	12.11	-4.5	5.0	3.422E-08	327.1	42.5
QWL01C	12.11	-4.5	10.0	2.884E-08	326.3	40.4
QWL01C	12.11	-4.5	20.0	2.529E-08	332.4	40.7
QWL01C	12.11	-4.5	30.0	2.150E-08	329.2	32.5
QWL01C	12.11	-4.5	40.0	1.944E-08	329.8	34.5
QWL01C	12.11	-4.5	60.0	1.537E-08	329.8	34.9
QWL01C	12.11	-4.5	80.0	1.406E-08	328.2	34.2
QWL01C	12.11	-4.5	100.0	8.101E-09	342.7	45.5
QWV01C	11.38	-12.0	0.0	3.198E-08	353.2	52.0
QWV01C	11.38	-12.0	2.5	3.312E-08	347.2	47.5
QWV01C	11.38	-12.0	5.0	3.031E-08	351.3	44.8
QWV01C	11.38	-12.0	10.0	2.557E-08	349.7	43.9
QWV01C	11.38	-12.0	20.0	2.015E-08	349.3	39.0
QWV01C	11.38	-12.0	30.0	1.797E-08	350.3	44.2
QWV01D	11.72	-12.0	0.0	4.351E-08	342.2	60.0
QWV01D	11.72	-12.0	5.0	3.764E-08	355.0	58.2
QWV01D	11.72	-12.0	10.0	3.400E-08	357.4	57.6
QWV01D	11.72	-12.0	20.0	2.919E-08	357.7	55.8
QWN01C	12.01	-34.5	0.0	3.944E-08	307.1	43.8

QWN01C	12.01	-34.5	2.5	3.921E-08	308.9	39.9
QWN01C	12.01	-34.5	5.0	3.747E-08	307.3	41.3
QWN01C	12.01	-34.5	10.0	3.406E-08	306.7	39.7
QWN01C	12.01	-34.5	20.0	2.535E-08	303.5	38.7
QWN01C	12.01	-34.5	30.0	2.433E-08	305.5	39.0
QWQ01A	10.70	-57.5	0.0	5.413E-08	320.4	51.5
QWQ01A	10.70	-57.5	5.0	5.027E-08	325.8	49.1
QWQ01A	10.70	-57.5	10.0	4.479E-08	329.7	48.3
QWQ01A	10.70	-57.5	20.0	3.798E-08	332.0	48.0
QWQ01B	11.07	-57.5	0.0	5.260E-08	325.3	40.0
QWQ01B	11.07	-57.5	2.5	5.262E-08	328.9	38.6
QWQ01B	11.07	-57.5	5.0	4.830E-08	330.5	36.7
QWQ01B	11.07	-57.5	10.0	4.474E-08	332.4	38.5
QWQ01B	11.07	-57.5	20.0	3.762E-08	332.4	37.9
QWR01B	11.75	-79.5	0.0	2.500E-08	274.3	24.2
QWR01B	11.75	-79.5	5.0	2.036E-08	274.7	29.4
QWR01B	11.75	-79.5	10.0	1.889E-08	277.1	27.5
QWR01B	11.75	-79.5	20.0	1.269E-08	268.4	32.3
QWR01C	11.82	-79.5	0.0	2.825E-08	253.5	51.2
QWR01C	11.82	-79.5	2.5	2.404E-08	261.6	52.8
QWR01C	11.82	-79.5	5.0	2.329E-08	264.8	54.7
QWR01C	11.82	-79.5	10.0	2.164E-08	259.8	55.0
QWR01C	11.82	-79.5	20.0	1.802E-08	256.8	56.2
QWR01C	11.82	-79.5	30.0	1.470E-08	258.9	53.4
QSJ01B	11.14	154.5	0.0	2.788E-08	47.7	68.1
QSJ01B	11.14	154.5	5.0	2.226E-08	43.0	69.5
QSJ01B	11.14	154.5	10.0	1.972E-08	31.2	73.0
QSJ01B	11.14	154.5	20.0	1.641E-08	41.1	72.8
QSJ01C	10.54	154.5	0.0	2.553E-08	3.6	67.0
QSJ01C	10.54	154.5	10.0	2.066E-08	337.9	72.8
QSJ01C	10.54	154.5	20.0	1.749E-08	7.6	75.1
QSI01B	11.50	134.0	0.0	4.919E-08	71.0	73.2
QSI01B	11.50	134.0	5.0	5.289E-08	70.5	80.5

Diversion Lake Section

QSI01B	11.50	134.0	10.0	5.359E-08	62.2	81.2
QSI01B	11.50	134.0	20.0	4.331E-08	40.3	81.3
QSI01C	12.00	134.0	0.0	6.298E-08	39.7	69.4
QSI01C	12.00	134.0	10.0	5.176E-08	26.3	73.8
QSI01C	12.00	134.0	20.0	4.274E-08	29.7	74.9
QSH01B	10.50	111.0	0.0	8.053E-08	26.7	69.5
QSH01B	10.50	111.0	5.0	6.950E-08	8.5	69.0
QSH01B	10.50	111.0	10.0	6.312E-08	11.7	70.1
QSH01B	10.50	111.0	20.0	4.694E-08	2.2	72.4
QSH01C	10.77	111.0	0.0	5.187E-08	22.3	67.6
QSH01C	10.77	111.0	10.0	4.099E-08	18.1	71.6
QSH01C	10.77	111.0	20.0	3.046E-08	15.4	72.8
QSG01B	11.76	90.5	0.0	4.195E-08	10.7	71.2
QSG01B	11.76	90.5	5.0	3.581E-08	1.9	73.3
QSG01B	11.76	90.5	10.0	3.674E-08	-7.5	75.9
QSG01B	11.76	90.5	20.0	2.178E-08	-15.7	76.2
QSG01C	10.33	90.5	0.0	2.632E-08	-2.3	72.9

QSG01C	10.33	90.5	10.0	1.881E-08	-24.5	61.0
QSF01A	12.39	70.0	0.0	6.800E-08	30.3	63.3
QSF01A	12.39	70.0	5.0	6.655E-08	13.6	70.1
QSF01A	12.39	70.0	10.0	5.875E-08	13.8	68.3
QSF01A	12.39	70.0	20.0	4.272E-08	10.8	71.0
QSF01B	10.46	70.0	0.0	8.050E-08	36.2	70.6
QSF01B	10.46	70.0	10.0	6.088E-08	25.2	72.1
QSF01B	10.46	70.0	20.0	4.834E-08	6.6	75.8
QSE01B	10.49	21.5	0.0	2.740E-08	30.7	56.4
QSE01B	10.49	21.5	5.0	2.922E-08	15.0	68.3
QSE01B	10.49	21.5	10.0	1.961E-08	12.5	64.5
QSE01B	10.49	21.5	20.0	1.831E-08	0.8	68.3
QSE01C	11.17	21.5	0.0	4.181E-08	29.7	69.4
QSE01C	11.17	21.5	10.0	2.566E-08	14.7	71.0
QSE01C	11.17	21.5	20.0	2.190E-08	358.8	74.0
QSD01B	11.43	9.0	0.0	8.554E-08	46.2	60.3
QSD01B	11.43	9.0	5.0	6.844E-08	26.1	68.5
QSD01B	11.43	9.0	10.0	4.307E-08	21.5	69.5
QSD01B	11.43	9.0	20.0	4.591E-08	18.0	70.2
QSC01B	11.04	-3.5	0.0	5.021E-08	44.1	64.1
QSC01B	11.04	-3.5	5.0	3.689E-08	31.8	68.0
QSC01B	11.04	-3.5	10.0	3.271E-08	25.2	68.5
QSC01B	11.04	-3.5	20.0	2.544E-08	20.2	67.8
QSB01A	11.87	-9.0	0.0	6.634E-08	32.2	70.9
QSB01A	11.87	-9.0	5.0	5.304E-08	27.9	76.1
QSB01A	11.87	-9.0	10.0	4.000E-08	13.7	69.9
QSB01A	11.87	-9.0	20.0	2.988E-08	31.7	66.7
QSB01B	11.23	-9.0	0.0	7.273E-08	65.5	72.9
QSB01B	11.23	-9.0	10.0	4.667E-08	57.5	80.4
QSB02B	11.84	-10.0	0.0	9.011E-08	12.9	60.4
QSB02B	11.84	-10.0	5.0	7.259E-08	-2.6	63.1
QSB02B	11.84	-10.0	10.0	5.944E-08	-15.6	62.6
QSB02B	11.84	-10.0	20.0	4.714E-08	-11.9	60.7
QSB02C	11.56	-10.0	0.0	8.923E-08	2.2	69.6
QSB02C	11.56	-10.0	10.0	7.477E-08	323.8	68.3
QSB02C	11.56	-10.0	20.0	5.166E-08	4.8	66.6
QSA01B	11.84	-26.0	0.0	4.997E-08	9.4	47.0
QSA01B	11.84	-26.0	10.0	3.491E-08	31.5	55.1
QSA01B	11.84	-26.0	20.0	2.896E-08	17.4	55.6
QSA01C	11.82	-26.0	0.0	4.727E-08	6.0	54.7
QSA01C	11.82	-26.0	5.0	3.041E-08	15.9	61.2
QSA01C	11.82	-26.0	10.0	3.115E-08	49.7	63.0

APPENDIX 3

The data used in Chapter 3 is listed here in the same format used Appendix 2. Distances are measured from the Cherryville Tephra.

Riggins Road Data

QJA01	9.52	0.0	0.0	1.401E-06	8.1	54.3
QJA01	9.52	0.0	2.5	1.335E-06	9.1	53.5
QJA01	9.52	0.0	5.0	1.237E-06	11.2	52.7
QJA01	9.52	0.0	10.0	1.019E-06	12.2	47.9
QJA01	9.52	0.0	15.0	9.230E-07	15.0	49.3
QJA01	9.52	0.0	20.0	7.622E-07	16.6	47.0
QJA01	9.52	0.0	30.0	1.520E-06	18.2	72.7
QJA01	9.52	0.0	40.0	2.316E-07	22.7	44.4
QJA02	9.68	0.0	0.0	1.624E-06	1.7	63.2
QJA02	9.68	0.0	10.0	1.245E-06	4.6	59.0
QJB01	10.03	-15.0	0.0	3.649E-07	7.1	64.0
QJB01	10.03	-15.0	10.0	3.181E-07	11.4	61.4
QJB02	10.91	-15.0	0.0	3.940E-07	14.2	66.8
QJB02	10.91	-15.0	10.0	3.363E-07	15.2	64.1
QJC01	11.44	-30.0	0.0	1.474E-07	356.5	65.3
QJC01	11.44	-30.0	10.0	1.248E-07	0.2	63.3
QJC02	10.93	-30.0	0.0	2.103E-07	5.7	69.9
QJC02	10.93	-30.0	10.0	1.484E-07	9.0	66.7
QJD01	10.68	-46.0	0.0	2.521E-06	8.5	66.9
QJD01	10.68	-46.0	10.0	2.356E-06	8.0	66.6
QJD02	10.78	-46.0	0.0	2.261E-06	7.3	69.0
QJD02	10.78	-46.0	10.0	2.133E-06	7.8	68.8
QJE01	10.43	-64.0	0.0	9.361E-07	7.1	73.4
QJE01	10.43	-64.0	10.0	8.539E-07	6.8	73.1
QJE02	10.34	-64.0	0.0	7.209E-07	14.2	68.6
QJE02	10.34	-64.0	10.0	6.989E-07	13.8	56.2
QJF01	10.44	-88.0	0.0	2.047E-07	3.4	63.0
QJF01	10.44	-88.0	10.0	1.339E-07	2.4	59.4
QJF02	10.46	-88.0	0.0	1.895E-07	1.5	71.1
QJF02	10.46	-88.0	10.0	1.151E-07	0.9	68.4
QJG01	10.23	-108.0	0.0	4.092E-07	3.5	71.4
QJG01	10.23	-108.0	10.0	3.268E-07	4.8	72.2
QJG02	10.60	-108.0	0.0	3.244E-07	2.1	67.4
QJG02	10.60	-108.0	10.0	2.587E-07	6.3	67.0
QJH01	9.32	-122.0	0.0	7.362E-07	8.3	70.8
QJH01	9.32	-122.0	2.5	7.156E-07	7.6	70.4
QJH01	9.32	-122.0	5.0	6.940E-07	7.5	70.4
QJH01	9.32	-122.0	10.0	6.477E-07	7.9	69.7
QJH01	9.32	-122.0	15.0	5.762E-07	7.9	69.4
QJH01	9.32	-122.0	20.0	5.183E-07	7.8	69.1
QJH01	9.32	-122.0	30.0	3.739E-07	9.3	66.8
QJH01	9.32	-122.0	40.0	2.329E-07	10.1	70.9

QJH02	10.77	-122.0	0.0	1.474E-06	12.8	68.8
QJH02	10.77	-122.0	10.0	1.184E-06	11.7	64.9
QJI01	10.19	-137.0	0.0	8.113E-07	5.9	68.1
QJI01	10.19	-137.0	10.0	6.618E-07	0.9	66.9
QJI02	10.35	-137.0	0.0	3.308E-07	6.6	66.6
QJI02	10.35	-137.0	10.0	2.681E-07	4.0	64.1
QJJ01	10.15	-155.0	0.0	2.255E-06	353.0	74.8
QJJ01	10.15	-155.0	10.0	1.825E-06	352.6	72.4
QJJ02	10.21	-155.0	0.0	1.407E-06	357.6	70.9
QJJ02	10.21	-155.0	10.0	1.115E-06	360.0	68.2
QJK01	10.00	-171.0	0.0	2.333E-06	7.6	71.5
QJK01	10.00	-171.0	10.0	1.980E-06	7.7	70.8
QJK02	9.92	-171.0	0.0	1.894E-06	13.2	70.1
QJK02	9.92	-171.0	10.0	1.584E-06	14.8	69.8
QJL01	9.89	-188.0	0.0	6.314E-07	12.3	69.2
QJL01	9.89	-188.0	10.0	4.286E-07	13.6	67.8
QJL02	10.00	-188.0	0.0	6.365E-07	6.1	67.0
QJL02	10.00	-188.0	10.0	4.305E-07	7.5	64.0
QJM01	10.26	-208.0	0.0	1.341E-06	3.6	72.3
QJM01	10.26	-208.0	10.0	1.045E-06	0.5	70.7
QJM02	10.40	-208.0	0.0	9.938E-07	347.5	76.7
QJM02	10.40	-208.0	10.0	7.537E-07	351.3	75.2
QJN01	10.39	-224.0	0.0	1.449E-06	1.1	69.8
QJN01	10.39	-224.0	10.0	1.233E-06	359.6	68.6
QJN02	10.32	-224.0	0.0	2.263E-06	15.2	71.6
QJN02	10.32	-224.0	10.0	1.956E-06	9.2	69.1
QJO01	7.85	-244.0	0.0	1.652E-06	4.1	71.2
QJO01	7.85	-244.0	10.0	1.389E-06	0.2	69.6
QJO02	9.55	-244.0	0.0	1.817E-06	12.9	71.8
QJO02	9.55	-244.0	10.0	1.482E-06	5.5	68.4
QJP01	10.96	-268.0	0.0	2.499E-07	1.1	70.9
QJP01	10.96	-268.0	2.5	2.330E-07	2.6	71.4
QJP01	10.96	-268.0	5.0	2.201E-07	1.7	70.7
QJP01	10.96	-268.0	10.0	2.137E-07	359.3	69.9
QJP01	10.96	-268.0	15.0	1.924E-07	0.6	69.4
QJP01	10.96	-268.0	20.0	1.631E-07	357.2	70.4
QJP01	10.96	-268.0	30.0	1.172E-07	5.1	66.2
QJP01	10.96	-268.0	40.0	1.087E-07	28.9	41.1
QJP02	11.02	-268.0	0.0	4.128E-07	0.1	70.6
QJP02	11.02	-268.0	10.0	3.437E-07	357.1	70.3
QJQ01	10.36	-289.0	0.0	3.255E-07	344.9	66.9
QJQ01	10.36	-289.0	10.0	2.465E-07	347.0	64.7
QJQ02	10.48	-289.0	0.0	1.682E-07	3.5	70.0
QJQ02	10.48	-289.0	10.0	1.180E-07	7.7	67.9
QJR01	10.91	-304.0	0.0	2.409E-07	7.8	72.3
QJR01	10.91	-304.0	10.0	1.423E-07	6.9	71.1
QJR02	11.00	-304.0	0.0	2.244E-07	14.3	74.2
QJR02	11.00	-304.0	10.0	1.472E-07	13.2	72.1
QJS01	10.45	-328.0	0.0	1.425E-07	20.9	75.0
QJS01	10.45	-328.0	10.0	9.293E-08	14.9	70.6
QJS02	10.41	-328.0	0.0	1.671E-07	3.3	72.7
QJS02	10.41	-328.0	10.0	8.585E-08	2.9	70.5
QJT01	10.67	-346.0	0.0	2.331E-07	11.9	67.5
QJT01	10.67	-346.0	2.5	2.125E-07	11.6	66.8

QJT01	10.67	-346.0	5.0	2.094E-07	11.1	65.4
QJT01	10.67	-346.0	10.0	1.618E-07	9.9	66.9
QJT01	10.67	-346.0	15.0	1.036E-07	9.6	66.2
QJT01	10.67	-346.0	20.0	6.219E-08	11.4	64.0
QJT01	10.67	-346.0	30.0	4.946E-08	10.4	65.3
QJT01	10.67	-346.0	40.0	3.127E-08	9.0	69.7
QJT02	10.56	-346.0	0.0	2.033E-07	6.8	68.4
QJT02	10.56	-346.0	10.0	1.362E-07	5.7	65.5
QJU01	10.40	-365.0	0.0	2.312E-07	358.0	75.1
QJU01	10.40	-365.0	10.0	1.622E-07	357.6	74.1
QJU02	10.76	-365.0	0.0	1.972E-07	0.1	64.4
QJU02	10.76	-365.0	10.0	1.280E-07	358.9	61.8
QIK01	10.44	-380.0	0.0	2.013E-07	14.1	66.5
QIK01	10.44	-380.0	10.0	1.610E-07	11.2	64.1
QIK02	10.66	-380.0	0.0	1.812E-07	3.1	72.5
QIK02	10.66	-380.0	10.0	1.315E-07	3.0	67.6
QJV01	10.88	-400.0	0.0	1.405E-07	359.6	70.0
QJV01	10.88	-400.0	10.0	8.296E-08	359.0	69.5
QJV02	10.42	-400.0	0.0	1.231E-07	357.4	59.6
QJV02	10.42	-400.0	10.0	7.041E-08	354.6	51.9
QJW01	9.73	-419.0	0.0	3.167E-07	357.4	66.9
QJW01	9.73	-419.0	2.5	2.914E-07	357.1	65.0
QJW01	9.73	-419.0	5.0	2.639E-07	353.9	63.4
QJW01	9.73	-419.0	10.0	2.011E-07	354.4	62.1
QJW01	9.73	-419.0	15.0	1.415E-07	356.7	58.7
QJW01	9.73	-419.0	20.0	1.067E-07	352.8	61.5
QJW01	9.73	-419.0	30.0	6.084E-08	330.5	69.5
QJW01	9.73	-419.0	40.0	4.063E-08	1.1	48.1
QJW02	9.97	-419.0	0.0	2.380E-07	13.0	67.8
QJW02	9.97	-419.0	10.0	1.210E-07	6.3	61.7
QJX01	9.56	-439.0	0.0	6.518E-07	3.4	63.1
QJX01	9.56	-439.0	10.0	4.113E-07	2.4	60.9
QJX02	10.03	-439.0	0.0	6.427E-07	8.5	65.1
QJX02	10.03	-439.0	10.0	4.031E-07	7.3	63.1
QJY01	9.60	-459.0	0.0	1.347E-07	17.0	63.9
QJY01	9.60	-459.0	10.0	8.951E-08	15.5	57.8
QJY02	8.10	-459.0	0.0	1.226E-07	15.6	77.9
QJY02	8.10	-459.0	10.0	6.637E-08	13.9	74.3
QJZ01	8.99	-502.0	0.0	7.572E-08	18.9	63.1
QJZ01	8.99	-502.0	2.5	6.983E-08	16.4	61.2
QJZ01	8.99	-502.0	5.0	6.209E-08	12.0	61.2
QJZ01	8.99	-502.0	10.0	4.854E-08	17.3	59.0
QJZ01	8.99	-502.0	15.0	4.214E-08	13.6	54.0
QJZ01	8.99	-502.0	20.0	3.461E-08	22.0	75.0
QJZ01	8.99	-502.0	30.0	2.524E-08	19.1	56.6
QJZ01	8.99	-502.0	40.0	1.817E-08	71.0	79.1
QJZ02	8.77	-502.0	0.0	4.532E-08	7.7	65.9
QJZ02	8.77	-502.0	10.0	2.552E-08	357.2	60.7
QIA01	10.69	-519.0	0.0	1.148E-07	16.0	59.6
QIA01	10.69	-519.0	10.0	6.782E-08	13.2	57.0
QIA02	10.98	-519.0	0.0	9.545E-08	21.1	58.0
QIA02	10.98	-519.0	10.0	4.273E-08	22.3	57.3
QIB01	10.24	-540.0	0.0	2.899E-07	12.6	74.0
QIB01	10.24	-540.0	10.0	1.401E-07	11.9	69.3

QIB02	10.33	-540.0	0.0	2.215E-07	23.2	78.3
QIB02	10.33	-540.0	10.0	9.641E-08	15.6	71.7
QIC01	10.04	-557.0	0.0	8.892E-07	6.7	66.4
QIC01	10.04	-557.0	10.0	6.968E-07	6.7	63.3
QIC02	9.94	-557.0	0.0	1.536E-06	6.8	71.6
QIC02	9.94	-557.0	10.0	1.274E-06	4.4	70.1
QID01	10.87	-576.0	0.0	5.210E-07	5.9	71.5
QID01	10.87	-576.0	10.0	4.346E-07	1.6	70.0
QID02	10.45	-576.0	0.0	2.288E-07	358.5	69.8
QID02	10.45	-576.0	10.0	1.820E-07	349.1	67.9
QIE01	11.38	-596.0	0.0	9.711E-08	358.6	76.9
QIE01	11.38	-596.0	2.5	7.281E-08	356.3	75.3
QIE01	11.38	-596.0	5.0	6.975E-08	357.5	74.2
QIE01	11.38	-596.0	10.0	5.599E-08	357.2	73.7
QIE01	11.38	-596.0	15.0	4.902E-08	353.0	79.4
QIE01	11.38	-596.0	20.0	5.903E-08	43.6	56.8
QIE01	11.38	-596.0	30.0	5.967E-08	27.7	17.7
QIE01	11.38	-596.0	40.0	2.629E-08	353.0	60.1
QIE01	11.38	-596.0	50.0	1.659E-08	25.6	69.6
QIE01	11.38	-596.0	60.0	4.380E-09	306.2	75.9
QIE02	10.71	-596.0	0.0	2.249E-07	6.6	77.4
QIE02	10.71	-596.0	10.0	1.503E-07	0.6	74.6
QIE02	10.71	-596.0	15.0	1.240E-07	1.8	73.0
QIE02	10.71	-596.0	17.5	1.025E-07	4.0	71.7
QIE02	10.71	-596.0	20.0	1.157E-07	9.9	73.5
QIE02	10.71	-596.0	22.5	1.027E-07	26.5	72.7
QIE02	10.71	-596.0	25.0	9.383E-08	6.5	73.6
QIE02	10.71	-596.0	27.5	9.083E-08	15.5	73.9
QIE02	10.71	-596.0	30.0	8.779E-08	10.3	71.4
QIE02	10.71	-596.0	32.5	8.195E-08	11.5	72.7
QIE02	10.71	-596.0	35.0	7.190E-08	357.3	71.6
QIE02	10.71	-596.0	37.5	7.100E-08	63.1	65.2
QIE02	10.71	-596.0	40.0	6.521E-08	21.5	69.7
QIE02	10.71	-596.0	42.5	6.949E-08	1.6	69.7
QIE02	10.71	-596.0	45.0	5.760E-08	1.8	69.4
QIE02	10.71	-596.0	47.5	5.292E-08	13.7	73.1
QIE02	10.71	-596.0	50.0	4.550E-08	7.2	70.3
QIE02	10.71	-596.0	52.5	4.835E-08	6.6	71.4
QIE02	10.71	-596.0	55.0	3.507E-08	14.3	70.2
QIE02	10.71	-596.0	60.0	2.693E-08	22.9	67.1
QIE02	10.71	-596.0	65.0	2.270E-08	341.6	66.5
QIE02	10.71	-596.0	70.0	1.384E-08	39.3	75.9
QIF01	10.98	-616.0	0.0	1.181E-07	10.0	75.4
QIF01	10.98	-616.0	10.0	7.326E-08	6.4	71.8
QIF02	11.56	-616.0	0.0	1.068E-07	1.0	80.9
QIF02	11.56	-616.0	10.0	6.841E-08	4.5	73.6
QIG01	10.51	-634.0	0.0	1.776E-07	15.0	73.1
QIG01	10.51	-634.0	10.0	1.134E-07	12.7	70.0
QIG02	10.64	-634.0	0.0	1.719E-07	20.9	72.0
QIG02	10.64	-634.0	10.0	1.115E-07	14.1	68.6
QIH01	10.86	-655.0	0.0	2.622E-07	3.2	75.0
QIH01	10.86	-655.0	2.5	2.240E-07	5.1	74.9
QIH01	10.86	-655.0	10.0	1.681E-07	6.6	73.1
QIH01	10.86	-655.0	15.0	1.347E-07	8.0	68.7

QIH01	10.86	-655.0	20.0	1.058E-07	0.2	72.6
QIH01	10.86	-655.0	30.0	7.916E-08	14.7	48.1
QIH01	10.86	-655.0	40.0	5.204E-08	10.2	51.6
QIH02	10.33	-655.0	0.0	1.149E-07	333.2	83.9
QIH02	10.33	-655.0	10.0	5.291E-08	8.9	77.5
QIH02	10.33	-655.0	15.0	4.047E-08	358.8	78.2
QIH02	10.33	-655.0	20.0	2.672E-08	6.1	76.5
QII01	9.83	-670.0	0.0	1.348E-07	7.8	70.3
QII01	9.83	-670.0	10.0	7.203E-08	2.7	65.4
QII02	10.81	-670.0	0.0	2.005E-07	7.2	74.0
QII02	10.81	-670.0	10.0	1.083E-07	3.8	72.2
QIJ01	11.01	-686.0	0.0	7.046E-07	3.9	71.6
QIJ01	11.01	-686.0	10.0	4.962E-07	1.8	68.9
QIJ02	11.28	-686.0	0.0	8.460E-07	8.3	62.7
QIJ02	11.28	-686.0	10.0	5.971E-07	5.7	60.8

APPENDIX 4

FORTRAN Listing of Synthetic Data Generating Program "WRTFREQ"

```
      COMPLEX CX(50),CX1,CX2,CX3
C     This program (WRTFREQ) produces a synthetic sequence of
C     paleomagnetic directions (specified length N)
C     containing a maximum of three superimposed looping
C     signals of arbitrary frequency, sense,
C     ellipticity, and amplitude.
C     Fisherian noise of arbitrary level may
C     be added to the data.
C     The data can be produced at non uniform intervals of
C     time if a file containing N times is provided through
C     unit 2 (format (7f9.4)).
C     Output is onto a file attached to unit 1 and is a
C     sequence of declinations and inclinations suitable for
C     input into Maxent (2f9.4).
C     If this program is compiled along with the attached
C     subroutine (Rotate) then it can be run as follows:
C    R -LOAD#+*IMSLLIB 1=OUTPUT 2=TIMES
      REAL LEVEL(50),INC,DINC2(50),THETA(50)
      SCALE=1.0
      RAD=57.29576
      PI=2.0*ARCOS(-1.0)
      WRITE(6,101)
      READ(5,100) P1,P2,P3
      WRITE(3,102)
      READ(8,100) B1,B2,B3,A1,A2,A3,SD
      SD=SD/RAD
      SD=(1.-COS(SD))
      WRITE(6,103)
      READ(5,100) AVEDEC,AVEINC
      AVEDEC=AVEDEC/RAD
      AVEINC=(90.-AVEINC)/RAD
      F1=1./P1
      F2=1./P2
      F3=1./P3
      WRITE(6,105)
      READ(7,106) IX
      CALL GGUB(IX,1,VV)
      W1=F1*PI
      W2=F2*PI
      W3=F3*PI
      WRITE(6,104)
      READ(5,100) SPACE
      IF(SPACE.EQ.0.0) GOTO 3
      DO 4 I=1,50
    4 READ(2,100) LEVEL(I)
      SCALE=50.0/LEVEL(50)
    3 CONTINUE
      XTOT=0.
      CALL GGUB(IX,50,THETA)
```

```
      CALL GGEXP(IX,SD,50,DINC2)
      DO 1 I=1,50
      IF(SPACE.EQ.0.0) LEVEL(I)=FLOAT(I)
      LEVEL(I)=LEVEL(I)*SCALE
      CX1=CMPLX(COS(W1*LEVEL(I)),SIN(W1*LEVEL(I)))
      CX2=CMPLX(COS(W2*LEVEL(I)),SIN(W2*LEVEL(I)))
      CX3=CMPLX(COS(W3*LEVEL(I)),SIN(W3*LEVEL(I)))
      CX(I)=A1*CX1+B1*CONJG(CX1)+A2*CX2+B2*CONJG(CX2)
     #+A3*CX3+B3*CONJG(CX3)
      DEC=ATAN2(-AIMAG(CX(I)),REAL(CX(I)))
      INC=(90.-CABS(CX(I)))/RAD
      X=COS(DEC)*COS(INC)
      Y=SIN(DEC)*COS(INC)
      Z=SIN(INC)
      DINC1=PI/4.-INC
      DINC2(I)=ARCOS(1.-ABS(DINC2(I)))+DINC1
      CALL ROTATE(X,Y,-DEC)
      CALL ROTATE(Z,X,-DINC2(I))
      THETA(I)=THETA(I)*PI
      CALL ROTATE(X,Y,THETA(I))
      CALL ROTATE(Z,X,DINC1)
      CALL ROTATE(X,Y,DEC)
      CALL ROTATE(Z,X,AVEINC)
      CALL ROTATE(X,Y,AVEDEC)
      DEC=ATAN2(Y,X)*RAD
      INC=ARSIN(Z/SQRT(X*X+Y*Y+Z*Z))*RAD
    1 WRITE(1,100) DEC,INC
      WRITE(4,106) IX
      WRITE(3,100) F1,F2,F3
  100 FORMAT(7F9.4)
  101 FORMAT('ENTER 3 PERIODS (REAL)')
  102 FORMAT('ENTER 3 CLOCKWISE THEN 3 COUNTERCLOCKWISE ',
     #'AMPLITUDES THEN STANDARD DEVIATION (DEGREES)')
  103 FORMAT('AVERAGE DECLINATION, AVERAGE INCLINATION;')
  104 FORMAT('ENTER 0.0 FOR EQUAL SPACING; ',
     #'ENTER 1.0 OTHERWISE')
  105 FORMAT('ENTER IX')
  106 FORMAT(I20)
      STOP
      END
      SUBROUTINE ROTATE(X,Y,ANGLE)
C     SUBROUTINE ROTATE WILL ROTATE A UNIT VECTOR CLOCKWISE
C     ABOUT THE X, Y, OR Z AXIS BY THE NUMBER OF RADIANS
C     GIVEN IN THE INPUT PARAMETER "ANGLE". THE FIRST TWO
C     PARAMETERS ARE THE VECTOR COMPONENTS WHICH WILL BE
C     AFFECTED BY THE ROTATION. IT IS IMPORTANT THAT THEY
C     BE ENTERED IN THE ORDER (Y FOLLOWS X, Z FOLLOWS Y,
C     OR X FOLLOWS Z). THE MODIFIED COMPONENTS ARE STORED
C     BACK INTO THESE TWO INPUT VARIABLES.
      XX=X*COS(ANGLE)-Y*SIN(ANGLE)
      Y=Y*COS(ANGLE)+X*SIN(ANGLE)
      X=XX
      RETURN
      END
```

Seed Integers Used in Chapter 4

926686201
748021105
1448281358
630620298
840290746
1680343038
1310233148
1397963139
1154274150
1116012542
840290746
1577741978
1607589824

APPENDIX 5

FORTRAN Listing of Complex Maximum Entropy Routine for Analysing Paleomagnetic Data

```
      COMPLEX CX(120),CB1(120),CB2(120),COM,CA(120),
     #CAA(120),CONJ
C     This program (Maxent) calculates and plots the
C     complex spectrum of a paleomagnetic time sequence.
C     Input is through unit 1 and is assumed to be a file
C     containing declination and inclination pairs
C     (one pair to a line) in the format (2f9.2).
C     Equal spacing in time between consecutive pairs
C     is also assumed.
C     The remanance directions are mapped onto
C     the complex plane about their vector mean
C     as suggested by Denham (1975).
C     The resulting time series is then analysed using the
C     maximum entropy routine given in Anderson (1974)
C     (Anderson's routine had to be modified slightly so
C     that it would accept complex data).
C     The program can simply list the power densities (in
C     degrees squared per unit frequency) associated
C     with the principal peaks of the spectrum or it can
C     produce a power density plot (on Calcomp) as well.
C     The user may also integrate under spectral peaks to
C     obtain the power (amplitude squared) over a given
C     frequency range.
C     The FPE criterion of Ulrich and Bishop (1975) will
C     be used to automatically choose a filter length
C     appropriate for the data if the user wishes.
C     If the automatic picking feature is used, then only
C     filter lengths between 6 and N/2 (N = number of
C     data points) will be considered.
C     The FPE must also have a "proper" minimum within
C     this range of filter lengths or no filter length
C     will be chosen.
C     If this program is compiled along with the attached
C     subroutines it may then be run as follows:
C    R -LOAD#+*IMSLLIB+*PLOTLIB+ALAB:ARCHIVE
C     +ALAB:O.BLOCKDATA 1=I 9=-P T=1M
C     Where "I" is the input file of remanance directions
C     and "-P" is the plot description file.
      REAL X(430),Y2(430),Y(430),INC,Z(120),F(50),PO1(50)
     #,PO2(3),PHS(50)
      INTEGER ITITLE(10),IR(430)
      DATA RAD,AVEX,AVEY,AVEZ,AVEDEC,AVEPOW,CC,XMIN,XMAX,
     #SCALE,ISPEC/57.29576,
     #0.,0.,0.,0.,0.,.1E07,-.5,.5,1.,0/
      PI=6.2831853
      DO 1 I=1,100
      READ(1,99,END=10) DEC,INC
      DEC=DEC/RAD
      INC=INC/RAD
```

```
      X(I)=COS(INC)*COS(DEC)
      Z(I)=SIN(INC)
      Y(I)=COS(INC)*SIN(DEC)
      AVEX=AVEX+X(I)
      AVEY=AVEY+Y(I)
    1 AVEZ=AVEZ+Z(I)
   10 N=I-1
      C=CC/FLOAT(N)
      AVEX=AINT(AVEX*C)/CC
      AVEY=AINT(AVEY*C)/CC
      AVEZ=AVEZ/FLOAT(N)
      IF(ABS(AVEX)+ABS(AVEY).NE.0.0) AVEDEC=
     #-ATAN2(AVEY,AVEX)
      AVEINC=-ARCOS(AVEZ/SQRT(AVEX**2+AVEY**2+AVEZ**2))
      DO 2 I=1,N
      CALL ROTATE(X(I),Y(I),AVEDEC)
      CALL ROTATE(Z(I),X(I),AVEINC)
      DEC=ATAN2(Y(I),X(I))
      INC=ARSIN(Z(I))*RAD
      X(I)=(90.0-INC)*COS(DEC)
    2 Y(I)=(90.0-INC)*SIN(DEC)
      DO 3 I=1,N
    3 CX(I)=CMPLX(X(I),Y(I))
      DO 60 I=1,N
   60 AVEPOW=AVEPOW+CABS(CX(I))**2
      AVEPOW=AVEPOW/FLOAT(N)
      WRITE(6,107) AVEPOW
      WRITE(6,116)
      READ(5,101) IFPE
      IF(IFPE.EQ.0) GOTO 64
      MM=N/2
      GOTO 65
   64 WRITE(6,102)
      READ(5,101) MM
      IF(MM.EQ.0) STOP
      mm=mm-1
   66 WRITE(6,108)
      READ(5,101) ISPEC
   65 CONTINUE
      COMMON CX,CAA,CB1,CB2,CA,COM,CONJ,Z,P0,PI,MM,N,ERR
      EXTERNAL POWER
      CALL MAXENT
      IF(ISPEC.EQ.1) GOTO 89
      IF(IFPE.EQ.0) GOTO 62
      MM=MM+1
      DO 61 I=1,MM
   61 IR(I)=I
      IF(IFPE.EQ.1) GOTO 63
      IF(IFPE.GE.2) WRITE(6,98)(IR(I),Z(I),I=1,MM)
      IF(IFPE.EQ.3) GOTO 63
      IFPE=0
      GOTO 64
   63 MN=MM-4
      CALL VSORTP(Z(5),MN,IR(5))
```

```
      KL=MM
      KM=5
      DO 49 I=5,MM
      IF(KM.GT.KL) GOTO 52
      IF(IR(I).EQ.KM) GOTO 51
      IF(IR(I).EQ.KL) GOTO 53
      GOTO 50
   51 KM=KM+1
      GOTO 49
   53 KL=KL-1
   49 CONTINUE
   52 WRITE(6,150)
  150 FORMAT('NO PROPER FPE MINIMUM CAN BE FOUND. PLEASE
     # PICK YOUR OWN FILTER LENGTH.')
      STOP
   50 WRITE(6,119) IR(I)
      MM=IR(I)-1
      IFPE=0
      GOTO 66
   62 CB1(1)=(1.0,0.)
      MM2=MM+1
      DO 20 I=2,MM2
   20 CB1(I)=-CA(I-1)
      CALL ZCPOLY(CB1,MM,CB2,IER)
      DO 28 I=1,MM
      F(I)=ATAN2(AIMAG(CB2(I)),REAL(CB2(I)))/PI
      PO1(I)=POWER(F(I))
      COM=P0/COM
      PHS(I)=ATAN2(AIMAG(COM),REAL(COM))*RAD
      J=I+360
      Y(J)=PO1(I)
      X(J)=F(I)
   28 IR(J)=J
      DO 47 I=1,MM
   47 IR(I)=I
      CALL VSORTP(F,MM,IR)
      WRITE(6,120) (F(I),PO1(IR(I)),I=1,MM)
      WRITE(6,110)
      READ(5,101) IPLT
      IF(IPLT.EQ.0) STOP
      N=360+MM
      DO 18 I=1,360
      IR(I)=I
      X(I)=-.5+.5*FLOAT(I)/180.0
   18 Y(I)=POWER(X(I))
      CALL USMNMX(Y,N,1,C,YMAX)
      CALL VSORTP(X,N,IR)
      DO 69 I=1,N
   69 Y2(I)=Y(IR(I))
      IF(ERR.EQ.1.0) WRITE(6,103)
      DO 67 I=1,76
      IF(YMAX.LT.10.**I) GOTO 68
   67 CONTINUE
   68 FOUR=4.*10**(I-2)
```

```
      YMAX=FLOAT(INT(YMAX/FOUR)+1)*FOUR
      WRITE(6,114)
      READ(5,115) ITITLE
      CALL PLOTS
      CALL FACTOR(SCALE)
      CALL PLOT(1.0,1.0,-3)
      X(N+1)=XMIN
      X(N+2)=(XMAX-XMIN)/5.
      Y2(N+1)=0.0
      Y2(N+2)=YMAX/4.0
      CALL AXIS2(0.0,0.0,'FREQUENCY',-9,5.0,0.0,XMIN
     #,X(N-2),0.5)
      CALL AXIS2(0.0,0.0,'POWER DENSITY',13,4.0,90.0
     #,0.0,Y2(N+2),-1.0)
      CALL LINE(X,Y2,N,1,0,003)
      CALL SYMBOL(1.0,4.1,.20,ITITLE,0.,40)
      CALL PLOT(0.0,0.0,999)
      STOP
   89 WRITE(6,106)
    4 READ(5,113) F1,F2,FINC
      IF(F1.EQ.F2) STOP
      NX=INT((F2-F1)/FINC)+1
      FF1=F1
      TOT=0.0
      DO 31 J=1,NX
      TOT=TOT+GLQ96(POWER,FF1,FF1+FINC,144)
   31 FF1=FF1+FINC
      RTOT=SQRT(TOT)
      WRITE(6,105) TOT,RTOT,F1,F2,FINC
      GOTO 4
   98 FORMAT (//'FILTER LENGTH  NORMALIZED FPE'//(I7,E22.5))
   99 FORMAT(2F9.4)
  100 FORMAT(F13.5,E13.5)
  101 FORMAT(I2)
  102 FORMAT(/'ENTER FILTER LENGTH (2-DIGIT INTEGER);',
     #' TO STOP ENTER 0;')
  103 FORMAT('POWER SPECTRUM UNSCALED (INSUFFICIENT NOISE)')
  105 FORMAT(2E13.5,3F13.5)
  106 FORMAT(/1X,'INPUT LOWER FREQ, UPPER FREQ, FREQ',
     #'INCREMENT;'/1X,'OUTPUTS POWER, SQRT(POWER), INPUT;'
     #/1X,'TO STOP ENTER ZEROS')
  107 FORMAT('MEAN POWER OF THE DATA =',E10.5)
  108 FORMAT(/'ENTER 0; FOR SPECTRUM OR 1; FOR INTEGRATION')
  110 FORMAT(/'FOR SPECTRUM PLOT TYPE 1; OTHERWISE TYPE 0;')
  113 FORMAT(6F9.5)
  114 FORMAT('ENTER TITLE')
  115 FORMAT(10A4)
  116 FORMAT('AUTOPICK ENTER 1; FPE LIST 2; BOTH 3; ',
     #'NEITHER 0;')
  119 FORMAT(/'FILTER LENGTH=',I2)
  120 FORMAT(//5X,'SPECTRAL PEAKS'/'FREQUENCY  POWER ',
     #'DENSITY'/(1X,F8.5,E15.5))
      END
      SUBROUTINE MAXENT
```

```
      IMPLICIT COMPLEX(C)
      COMMON CX(120),CAA(120),CB1(120),CB2(120),CA(120),
     #COM,CONJ,FPE(120),P0,PI,MM,N,ERR
      ERR=0.0
      PP=0.0
      DO 11 I=1,N
   11 PP=PP+CABS(CX(I))**2
      P0=PP/FLOAT(N)
      FPE(1)=FLOAT(N+1)*P0/FLOAT(N-1)
      FTEMP=FPE(1)
      FPE(1)=0.0
      M=1
      CB1(1)=CX(1)
      CB2(N-1)=CX(N)
      NN=N-1
      DO 12 I=2,NN
      CB1(I)=CX(I)
   12 CB2(I-1)=CX(I)
      COM=(0.0,0.0)
      DEN=0.0
      DO 13 I=1,NN
      COM=COM+CONJG(CB1(I))*CB2(I)
   13 DEN=DEN+CABS(CB1(I))**2+CABS(CB2(I))**2
      CA(M)=2.0*CMPLX(REAL(COM)/DEN,AIMAG(COM)/DEN)
      P0=P0*(1.0-CABS(CA(M))**2)
      FPE(2)=ALOG10((FLOAT(N+2)*P0/FLOAT(N-2))/FTEMP)
      IF(P0.LE.0.0) P0=1.001
      IF(P0.LE.0.0) ERR=1.0
      DO 14 M=2,MM
      M1=M+1
      NN=M-1
      NM=N-M
      DO 15 I=1,NN
   15 CAA(I)=CA(I)
      COM=(0.0,0.0)
      DEN=0.0
      CONJ=CONJG(CAA(NN))
      DO 16 I=1,NM
      CB1(I)=CB1(I)-CONJ*CB2(I)
      CB2(I)=CB2(I+1)-CAA(NN)*CB1(I+1)
      COM=COM+CONJG(CB1(I))*CB2(I)
   16 DEN=DEN+CABS(CB1(I))**2+CABS(CB2(I))**2
      CA(M)=2.0*CMPLX(REAL(COM)/DEN,AIMAG(COM)/DEN)
      P0=P0*(1.0-CABS(CA(M))**2)
      FPE(M1)=ALOG10((FLOAT(N+M1)*P0/FLOAT(N-M1))/FTEMP)
      DO 17 I=1,NN
   17 CA(I)=CAA(I)-CA(M)*CONJG(CAA(M-I))
   14 CONTINUE
      RETURN
      END
      FUNCTION POWER(F)
      COMPLEX CA(120),COM,CSPACE(480),CONJ
      COMMON CSPACE,CA,COM,CONJ,Z(120),P0,PI,MM
      COM=(0.0,0.0)
```

```
      DO 19 J=1,MM
      ZZ=-PI*F*J
   19 COM=COM+CMPLX(COS(ZZ),SIN(ZZ))*CA(J)
      COM=1.0-COM
      POWER=P0/CABS(COM)**2
      RETURN
      END
      SUBROUTINE ROTATE(X,Y,ANGLE)
C     SUBROUTINE ROTATE WILL ROTATE A UNIT VECTOR CLOCKWISE
C     ABOUT THE X, Y, OR Z AXIS BY THE NUMBER OF RADIANS
C     GIVEN IN THE INPUT PARAMETER "ANGLE". THE FIRST TWO
C     PARAMETERS ARE THE VECTOR COMPONENTS WHICH WILL BE
C     AFFECTED BY THE ROTATION. IT IS IMPORTANT THAT THEY BE

C     ENTERED IN THE CORRECT ORDER (Y FOLLOWS X, Z FOLLOWS Y,
C     OR X FOLLOWS Z). THE MODIFIED COMPONENTS ARE STORED
C     BACK INTO THESE TWO INPUT VARIABLES.
      XX=X*COS(ANGLE)-Y*SIN(ANGLE)
      Y=Y*COS(ANGLE)+X*SIN(ANGLE)
      X=XX
      RETURN
      END
```

APPENDIX 6

Chi-squared Test for Log-normal Distribution of Power Densities

Expected Frequency (E)	Observed Frequency (O)	$(O - E)^2/E$
6.45	10	1.95
18.10	15	0.53
27.51	24	0.45
22.67	28	1.25
10.11	8	0.44
2.44	3	0.13

Third column total (chi-squared) = 4.75

Degrees of freedom = 6 - 3 = 3

Maximum "passing" value (5 percent level) = 7.82